

# Beryllium and Alpha-Element Abundances in a Large Sample of Metal-Poor Stars

Ann Merchant Boesgaard<sup>1</sup>, Jeffrey A. Rich<sup>1</sup>, Emily M. Levesque<sup>1,2</sup> & Brendan P. Bowler<sup>1</sup>

*Institute for Astronomy, University of Hawai'i at Manoa,  
2680 Woodlawn Drive, Honolulu, HI 96822*

boes@ifa.hawaii.edu

jrich@ifa.hawaii.edu

Emily.Levesque@colorado.edu

bpbowler@ifa.hawaii.edu

## ABSTRACT

The light elements, Li, Be, and B, provide tracers for many aspects of astronomy including stellar structure, Galactic evolution, and cosmology. We have made observations of Be in 117 metal-poor stars ranging in metallicity from  $[\text{Fe}/\text{H}] = -0.5$  to  $-3.5$  with Keck I + HIRES. Our spectra are high-resolution ( $\sim 42,000$ ) and high signal-to-noise (the median is 106 per pixel). We have determined the stellar parameters spectroscopically from lines of Fe I, Fe II, Ti I and Ti II. The abundances of Be and O were derived by spectrum synthesis techniques, while abundances of Fe, Ti, and Mg were found from many spectral line measurements. There is a linear relationship between  $[\text{Fe}/\text{H}]$  and  $A(\text{Be})$  with a slope of  $+0.88 \pm 0.03$  over three orders of magnitude in  $[\text{Fe}/\text{H}]$ . We find that Be is enhanced relative to Fe;  $[\text{Be}/\text{Fe}]$  is  $+0.40$  near  $[\text{Fe}/\text{H}] \sim -3.3$  and drops to  $0.0$  near  $[\text{Fe}/\text{H}] \sim -1.7$ . For the relationship between  $A(\text{Be})$  and  $[\text{O}/\text{H}]$  we find a gradual change in slope from  $0.69 \pm 0.13$  for the Be-poor/O-poor stars to  $1.13 \pm 0.10$  for the Be-rich/O-rich stars. Inasmuch as the relationship between  $[\text{Fe}/\text{H}]$  and  $[\text{O}/\text{H}]$  seems robustly linear (slope =  $+0.75 \pm 0.03$ ), we conclude that the slope change in Be vs. O is due to the Be abundance. Much of the Be would have been formed in the vicinity of SN II in the early history of the Galaxy and by Galactic

---

<sup>1</sup>Visiting Astronomer, W. M. Keck Observatory jointly operated by the California Institute of Technology and the University of California.

<sup>2</sup>University of Colorado

cosmic-ray (GCR) spallation in the later eras. Although Be is a by-product of CNO, we have used Ti and Mg abundances as alpha-element surrogates for O in part because O abundances are rather sensitive to both stellar temperature and surface gravity. We find that  $A(\text{Be})$  tracks  $[\text{Ti}/\text{H}]$  very well with a slope of  $1.00 \pm 0.04$ . It also tracks  $[\text{Mg}/\text{H}]$  very well with a slope of  $0.88 \pm 0.03$ . We have kinematic information on 114 stars in our sample and they divide equally into dissipative and accretive stars. Almost the full range of  $[\text{Fe}/\text{H}]$  and  $[\text{O}/\text{H}]$  is covered in each group. There are distinct differences in the relationships of  $A(\text{Be})$  and  $[\text{Fe}/\text{H}]$  and of  $A(\text{Be})$  and  $[\text{O}/\text{H}]$  for the dissipative and the accretive stars. It is likely that the formation of Be in the accretive stars was primarily in the vicinity of SN II while the Be in the dissipative stars was primarily formed by GCR spallation. We find that Be is not as good a cosmochronometer as Fe. We have found a spread in  $A(\text{Be})$  that is valid at the  $4\sigma$  level between  $[\text{O}/\text{H}] = -0.5$  to  $-1.0$  which corresponds to  $-0.9$  to  $-1.6$  in  $[\text{Fe}/\text{H}]$ .

*Subject headings:* stars: abundances; stars: evolution; stars: late-type; stars Population II; Galaxy: halo; Galaxy: disk

## 1. INTRODUCTION

The rare light elements, Li, Be, and B, are rare relative to their neighbors on the periodic table, light H and He and heavier C, N, and O, because their origins are not in stellar interiors. A method other than stellar nucleosynthesis is needed to form LiBeB. Although they can be formed by nuclear fusion in stellar interiors, they are readily destroyed at temperatures lower than the formation temperatures, i.e. at shallower depths in the interiors.

Beryllium can be formed outside of stars in different ways. The “supernovae mechanism” occurs in the vicinity of massive stars which accelerate plentiful nuclei like C, N, and O during the explosion into the surrounding gas. The collisions break up these abundant elements into smaller units, among which are Li, Be, and B nuclei (e.g. Duncan et al. (1997, 1998) Lemoine et al. (1998). In the general vicinity of SN II the number of Be nuclei would be proportional to the number of CNO nuclei. This mechanism might be the prevalent one in the early history of the Galaxy (Boesgaard et al. 1999, Rich & Boesgaard 2009, Tan et al. 2009) and Smiljanic et al. 2009). The slope between  $A(\text{Be}) = \log N(\text{Be})/N(\text{H}) + 12.00$  and  $[\text{O}/\text{H}]$  would be  $\leq 1$ .

A variation on this is the “hypernovae mechanism” (Fields et al. 2002; Nakamura et al. 2006) which could enrich certain regions with excess light elements. Similarly, Parizot

(2000) suggests the idea that superbubbles containing multiple supernovae would lead to local enrichments of light elements. This mechanism has been suggested by Boesgaard & Novicki (2006) and by Smiljanic et al. (2008) to account for some stars with strong Be enrichments.

Another external source of formation of the rare light elements is the classical Galactic Cosmic Ray = “GCR spallation” reactions outside of stars in the general interstellar medium first proposed by (Reeves et al. 1970). Energetic cosmic rays ( $> 150$  MeV) bombard CNO atoms in the ambient interstellar gas and break them into smaller pieces, including Li, Be, B. This process has been described and element ratios were predicted by Meneguzzi et al. (1971). In this case the number of CNO nuclei would be proportional to the cumulative number of SN II ( $N$ ) and the number of cosmic rays would be proportional to the instantaneous rate of SN II ( $dN$ ). The spallation products would be  $\int NdN = kN^2$ . This mechanism might be the more dominant one now producing light elements in the Galactic disk. Then the slope between  $A(\text{Be})$  and  $[\text{O}/\text{H}]$  would be  $\leq 2$ . Processes such as mass outflow during star formation would reduce the predicted slope to lower values.

The early observations of Be and B did not demonstrate the expected quadratic relationship of Be and B with metallicity as predicted by the classic GCR spallation. More complex models of the production of the light elements were then made by several groups (e.g. Ryan et al. 1992, Ramaty et al. 1997, Prantzos et al. (1993), Yoshii et al. 1997, Suzuki et al. (1999), Suzuki & Yoshii 2001). Ryan et al. suggest a model with outflow from the Galactic halo and time-dependent cosmic ray flux. The model of Prantzos et al. that best fit the data at the time consists of two zones - one with gas outflow for the halo and one with gas inflow for the disk. Suzuki & Yoshii produce a self-consistent model which includes inhomogeneous conditions for the halo; they also discuss the effect of an AGN in our Galaxy as a producer of energetic particles as spallation “bullets.” Their model (their Figure 3) does show a fit between Be and metallicity with a slope of 1.0.

Rich & Boesgaard (2009) identified a change in slope between the abundance of Be and O, suggesting such that the “supernovae mechanism” dominated in the early times of Galactic evolution and the “GCR mechanism” became the more dominant one in the later stages of evolution. They found a slope for the the metal-poorer stars to be  $0.74 \pm 0.11$  and for the metal-richer stars to be  $1.59 \pm 0.15$ .

Beryllium has some advantages in the study of light elements over Li and B. It has only one stable isotope,  $^9\text{Be}$ , while Li has both  $^6\text{Li}$  and  $^7\text{Li}$  and B has both  $^{10}\text{B}$  and  $^{11}\text{B}$ . The small non-LTE effects tend to cancel each other out whereas there are non-LTE effects for both Li and B. Beryllium is apparently not produced by the  $\nu$ -process, but both Li and B are predicted to be formed by that mechanism (Woosley et al. 1990). It is less fragile than

Li to  $(p, \alpha)$  reactions (but more fragile than B). Although it is less easily observed than Li, Be is observable from the ground while B is not. It may be that Be will be a good cosmochronometer as suggested by Suzuki & Yoshii (2001) and Pasquini et al. (2005); this is not the case for Li due to the Big Bang component of Li.

The study of the Be abundances in metal-poor stars has been the topic of many papers following the detection of Be in the metal-poor star, HD 140283, by Gilmore et al. (1991). Prior to that study only upper limits had been determined for several stars with  $[\text{Fe}/\text{H}] < -1.3$  (Rebolo et al. 1988, Ryan et al. 1990). Some recent compilations of Be abundances in metal-poor stars include Boesgaard et al. (1999), Boesgaard & Novicki (2006), Tan et al. (2009), Smiljanic et al. (2009), Rich & Boesgaard (2009).

Primas et al. (2000a, 2000b) found Be abundances in two of the three very metal-poor stars that they studied. They compared their results for Be and Fe with those determined by Boesgaard et al. (1999), finding that their Be abundances were “significantly” higher than expected. Rich & Boesgaard (2009), however, found no evidence for a plateau with constant Be abundance. They did find that the four lowest metallicity stars have enhanced  $[\text{Be}/\text{Fe}]$  by about  $1 \sigma$ .

In this paper we report on an extensive collection of high-resolution, high signal-to-noise spectra of Be in 117 metal-poor stars. We have determined abundances for Be, Fe, and O in these stars and have derived abundances for Ti and Mg in the 99 stars observed with the upgraded version of HIRES on the Keck I telescope. Abundances of Li from the literature have been used to assess the possibility of Be depletions. We have found kinematic data for 114 stars and examine the relationship between Be abundance and kinematic properties for these stars.

## 2. OBSERVATIONS AND REDUCTIONS

Altogether 17 nights have been allocated for several programs on various aspects of Be research. Two of those were cancelled before they even began by the Keck Observatory due to a snowstorm that closed the mountain access road (2006 March 19/20) and because of damage resulting from 6.7 and 6.0 magnitude earthquakes (2006 October 15/16). Two other nights had some weather problems. Altogether we obtained data on 15 nights between September 2004 and July 2010. (None of our data was obtained in “service” mode.) The median seeing for the 15 nights was  $0.7''$ .

The HIRES instrument (Vogt et al. 1994) on the Keck I was upgraded in 2004 and was used to observe the Be II resonance doublet at 3130.421 and 3131.065 Å. We restricted our

targets to those within declination of  $-30^\circ$  to  $+60^\circ$  to minimize the effects of atmospheric dispersion on the ultraviolet spectral region of the Be II lines; the latitude of Mauna Kea is  $+19^\circ 45'$ . In addition we tried to observe all the stars near the meridian, at the lowest possible airmass, usually within  $\pm 2$  hours of crossing the meridian. The upgraded HIRES CCD has 3 chips: blue, green, and red. The blue chip has a quantum efficiency of 93% at 3130 Å. This is important to counter the effects of atmospheric absorption and weak stellar output at this wavelength in solar-temperature stars. In the low metallicity stars the Be II lines are weak so we tried to obtain a signal-to-noise ratio per pixel (S/N) of at least 100. The median S/N for our stars is 106 per pixel. The measured spectral resolution in the ultraviolet region is  $\sim 42,000$ .

The upgraded chips are each 2048 x 2048 pixels and have a pixel size of 15  $\mu\text{m}$ . Our grating settings produced a spectral range on the three chips of approximately 3000-6000 Å. Quartz flat-fields were obtained with exposures tailored to the sensitivity of each chip: 50 s for the UV (blue chip), 3-5 s for the green chip and 1 s for the red chip. We obtained 7-9 exposures for each chip. Typically 9-11 bias frames were obtained each night and Th-Ar comparison spectra were taken at the beginning and end of each night. The individual integration times for the stellar spectra were not longer than 30-45 minutes in order to both minimize the effects of cosmic ray hits and maximize the signal so that multiple spectra of the same star could be co-added reliably.

The log of the observational data is presented in Table 1 where the final two columns give the total exposure time in minutes and the S/N of the combined spectra. The S/N measurements are per pixel and are made near 3130 Å. In this paper in addition to these new observations, we have included the data and results for the most metal-poor stars as presented in Rich & Boesgaard (2009). We have also included the stars from Boesgaard et al. (1999) as reanalyzed in Rich & Boesgaard (2009) (Table 4). We have reanalyzed the Subaru spectra of Boesgaard & Novicki (2006) and the four most metal-poor stars from Boesgaard & Hollek (2009). The observing log for these stars are in the original papers and do not appear in Table 1.

We have observed 18 stars in common with Smiljanic et al. (2009), six which they obtained from the archive and 12 which were observed for them in service mode. We have compared our exposure times and S/N ratios with theirs. On average our exposure times are 70% of theirs while the data quality in terms of S/N is 2.8 times better. In addition our spectral resolution is  $\sim 42,000$  compared to their  $\sim 35,000$ . Including the effect of the size of the primary mirrors, we can see that Keck+HIRES is  $\sim 5$  times better for UV spectroscopy than VLT+UVES.

For the data reduction we have used the IDL pipeline<sup>1</sup> made for the upgraded HIRES courtesy of J. Prochaska and standard IRAF<sup>2</sup> routines. The pipeline performed bias subtraction, flat field normalization (with our flat fields, not the archived ones), spectral order extraction, and wavelength correction. We used IRAF to co-add multiple spectra of the same star (sometimes taken on multiple nights) and to fit continua to the final combined, calibrated spectra.

There are five stars in Table 1 for which we did not determine Be abundances. For two of the stars for which Li abundances have been published, our data shows that they are double-lined spectroscopic binaries: BD +9° 352 and BD +26° 2606. We have not tried to determine Be abundances for these stars. In addition, G 10-4 is Li depleted (Ryan & Deliyannis 1998) and too cool at 5000 K to determine a reliable Be abundance. Two other stars, HD 106516 and HD 221377, are deficient in Li and Be and we have not included those in this analysis.

### 3. ABUNDANCES

We have used both IRAF and MOOG<sup>3</sup> (Snedden 1973) to analyze the reduced spectra. Equivalent widths of Fe I, Fe II, Ti I, Ti II and Mg I were measured with the *splot* task in IRAF for each star. For each star for each line lists we removed lines weaker than 5 mÅ and stronger than  $\log W/\lambda = -4.82$ . The weak-line limit was chosen to exclude lines with potentially poor measurements while the strong-line limit was selected to ensure the lines we used would be on the straight-line portion of the curve of growth. We used IRAF (*listpix*) to make files of the wavelength versus intensity in the Be II order to use in the spectrum synthesis mode of MOOG.

#### 3.1. Stellar Parameter Determination

Our stars have a range in temperatures (5500 - 6400 K) and metallicities ( $-0.4$  to  $-3.5$ ) so our original line lists were reduced slightly differently for each star due to the limits above.

---

<sup>1</sup> <http://www.ucolick.org/~xavier/HIRedux>

<sup>2</sup> IRAF is distributed by the National Optical Astronomy Observatories, which are operated by the Association of Universities for Research in Astronomy, Inc., under cooperative agreement with the National Science Foundation.

<sup>3</sup> <http://www.as.utexas.edu/chris/moog.html>

We were left with 28-86 lines of Fe I, 9-14 lines of Fe II, 5-19 lines of Ti I, 5-13 lines of Ti II and 1-3 lines of Mg I.

We have written a collection of perl scripts that perform an iterative determination of  $T_{\text{eff}}$ ,  $\log g$ ,  $[\text{Fe}/\text{H}]$ , and  $\xi$  using the line lists for each star. These scripts utilize the *abfind* driver in MOOG. We found  $T_{\text{eff}}$  from the agreement of the Fe abundance from Fe I lines with a range of excitation potentials, i.e. the slope between  $\log \text{Fe}/\text{H}$  and excitation potential ( $\chi$ ) should be zero. We determined  $\log g$  from the ionization balance of both Fe I with Fe II and Ti I with Ti II, i.e. the abundances from the lines of the two ionization stages agreed at the preferred  $\log g$  value. For almost all our stars we used the  $\log g$  values from Ti I and Ti II in part because there were more lines of Ti II than Fe II in general. However, the differences in  $\log g$  were typically  $<0.04$  and the ensuing differences in  $A(\text{Be})$  were typically  $<0.01$ . We found  $\xi$  by iterating so that the Fe I abundances were similar at all reduced equivalent widths. Our starting value was  $\xi = 1.5 \text{ km s}^{-1}$ ; for some stars this did not converge to a slope of zero so the iterations stopped and  $1.5 \text{ km s}^{-1}$  was used. The median value for the 42 stars where we did determine  $\xi$  is  $1.42 \text{ km s}^{-1}$ . This is virtually identical to the  $1.45 \text{ km s}^{-1}$  value found by Magain (1985).

Model atmospheres were made for the specific parameters for each star by interpolation with the Kurucz grid (1993). All elements were reduced by the amount that Fe is reduced relative to the sun, except for Be and O.

Table 2 contains the derived values for the stellar parameters in columns 2-5. We show in Figure 1 the distribution of our selected stars in the  $T_{\text{eff}}$  vs.  $[\text{Fe}/\text{H}]$  plane. We note that there are 6 stars with  $[\text{Fe}/\text{H}] < -3.00$ . We limited our lower temperature bound to 5500 K because below that the metallic and molecular blending lines become too strong and the Be II lines become too weak to obtain reliable Be abundances.

We have compared our derived parameters with those determined by Stephens & Boesgaard (2002) for the seven stars in common. (We have two other stars in common, but we adopted their parameters for G 64-12 and G 64-37.) The average of the temperature differences is +10 K, of the  $\log g$  differences is  $-0.02$  and of the  $[\text{Fe}/\text{H}]$  differences is  $-0.02$  dex (in the sense of this study minus theirs). One star, BD +34 2476, has a  $T_{\text{eff}}$  difference of 187 K. The other stars agreed well within the nominal uncertainty of  $\pm 50$  K. The largest difference in  $[\text{Fe}/\text{H}]$  was only +0.16. The range in the differences in  $\log g$  was  $\pm 0.36$ .

We have also compared our parameters with those used in the study by Smiljanic et al. (2009) for the 16 stars in common with theirs. (There are 18 stars in common but they used the Stephens & Boesgaard (2002) parameters for two of them). For 14 of the 16 stars they made use of the parameters derived spectroscopically by Fulbright (2002). For nine of

the stars the agreement in temperature is excellent, within  $\pm 50$  K. However, for seven stars their temperatures are systematically lower than ours by 250 to 600 K. For six of these seven stars we were able to make comparisons with effective temperatures found by Casagrande et al. (2010) from the infrared-flux method (IRFM). Those temperatures were in between our values and the ones used by Smiljanic et al. (2009), with five being closer to ours and one closer to theirs. On average our spectroscopic temperatures were 138 K hotter than those from the IRFM, while those of Smiljanic et al. were 285 K cooler. The seventh star was analyzed by Nissen et al. (2000) who found temperatures with IRFM; that value is also intermediate between the two spectroscopically determined temperatures with ours again being hotter.

Thirteen of our stars were also observed by Nissen & Schuster (2010) in their sample of 106 stars from which they found evidence for two different populations of halo stars in the solar neighborhood. They also determined their parameters spectroscopically. On average our values for  $T_{\text{eff}}$  are 28 K hotter than theirs, our values for  $\log g$  are smaller than theirs by 0.15 dex and we find  $[\text{Fe}/\text{H}]$  lower by -0.05 dex. (If we exclude HD 241253 for which we differ in temperature by 224 K, our mean difference is +12 K; for that star we agree in  $[\text{Fe}/\text{H}]$  by 0.03 dex.)

The Be abundance is particularly sensitive to  $\log g$ . As mentioned above, we found this parameter spectroscopically primarily from the ionization balance between Ti I and Ti II which compared well with what we found from Fe I and Fe II. This study has 20 stars in common with Tomkin et al. (1992) who found  $\log g$  values from the ionization balance between Fe I and Fe II. The average difference in  $\log g$  from the two studies is +0.008.

Smiljanic et al. (2009) used gravities derived from Hipparcos parallaxes or adopted literature values. The agreement for all but one of the 16 stars is within  $\pm 0.30$  and the mean difference is  $-0.04$ . For that one star, G 63-46, our  $\log g$  value is higher by 0.93 dex and our Be abundance is higher by a factor of four. We have also tried their  $\log g$  from Hipparcos in our analysis which we present in the next section. Neither our Be abundance nor theirs produce an outlier in the relationships produced in section 4.

We also compared our derived values of  $[\text{Fe}/\text{H}]$  for the 16 stars. All but one star agree to within  $\pm 0.12$  with a mean difference of  $-0.03$ . For BD +2 4651 we find  $[\text{Fe}/\text{H}] = -1.90$  while they find  $-1.50$ . This star is also not an outlier in any of the figures in section 4 with either set of values.



### 3.2. Beryllium Syntheses

We used MOOG with the *synth* driver to find Be and O abundances. We used the appropriate model for each star to create a synthetic spectrum from 3129 - 3133 Å to compare with the observed intensity-wavelength files. For Be we used four abundances to find the best match. We then plotted the best fit to the data with comparisons of  $A(\text{Be})$  of +0.30 dex and -0.30 dex and one with no Be at all. For O we tried four abundances differing by 0.20 dex (or in some cases 0.10 dex.) As part of the fitting procedure we could adjust the width of the gaussian we used for the line profile, the continuum level, and the exact wavelength. For some stars there was some broadening beyond the instrumental width, but the determination of the continuum level was not a problem in the metal-poor stars and the wavelength corrections made during the data reduction were very accurate.

In Figure 2 we show the syntheses for two stars of very different metallicities:  $[\text{Fe}/\text{H}] = -1.01$  and  $-2.79$ . This illustrates the complexity of the spectra in the more metal-rich stars and the concomitant difficulty in getting a good synthetic fit. The metal-poor stars can be well fit, as seen in the figure for BD  $-10^\circ$  388 and reliable Be abundances can be determined. However, the Be II lines grow weaker as the metallicity decreases (see, e.g. Gilmore et al. 1991, 1992, Molaro et al. (1997), Boesgaard & King 1993, Boesgaard et al. 1999, Rich & Boesgaard 2009). The need for very high S/N is clear for the lowest metallicity stars. For example, our spectrum of BD  $-10^\circ$  388, shown in Figure 2, has a S/N of 120.

Figure 3 shows the observed spectra and synthetic spectra for two stars with the same temperature, but different values for  $\log g$  and  $[\text{Fe}/\text{H}]$ . The lower metallicity star has the lower Be and O abundances. In BD  $+28^\circ$  2137 the value for  $[\text{Fe}/\text{H}]$  is lower by 0.41 dex, for  $[\text{O}/\text{H}]$  by 0.39 dex, for  $A(\text{Be})$  by 0.31 dex compared to those values in BD  $-17^\circ$  484.

For stars with lower  $\log g$  values the Be II lines are stronger for a given Be abundance which can be seen in Figure 4. For G 180-24  $\log g$  is 3.77, which is lower than 3.98 for G 24-3 and the Be II lines can both be seen to be stronger in G 180-24. The Be abundances are comparable; G 180-24 does have a higher  $A(\text{Be})$ , but not by much: 0.10 dex. The syntheses for these two stars are shown in Figure 5. This implies that Be II will be more easily detected in subgiants than in dwarfs at low metallicities.

One of our stars, G 268-32, with  $[\text{Fe}/\text{H}] = -2.51$  seemed to be very difficult to fit with an ordinary synthetic spectrum. According to the analysis by Aoki et al. (2002), it is a carbon-enhanced metal-poor star (CEMP) with  $[\text{C}/\text{Fe}] = 2.1$  and  $[\text{N}/\text{Fe}] = 1.2$ . When we used those values in the synthesis, we derived a much better fit. Our parameters are very similar to those of Aoki et al. (2002): we derive 6230/4.60/-2.51/1.46, while they find

6250/4.5/−2.55/1.5 for  $T_{\text{eff}}$ ,  $\log g$ ,  $[\text{Fe}/\text{H}]$ , and  $\xi$ .

Then following the example of Ito et al. (2009), we removed the CH (and CN) lines from the line list in order to find an upper limit for the Be abundance. Figure 6 shows an expanded view of the region of the 3131 line of Be II. The feature at 3130.8 Å, primarily Ti II, is well-fit. For Be the synthetic spectrum with no Be best matches the observed spectrum, but we adopt an upper limit of  $A(\text{Be}) < -1.5$ . This is now the second CEMP star with no Be; Ito et al. (2009) found  $A(\text{Be}) < -2.00$  in BD +44° 493. Unlike BD +44° 493, G 268-32 has enhanced s-process elements; Aoki et al. (2002) find  $[\text{Ba}/\text{Fe}] = +1.98$ . The group of CEMP stars that are enhanced by s-process nucleosynthesis, CEMP-*s*, are thought to result from mass transfer from an AGB companion. This AGB connection may provide an answer to the problem of the low (or no) Be in light of a normal Li abundance in G 268-32; Thorburn (1994) found  $A(\text{Li}) = +2.09$ , but with a lower temperature, 5841 K, and a lower  $[\text{Fe}/\text{H}] = -3.50$ . When we use our model with her Li equivalent width, we find  $A(\text{Li}) = 2.32$ .

Smiljanic et al. (2008) discovered a Be-rich halo dwarf, HD 106038 which has  $[\text{Fe}/\text{H}] = -1.26$  (Nissen & Shuster 1997). They found a Be abundance of  $A(\text{Be}) = 1.40$  near the meteoritic value of 1.42 (Grevesse & Sauval 1998) and 1.41 (Lodders 2003). We observed this star on our 2008 Jan 16 Keck night and obtained a S/N of 100 in a 25 min. integration. Our derived parameters ( $T_{\text{eff}} = 6085$  K,  $\log g = 4.63$ ,  $[\text{Fe}/\text{H}] = -1.34$ ,  $\xi = 1.46$ ) are very similar to the ones they used and our Be abundance is similar,  $A(\text{Be}) = 1.47$ . Tan et al. (2009) also analyzed HD 106038 and derived  $A(\text{Be}) = 1.37$ .

The upper part of Figure 7 shows our observed spectrum of HD 106038 compared to BD −8° 4501, which has similar parameters. The difference in the Be II lines is dramatic. The lower half of the figure is our spectrum synthesis for HD 106038 showing good fits for both Be and OH. This OH line gives  $[\text{O}/\text{H}] = -0.95$ ; the other two OH features give  $-0.92$  and  $-0.90$  (see O synthesis section below).

In section 3.1 we noted that our spectroscopic  $\log g$  was quite different from the Hipparcos one used by Smiljanic et al. (2009) for G 63-46. The parallax for this star is  $7.44 \pm 1.70$  mas resulting in their value of 3.77 ( $\pm 0.10$ ). We have done a Be- and O-synthesis with that  $\log g$  and find  $A(\text{Be}) = 0.66$ , lower than the +0.98 with our  $\log g$  but higher than the +0.37 found by Smiljanic et al. The OH lines are not fit as well using the lower  $\log g$ , however. We also tried a synthesis with all four parameters used by Smiljanic et al.; that does not fit our data at all well, mostly because their temperature is so low that all the blending lines near the 3130 line of Be II are too strong.

### 3.3. Oxygen Syntheses

Beryllium is a direct by-product of O via spallation so it is useful to find the abundance of O in our stars. As pointed out in Rich & Boesgaard (2009) determining reliable O abundances in stars is not easy and the three common features used (O I triplet, [O I], and the electronic transitions of OH in the UV) all have drawbacks. Our spectra do not extend beyond 6000 Å, so we could only use the OH features in the UV. In addition to the OH feature between the two Be II lines at 3130.6 Å, we used two additional OH features at 3139 and 3140 Å. There are seven OH lines in the 3139 region and five OH transitions in the 3140 region as well as atomic lines. Our line lists for the OH regions are from B. Gustafsson (private communication).

Figure 8 shows the syntheses for these regions in two of our stars with different values of [Fe/H]. We used the value for the Gaussian smoothing that we found in the Be II synthesis because it was constrained there by many more features. Similarly, if needed, we used those values for the continuum and wavelength adjustments. In the figure we show the best fit for O and for amounts of  $\pm 0.20$  dex as well as the result with no O at all.

We derive an average [O/H] abundance by weighing the O abundance derived from 3130 Å region by a factor of two. That extra weight was used because 1) the 3130 Å line list is better determined and 2) that region is closer to the center of the echelle order and thus has a somewhat higher S/N. Generally the O abundance from these two OH features agree well with the that found from the 3130 Å feature.

We used our spectrum of the Moon (see Table 1) to find a solar abundance of O from the same three OH features. From this we find  $\log O/H + 12.00 = 8.63 \pm 0.08$ . This is in good agreement with the revised value for the Sun of Asplund et al. (2009) of 8.69. The work of Asplund & García Perez (2001) indicates that the use of 3-D model atmospheres reduces the O abundance found from the OH lines, and also reduces it more at lower values of [Fe/H].

### 3.4. Alpha-Element Abundances: Ti and Mg

The O abundances are quite sensitive to the values for  $\log g$  and  $T_{\text{eff}}$  (see §3.5 below). There is an additional uncertainty from using 2-D instead of 3-D model atmospheres. We decided to use two other alpha-elements as surrogates for O and thus have determined the abundances of [Ti/H] and [Mg/H].

We have measured equivalent widths of 5-19 Ti I lines and 5-13 Ti II lines. We found Ti

abundances with the *abfind* driver in MOOG. The standard deviation of the Ti abundance from the agreement of the Ti I lines is 0.06 - 0.11 dex and from the Ti II lines is 0.08 - 0.11 dex. Table 3 gives our results for [Ti/H] for the newly observed stars and for the stars in Rich & Boesgaard (2009).

For Mg we have used three lines of Mg I at 4571, 4703, and 4730 Å. For the most metal-poor stars ([Fe/H]  $\lesssim$  -2.7) only the line at 4703 Å was strong enough to use. Conversely, in the more metal-rich stars ([Fe/H]  $\sim$  -0.5 to  $\sim$ -1.0) that line was too strong to use. Table 3 also gives the Mg abundances.

### 3.5. Abundance Uncertainties

Uncertainties in the abundances are due to uncertainties in the stellar parameters and the quality of the data, including the S/N ratio. We have calculated the errors in the abundances for all five elements which are due to the uncertainties in the stellar parameters. We have used  $\pm 100$  K as the uncertainty in  $T_{\text{eff}}$ ,  $\pm 0.2$  dex as the uncertainty in  $\log g$ ,  $\pm 0.10$  dex as the uncertainty in [Fe/H], and  $\pm 0.2$  km s $^{-1}$  as the uncertainty in  $\xi$ . We have chosen three representative stars that cover a range in parameters from 5768 to 6222 K in temperature, 3.04 to 4.07 in  $\log g$ , -1.35 to -2.79 in [Fe/H], and 1.14 to 1.54 km s $^{-1}$  in  $\xi$ ; the results are in Table 4. The adopted abundance error is the quadrature sum of the uncertainty from each parameter.

We can estimate the uncertainty in the equivalent width measurements from the S/N values and the spectral resolution. Eighty-seven percent of our stars have spectra with S/N  $> 80$  and 60% are  $> 100$ .

As can be seen from Figure 2, the more metal-rich stars have many blended lines in the Be II region; to determine reliable Be abundances the stellar parameters and the line list used in the synthesis must therefore be well-determined. For the metal-poorer stars the spectrum is less crowded, making the Be abundances easier to determine. However, in the most metal-poor stars the Be lines become very weak so it is especially important to obtain high S/N spectra. As can be noticed in Table 4 the Be abundance is particularly sensitive to the  $\log g$  value used.

The abundance of O from the OH features is particularly sensitive to the model temperature and gravity. Even though the three OH features we used give very similar abundances in each star, the uncertainties in the stellar parameters contribute substantial error. In addition there is the possibility of a more systematic trend seen when the 3-D model atmospheres are used (Asplund & García Pérez 2001) as mentioned in §3.3.

In the figures that follow we adopt these values as mean errors:  $[\text{Fe}/\text{H}] \pm 0.09$ ;  $[\text{Ti}/\text{H}] \pm 0.09$ ;  $[\text{Mg}/\text{H}] \pm 0.07$ ;  $A(\text{Be}) \pm 0.12$ ; and  $[\text{O}/\text{H}] \pm 0.22$ . For the element ratios we adopt these values:  $[\text{Ti}/\text{Fe}] \pm 0.13$ ;  $[\text{Mg}/\text{Fe}] \pm 0.11$ ;  $[\text{Be}/\text{Fe}] \pm 0.15$ ;  $[\text{O}/\text{Fe}] \pm 0.24$ .

## 4. RESULTS

Parameters and abundances given for 117 stars in Table 2. Only two of these stars have upper limits on the Be abundances: the CEMP star, G 268-32, and LP 831-70 which has  $[\text{Fe}/\text{H}] = -3.06$  and for which our S/N was only 52.

### 4.1. Beryllium and Iron

Figure 9 shows the relationship between  $[\text{Fe}/\text{H}]$  and  $A(\text{Be})$  for our stars. Two stars with enriched Be (HD 106038 and HD 132475) were not included in the determination of the least-squares fit to the data. A linear fit between these two logarithmic quantities is a good match over three orders of magnitude in  $[\text{Fe}/\text{H}]$ .

$$A(\text{Be}) = 0.877(\pm 0.030)[\text{Fe}/\text{H}] + 1.207(\pm 0.060) \quad (1)$$

As Rich & Boesgaard (2009) pointed out there is no substantial evidence for a plateau of Be at the lowest metallicities.

Smiljanic et al. (2009) list the linear relations found between Be and Fe by several different studies and for four subsets of their own data. Those slopes are all steeper than ours because none of those studies has the large number of very metal-poor stars that we have here. Our single slope fit is influenced by our stars with  $[\text{Fe}/\text{H}] < -2.2$ . When we just consider the more metal-rich stars with  $[\text{Fe}/\text{H}] > -2.2$ , we find a slope of  $1.04 \pm 0.06$ . This agrees, within the errors, with the slope of  $1.16 \pm 0.07$  found by Smiljanic et al. (2009) for their thick disk star sample.

When the Be results are normalized to the Fe abundance,  $[\text{Be}/\text{Fe}]$ , as seen in Figure 10, we can see that Be is somewhat enriched over Fe from  $[\text{Be}/\text{Fe}] = +0.19$  at  $[\text{Fe}/\text{H}] \sim -3.3$  and reducing to  $[\text{Be}/\text{Fe}] = 0$  at  $[\text{Fe}/\text{H}] = -1.7$ . The formation of Be can occur in the earliest generations of massive stars during supernovae when CNO atoms accelerate out from the explosion into the ambient gas. These ejecta strike protons and neutrons at high energies and split into smaller atoms like Li, Be, and B. So it is not surprising that Be is enhanced relative to Fe in the most metal-poor stars. According to Tsujimoto et al. (1995) the relative

contribution of SNe Ia to the solar Fe abundance is 57%.

## 4.2. Beryllium and Oxygen

Oxygen is directly connected to Be as a major “mother” nucleus for the rare light elements through various spallation reactions. The relationship we found between  $A(\text{Be})$  and  $[\text{O}/\text{H}]$  is shown in Figure 11. There is more scatter in this diagram than in Figure 9 which is due in part to the larger uncertainties in  $[\text{O}/\text{H}]$  as seen in Table 4.  $[\text{O}/\text{H}]$  is sensitive to both  $T_{\text{eff}}$  and  $\log g$ ; the error bar shown here is  $\pm 0.22$ .

The linear single-slope fit shown is:

$$A(\text{Be}) = 1.037(\pm 0.053)[\text{O}/\text{H}] + 0.893(\pm 0.073) \quad (2)$$

The scatter of the data in Figure 11 does not seem to be random, but rather the low O points are above the best fit line as are the high O points. We therefore tried a two-slope fit shown in Figure 12. This was also done by Rich & Boesgaard (2009). This change could be expected if the dominant source of Be in the O-poor and Be-poor stars is the acceleration of CNO atoms from SN II in the early days of Galactic evolution. The number of Be atoms would be proportional to the number of SN II and thus the number of O atoms. The slope would be  $\leq 1$  (as modified to lower values by processes like mass outflow during star formation). When the dominant source of Be atoms is from the classical GCR method with energetic cosmic rays hitting CNO atoms in the ambient interstellar gas as detailed by Meneguzzi et al. (1971), then the number of O atoms would depend on the cumulative rate of supernovae and the number of energetic cosmic rays proportional to the instantaneous rate of supernovae. The slope for the O-rich and Be-rich stars would be  $\leq 2$ . The slope we find between  $[\text{O}/\text{H}]$  and  $A(\text{Be})$  for the O- and Be-poor stars is  $0.69 \pm 0.13$  and for the O-rich and Be-rich stars is  $1.30 \pm 0.10$ , consistent with the notion of a change in the dominant production mechanism.

Those expressions are:

High-O and high-Be:

$$A(\text{Be}) = 1.295(\pm 0.100)[\text{O}/\text{H}] + 1.127(\pm 0.104) \quad (3)$$

Low-O and low-Be:

$$A(Be) = 0.690(\pm 0.129)[O/H] + 0.275(\pm 0.252) \quad (4)$$

The slope change does seem to be caused by the Be abundances rather than the O abundances. In Figure 13 we show the relationship between  $[Fe/H]$  and  $[O/H]$ . There is less scatter than found in Figures 9 (Be vs. Fe) and 11 (Be vs. O) and a well-defined linear fit given by:

$$[O/H] = 0.749(\pm 0.025)[Fe/H] + 0.126(\pm 0.050) \quad (5)$$

We have done two statistical tests (chi-squared and BIC = Bayesian information criterion) to evaluate whether the data for  $A(Be)$  and  $[O/H]$  are better fit by a single power law or a broken power law. Both tests indicate that the one-slope fit is better.

Figure 14 shows the O abundances normalized to the Fe abundances as a function of the Fe abundances. This too can be well-represented by a linear fit with the scatter due to the mean error in  $[O/Fe]$ .

$$[O/Fe] = -0.252(\pm 0.025)[Fe/H] + 0.121(\pm 0.050) \quad (6)$$

### 4.3. Beryllium and Alpha-Elements – Ti and Mg

As mentioned previously, the O abundance from the OH features has a large dependence on both  $T_{\text{eff}}$  and  $\log g$  from the models; in addition there is the issue of the abundance found from 3-D models vs. 1-D models as discussed above in §3.3. Therefore we have used two alpha-elements, Ti and Mg, as surrogates for O.

Figure 15 shows the relationship between the abundance of Ti and Fe as well as the Ti normalized to Fe compared to Fe. There is a remarkably tight correlation between  $[Ti/H]$  and  $[Fe/H]$  with a slope of  $0.86 \pm 0.01$ . The closeness of this relationship, and that between  $[Mg/H]$  and  $[Fe/H]$  (shown in Figure 17), indicates that the stellar parameters we have derived are well-determined. The relationship between  $[Ti/Fe]$  and  $[Fe/H]$  with a slope of  $-0.14 \pm 0.01$  is less steep than the one between  $[O/H]$  and  $[Fe/H]$  which has a slope of  $-0.25 \pm 0.02$ .

Figure 16 shows how  $A(Be)$  tracks  $[Ti/H]$  well with a slope of  $1.00 \pm 0.04$ . As in Figure 11 of  $A(Be)$  vs.  $[O/H]$  both the lowest values of  $[Ti/H]$  and the highest lie above the best fit but not as dramatically as for  $[O/H]$ .

$$A(Be) = 1.002(\pm 0.042)[Ti/H] + 1.069(\pm 0.072) \quad (7)$$

The relationship between [Mg/H] and [Fe/H] and the one between [Mg/Fe] and [Fe/H] are shown in Figure 17. There is a surprisingly close correlation between [Mg/H] and [Fe/H] with a slope of  $0.94 \pm 0.01$ . This is impressive in part because we have only 1-3 Mg I lines and only the strongest one could be used in the Fe-poor stars. The relationship between [Mg/Fe] and [Fe/H] (slope =  $-0.07 \pm 0.01$ ) is even flatter than those of [Ti/Fe] with [Fe/H] and [O/H] with [Fe/H].

The plot of [Mg/H] (as a surrogate for [O/H]) with A(Be) is shown in Figure 18. The slope of this relationship is  $0.87 \pm 0.03$  which is very similar to the slope between A(Be) and [Fe/H] of  $0.87 \pm 0.03$ . The relation between A(Be) and [Mg/H] is

$$A(Be) = 0.870(\pm 0.033)[Mg/H] + 0.815(\pm 0.056) \quad (8)$$

#### 4.4. Lithium

Table 3 also gives the abundance of Li from the literature for most of our stars along with the reference for each. This is not meant to be a comprehensive compilation where multiple studies of a given star are combined in some way. We did make use of the compilation done by Charbonnel & Primas (2005) when the Li abundances were available for our stars to give some consistency. Our purpose here is only to compare the Li and Be abundances in a general way and to check for potential Be depletions in Li-depleted stars.

In Figure 19 we show our Be abundances compared to Li abundances found in the literature. Most of our sample have values of A(Li) near 2.2, corresponding to the halo star Li plateau reflecting the Big Bang production of Li as first found by Spite & Spite (1982). There are seven stars in our sample that are Li-deficient: BD +37° 1458 at A(Li) = 1.37, HD 64090 at 1.21, HD 109303 at <1.65, HD 188510 at 1.61, HD 201889 at 1.04, G 74-5 at 1.48, and Ross 390 at 1.15. Although Li is depleted in those seven stars, the Be abundances are apparently normal for their [Fe/H] values. Four of the seven have  $T_{\text{eff}} < 5600$  K (HD 64090, HD 188510, HD 201889, and BD +37° 1458); these temperatures are cool enough for Li depletion to have occurred (e.g. Boesgaard et al. 2005). Only the coolest, BD +37° 1458 at 5492 K, might be mildly Be-deficient as judged by its position in Figure 9 where it is 0.35 dex below the fit. The other three stars have [Fe/H] values < -0.9, which are too metal-rich to be part of the halo star Li plateau; they may have suffered Li depletion like that in Pop I stars.



We could not find Li abundances in the literature for 21 of our 117 stars. Only one, HD 184499, may be cool enough to have had Li depletion, but it has normal Be. Our two stars with enhanced Be are also enhanced in Li. HD 106038 with  $A(\text{Be}) = 1.47$  has  $A(\text{Li}) = 2.48$  (Asplund et al. 2006) and 2.55 (Tan et al. 2009). HD 132475 was found by Novicki (2005) to have enhanced Li with  $A(\text{Li}) = 2.39$ . Boesgaard & Novicki (2006) determined a Be abundance of  $A(\text{Be}) = +0.57$  and Tan et al. (2009) found  $A(\text{Be}) = +0.62$ , i.e. it is Be-rich for its  $[\text{Fe}/\text{H}]$  of  $-1.50$ , as seen in Figure 9.

#### 4.5. Kinematics

Our kinematic classification of these stars is drawn from Gratton et al. (2003), who use Galactic orbit calculations to determine criteria for distinguishing between stellar populations corresponding to different Galactic components. Stars with a galactic rotation velocity larger than  $40 \text{ km s}^{-1}$  and an apogalactic distance ( $R_{apo}$ ) less than 15 kpc comprise a kinematic class associated with the dissipative collapse population (Eggen et al. 1962), including stars from the classical thick disk and halo. The remainder of the stars in our sample can be associated with the accretion-process population first proposed by Searle & Zinn (1978). These are mainly halo stars, a subset of which can be further distinguished due to their retrograde orbits. Retrograde stars have a  $V$  velocity of  $< -220 \text{ km s}^{-1}$ . The  $UVW$  velocities have positive  $U$  values away from the Galactic center, positive  $V$  values in the direction of the solar motion, and positive  $W$  values paralleling the direction of the north Galactic pole. To convert these values relative to the local standard of rest we used solar values of  $U_{\odot} = -9 \text{ km s}^{-1}$ ,  $V_{\odot} = +12 \text{ km s}^{-1}$ , and  $W_{\odot} = +7 \text{ km s}^{-1}$ . Here we define a star’s Galactic rotation velocity as  $v_{rot} = V + 220 \text{ km s}^{-1}$ , where  $220 \text{ km s}^{-1}$  is the rotational velocity of the local standard of rest with respect to the Galaxy (Fulbright 2002). The Galactic rest-frame velocities,  $v_{RF}$ , are  $[U^2 + (V + 220)^2 + W^2]^{1/2}$ .

Kinematic properties for our full sample are given in Table 5, which lists the stellar radial velocity, the  $U_{lsr}$ ,  $V_{lsr}$ , and  $W_{lsr}$  velocities relative to the local standard of rest, all in  $\text{km s}^{-1}$ , the distance to the apogalaticon of the orbit ( $R_{apo}$ ), and the distance above the Galactic plane  $Z_{max}$ , both in kpc. The reference for the orbital parameters is included in Table 5, with the majority from the compilation of Carney et al. (1994). For each star we also list  $v_{RF}$  in  $\text{km s}^{-1}$ . We include our final classification of each star as dissipative (D) or accretive (A) or accretive/retrograde (A,R). In total our sample consists of 57 dissipative stars and 57 accretive stars (33 of which are also classified as retrograde). For two stars in our sample (HD 24289 and BD  $-13$  3442), we were unable to make a conclusive kinematic classification as no data was available in the literature.

The distribution of  $A(\text{Be})$  with  $[\text{Fe}/\text{H}]$  for the four groups – all stars, dissipative, accretive, and retrograde – is shown in Figure 20. The stars in the dissipative group span nearly the full range in  $[\text{Fe}/\text{H}]$ . The slope we find for them is  $0.94 \pm 0.04$ . However, the slopes for the accretive and retrograde stars are both lower at  $0.68 \pm 0.04$ . These slopes are different at the  $4.6 \sigma$  level. For comparison, in Figure 21 we have plotted the accretive stars and the dissipative stars with the best fit linear relations overplotted. They separate well into two distinctive groups. The slopes intersect at  $[\text{Fe}/\text{H}]$  near  $-2.2$  which somewhat blurs the distinction in  $A(\text{Be})$  for low metallicity stars in the two populations. We suggest that the accretive stars may have originated in environments where less Be was formed. They may have had their Be formed in the vicinity of SN II through the acceleration of CNO atoms into the surrounding gas as discussed in §4.2.

Similar plots between  $A(\text{Be})$  and  $[\text{O}/\text{H}]$  are shown in Figures 22 and 23. In Figure 22 we see that the stars in the dissipative group span nearly the full range in  $[\text{O}/\text{H}]$ . The slope between  $A(\text{Be})$  and  $[\text{O}/\text{H}]$  for this group is  $1.13 \pm 0.08$ . As with Be and Fe, the accretive and retrograde stars have a shallower slope for Be and O of  $0.76 \pm 0.06$ . These slopes are different at the  $3.6 \sigma$  level. The two-slope fit that we see in Figure 12 of  $1.30 \pm 0.10$  and  $0.69 \pm 0.13$  may be partly due to the fact that there are two populations of stars. And this in turn may result from the formation of a larger fraction of Be made by the CNO cosmic rays produced by SN II for the accretive stars while most of the dissipative stars inherited Be from the galactic cosmic rays. A direct comparison between those two groups in Figure 23 shows that they follow distinct relations, but again the intersection of the two fits occurs at  $[\text{O}/\text{H}] \sim -1.9$  and the differences at Low  $[\text{O}/\text{H}]$  are cloudy.

In Figure 24 we show the distribution of the Be abundances with the rest-frame velocity ( $v_{RF}$ ). There are 4 panels showing the distribution for all stars, for just the dissipative stars, for just the accretive stars, and for just the retrograde stars. For the dissipative stars the full range of Be abundances is present, but there are no stars with  $v_{RF} > 280 \text{ km s}^{-1}$  (by definition). For the accretive and retrograde stars there are no stars with  $A(\text{Be}) > +0.35$  with the exception of the two with enriched Be (HD 106038 and HD 132475). Based on the  $A(\text{Li})$  values and the positions in the  $A(\text{Be})$ - $[\text{Fe}/\text{H}]$  plane, there is no evidence that there has been Be depletion (with the possible exception of BD +37° 1458). Therefore it seems plausible that the accretive and retrograde stars come from an environment that has *not* been as enriched in Be as the dissipative sample was. This is in qualitative agreement with Tan & Zhao (2011) who find that low- $\alpha$  (accretive) stars have generally lower Be abundances than high- $\alpha$  although their sample is only from  $[\text{Fe}/\text{H}] = -0.49$  to  $-1.55$ .

Figure 25 shows the distribution of Be normalized to Fe ( $[\text{Be}/\text{Fe}]$ ) with the rest-frame velocity ( $v_{RF}$ ). The accretive stars and their subset of retrograde stars show a flat distribution

of  $[\text{Be}/\text{Fe}]$  with  $v_{RF}$ ; the star with the highest velocity at  $409 \text{ km s}^{-1}$  is G 64-12 which has low values of  $A(\text{Be}) = -1.43$  and  $[\text{Fe}/\text{H}] = -3.45$  but a comparatively high value for  $[\text{Be}/\text{Fe}] = +0.60$ . The dissipative stars may be connected to  $v_{RF}$  with the lower velocity stars showing higher values of  $[\text{Be}/\text{Fe}]$ .

#### 4.6. Beryllium as a Cosmochronometer

Pasquini et al. (2005) have suggested that  $A(\text{Be})$  in stars can track early star formation in the Galaxy. They use  $[\text{O}/\text{Fe}]$  to reveal the variation in the star formation rate and  $A(\text{Be})$  as a measure of time, a cosmochronometer, from the beginning of star formation. They use the Galactic evolution model of Travaglio et al. (1999). Model predictions have been made by Valle et al. (2002) for Li, Be, and B. They take the stellar production of Fe and O from Thielemann et al. (1996) for SNe I and from Woosley & Weaver (1995) for SN II.

From observations of Be, Fe, and O from Boesgaard et al. (1999) they compare  $[\text{O}/\text{Fe}]$  with  $A(\text{Be})$  and find good agreement between the data for the dissipative stars and the model for the thick disk (see their Figure 2). That sample was only eight stars, however. Our sample size here is 116, excluding the CEMP star, G 268-32.

Figure 26 shows our data for  $[\text{O}/\text{Fe}]$  and  $A(\text{Be})$  for all 116 stars. We show a linear fit and the  $1\sigma$  error bars for  $[\text{O}/\text{Fe}]$ . The relationship is:

$$[\text{O}/\text{Fe}] = -0.269(\pm 0.029)A(\text{Be}) + 0.476(\pm 0.023) \quad (9)$$

We have also separated the data into dissipative, accretive, and retrograde sub-samples of 57, 57, and 33 stars. There is virtually no difference between the fits for the full sample and these sub-samples. The slopes are  $-0.26 \pm 0.04$ ,  $-0.25 \pm 0.05$ , and  $-0.29 \pm 0.08$ , respectively. The curve fit from Pasquini et al. (2005) does not match the data as well as the straight line fit. Note that in Figure 14 we have plotted  $[\text{O}/\text{Fe}]$  with  $[\text{Fe}/\text{H}]$  as the abscissa (as opposed to  $A(\text{Be})$  as the abscissa in Figure 26). In both plots there is a larger spread at higher values of the abscissa:  $[\text{Fe}/\text{H}] > -1.4$  and  $A(\text{Be}) > 0.0$ . The vast majority of these stars belong to the dissipative population. We conclude that Be is no better as a cosmochronometer than Fe, and may in fact be worse.

#### 4.7. Spread in Beryllium

Our Figure 7, top panel, shows two stars with similar metallicity and  $\log g$  values, but very different Be abundances. Smiljanic et al. (2009) show four pairs of stars from their paper in Figure 14 with similar parameters and very different values for  $A(\text{Be})$ . Another compelling example can be seen in Figure 14 of Boesgaard & Hollek (2009) of two stars differing by 35 K in temperature, 0.07 in  $\log g$ , 0.06 in  $[\text{Fe}/\text{H}]$ , but differing by a factor of 2 in both  $A(\text{Li})$  and  $A(\text{Be})$ ; their masses are similar at 0.95 and 0.96  $M_{\odot}$  as are their ages at 9.17 and 9.35 Gyr. These examples seem to indicate that there is a real spread in the Be abundance in stars of similar stellar parameters.

We have examined the possibility that there is a real spread in Be at a given interval of  $[\text{Fe}/\text{H}]$ ,  $[\text{O}/\text{H}]$ ,  $[\text{Ti}/\text{H}]$ , and  $[\text{Mg}/\text{H}]$ . Our approach is to determine whether the data show unusually large scatter within a given range of  $[X/\text{H}]$  compared to the rest of the observations outside that interval. This is done using a prediction interval, which is the expected range of an unobserved random variable  $Y$  (here abundance of Be) at a given confidence (defined by  $100(1-\alpha)\%$ ) based on a set of observed data (Casella & Berger 2002, Section 11.3). We assume the data are independent, obey a linear relationship, and are normally distributed about the line in  $y$ .

For each interval of interest  $\Delta[X/\text{H}]$  and confidence limit  $\alpha$  we use observations outside that region to derive the best-fit slope,  $y$ -offset, and prediction interval in that region of interest. We determine how many points within  $\Delta[X/\text{H}]$  lie inside and outside the prediction interval and then use the binomial distribution to calculate the probability of this occurring by chance. If the probability is  $<0.0063\%$  ( $>4\sigma$ ) and is not highly sensitive to either the width of  $\Delta[X/\text{H}]$  nor the chosen confidence limit  $\alpha$ , then we interpret that as evidence for a spread in  $A(\text{Be})$  for that particular  $\Delta[X/\text{H}]$ .

We ran our analysis for  $[\text{Fe}/\text{H}]$ ,  $[\text{O}/\text{H}]$ ,  $[\text{Ti}/\text{H}]$ , and  $[\text{Mg}/\text{H}]$  with a running interval in steps of 0.01 in  $[X/\text{H}]$  for  $\Delta[X/\text{H}] = 0.50, 0.30, \text{ and } 0.20$  ( $\pm 0.25, \pm 0.15, \pm 0.10$ ) and confidence levels  $\alpha = 0.01, 0.05, \text{ and } 0.10$  (99%, 95%, 90%). No significant spread in  $A(\text{Be})$  was observed in  $[\text{Fe}/\text{H}]$ ,  $[\text{Ti}/\text{H}]$ , or  $[\text{Mg}/\text{H}]$ . We did, however, find evidence of a spread for  $[\text{O}/\text{H}]$  from  $\sim -0.5$  to  $-1.1$  dex. In Figure 27 we show an example of the analysis for  $A(\text{Be})$  vs.  $[\text{O}/\text{H}]$ . At the  $[\text{O}/\text{H}]$  value of  $-0.8$  dex, an interval of  $\Delta[\text{O}/\text{H}] = 0.50$ , and a confidence limit of 95% for the prediction interval, 10 out of 30 stars fall outside the prediction interval (top panel). The probability of this occurring by chance given the 5% expectation rate is  $1.1 \times 10^{-6}$  (middle panel). Our results are independent of whether we include or exclude the two anomalously Be-rich stars HD 106038 and HD 132475 (bottom panel). The spread is real at the  $4^+\sigma$  level of confidence. It is also real at the  $3\sigma$  level of confidence when our  $\Delta[\text{O}/\text{H}] = 0.30$ .

The interval where there is the most spread in Be is between  $[O/H] = -0.5$  to  $-1.0$ , which corresponds to  $-0.9$  to  $-1.6$  in  $[Fe/H]$ .

## 5. SUMMARY AND CONCLUSIONS

The study of the light elements - Li, Be, and B - is important in advancing our knowledge of cosmology, Galactic evolution, and stellar structure and evolution. We have made observations to determine Be abundances in 117 stars, most of which were obtained from the upgraded HIRES spectrometer on the Keck 10-m telescope. Our spectral resolution is  $\sim 42,000$  and our median S/N ratio is 106 per pixel. We have also found abundances of Fe, O, Mg, and Ti. The Be and O abundances were found from spectrum synthesis from the Be II resonance lines and the OH electronic transitions in the ultraviolet spectral region near  $3100 \text{ \AA}$ . Equivalent widths were measured for Fe I, Fe II, Ti I, Ti II, and Mg I lines.

We have determined the stellar parameters spectroscopically from the Fe I lines for  $T_{\text{eff}}$  and the ionization balance of Ti I and Ti II or occasionally from Fe I and Fe II for  $\log g$ . The value for  $[Fe/H]$  comes from the Fe I lines. We have made error estimates from the uncertainties in the stellar parameters for three stars which cover the range in our stellar parameters in  $T_{\text{eff}}$ ,  $\log g$ ,  $[Fe/H]$ , and  $\xi$ .

One of our stars, G 268-32, is a carbon-enhanced metal-poor star (CEMP) according to Aoki et al. (2002). It has  $[Fe/H] = -2.51$ . Like BD +44 493, a CEMP star studied by Ito et al. (2009), G 268-32 seems to be devoid of Be and we set an upper limit of  $A(\text{Be}) = -1.5$ . Although the compilation by Charbonnel & Primas (2005) gives  $A(\text{Li}) = 1.99$  for G 268-32 (HIP 3446), when we use our model and Thorburn’s (1994) equivalent width for Li, we find  $A(\text{Li}) = 2.32$ .

We found a linear fit between the  $[Fe/H]$  and  $A(\text{Be})$  over three orders of magnitude in  $[Fe/H]$  with a slope of  $0.88 \pm 0.03$ . Although we found no support for the idea of a plateau in Be at low metallicities, we did find that Be is enriched relative to Fe changing from  $[Be/Fe]$  near  $+0.2$  at  $[Fe/H]$  near  $-3.3$  down to  $\sim 0.0$  near  $[Fe/H] \sim -1.7$ . This supports the idea that much of the Be was formed by the “supernovae” mechanism in the early history of the Galaxy. The Fe is formed primarily from intermediate mass stars from SNe Ia.

We examined the relationship between Be and O because they are directly related as the light elements are formed by spallation with CNO atoms. This relationship can also be fit by a straight line with a slope of  $1.04 \pm 0.05$  over two and a half orders of magnitude in  $[O/H]$ . There is more scatter in the Be-O data than in the Be-Fe data and the scatter is not uniformly distributed; both the lowest Be points and the highest Be points lie above the

best fit line. We tried fitting the results with two lines dividing the sample at  $[O/H] = -1.6$ . The Be-poor and O-poor stars are fit with a slope of  $0.69 \pm 0.13$  while the Be-rich/O-rich stars have a steeper slope of  $1.30 \pm 0.10$ . A change of slope between  $A(\text{Be})$  and  $[O/H]$  would be expected due to the change in the dominant mechanism of Be formation going from the “supernovae” mechanism to the classical GCR mechanism. It is clear that the change in slope is caused by the Be abundance rather than by the O abundance as indicated by the smaller scatter and clear linear fit between  $[Fe/H]$  and  $[O/H]$ .

The O abundance found from the UV lines of OH is sensitive to both the temperature and the gravity. Therefore, we decided to use the alpha-elements, Ti and Mg, as surrogates for O. We found a remarkably tight correlation between  $[Ti/H]$  and  $[Fe/H]$  and between  $[Mg/H]$  and  $[Fe/H]$ . This indicates that our stellar parameters are well-determined. The slope between  $[Mg/H]$  and  $[Fe/H]$  is  $0.94 \pm 0.01$ .

We found that  $A(\text{Be})$  tracks  $[Ti/H]$  very well with a slope of  $1.00 \pm 0.04$  and that  $A(\text{Be})$  tracks  $[Mg/H]$  very well with a slope  $0.88 \pm 0.03$ . As with the Be vs. O relation, both the lowest Be stars and the highest Be stars lie above the linear fit which may indicate that two slopes would be a better representation of the data.

We have searched the literature for Li abundances in our stars and found results for 96 of our 117 stars. Most of our stars have Li abundances near the observed Li plateau of  $A(\text{Li}) \sim 2.2$ . Seven stars were below  $A(\text{Li}) = 1.8$ . With the possible exception of our coolest star, BD +37° 1458, none of the Li-depleted stars are Be-deficient for their  $[Fe/H]$  values. If BD +37° 1458 is depleted in Be it is only a mild depletion. We note that our two stars with enhanced Be, HD 106038 and HD 132475, also have enhanced Li.

Gratton et al. (2003) have established kinematic criteria for distinguishing between a dissipative collapse population (mainly thick disk and halo stars) and an accretive population (mainly halo stars). We have kinematic information on 114 stars and our sample is equally divided between the two groups. Most of our stars have prograde motion, but 33 are on retrograde orbits with  $V < -220 \text{ km s}^{-1}$ . The stars in all three groups cover nearly the full range in both  $[Fe/H]$  and  $[O/H]$ .

The dependence of  $A(\text{Be})$  on  $[Fe/H]$  and on  $[O/H]$  shows distinct differences between the dissipative and the accretive groups. The dissipative stars have a steeper slope of  $A(\text{Be})$  with both  $[Fe/H]$  and  $[O/H]$  than the accretive and retrograde stars. For the Be relationship with  $[Fe/H]$  the slope for the accretive stars is  $0.68 \pm 0.04$  and for the dissipative stars is  $0.94 \pm 0.04$ . The slopes of  $A(\text{Be})$  with respect to  $[O/H]$  are both steeper than with  $[Fe/H]$ :  $0.76 \pm 0.06$  for the accretive stars and for  $1.13 \pm 0.08$  the dissipative stars. The Be in the accretive stars may have made in the vicinity of SN II stars in the early days of the Galaxy formation

and accretion of small stellar systems. The Be in the dissipative stars may have been made preferentially by GCR spallation reaction.

We have found that there are no stars in the accretive and retrograde groups with  $A(\text{Be}) > 0.35$ , except for the two stars with enhanced Be. Those two stars are thought to have originated in the vicinity of a hypernova or in entrained superbubbles with multiple supernovae (Boesgaard & Novicki 2006, Smiljanic et al. 2009). In general, the accretive and retrograde stars were not formed in an environment rich in Be.

The distribution of  $[\text{Be}/\text{Fe}]$  with the rest frame velocity is flat for the accretive and retrograde stars with the mean over the range of  $400 \text{ km s}^{-1}$  near  $[\text{Be}/\text{Fe}] = 0.0$ . The dissipative stars have higher  $[\text{Be}/\text{Fe}]$  at low values of  $v_{RF}$ .

It was suggested by Suzuki & Yoshii (2001) and Pasquini et al. (2005) and then further explored by Smiljanic et al. (2009) that the stellar abundance of Be can be used as a chronometer. In our large sample of 116 stars we find that Be is not as good as Fe as a chronometer. In the usual plot of  $[\text{O}/\text{Fe}]$  vs.  $A(\text{Be})$  there is more scatter in the data than in the plot of  $[\text{O}/\text{Fe}]$  vs.  $[\text{Fe}/\text{H}]$ . The Be abundance is less well-determined than the Fe abundance. If we divide the stars into the dissipative and accretive (and retrograde) subgroups, the fit to the data is no different from the fit with the full sample. For all plots there is more scatter in  $A(\text{Be})$  for data with  $A(\text{Be}) > 0.0$  and with  $[\text{Fe}/\text{H}] > -1.4$ , i.e. for the more recently formed stars.

Related to the use of Be as a chronometer is the issue of whether there is a spread in Be at a given metallicity, as measured by Fe, O, Ti, Mg. There is empirical evidence for a spread through comparisons of Be in pairs of stars with the same stellar parameters. Smiljanic et al. (2009) show four such pairs. Boesgaard et al. (2010) have done statistical tests which show a real dispersion in  $A(\text{Be})$  at a given  $[\text{O}/\text{H}]$  at the  $4\sigma$  level and at a given  $[\text{Fe}/\text{H}]$  at the  $3\sigma$  level. With a similar analysis done here with the larger sample, we find more support for the reality of the spread in  $A(\text{Be})$  with  $[\text{O}/\text{H}]$ . There is evidence at the  $4\sigma$  level for a spread in  $A(\text{Be})$  at  $[\text{O}/\text{H}]$  from  $-0.5$  to  $-1.0$  which corresponds to  $[\text{Fe}/\text{H}] = -0.9$  to  $-1.6$

We are grateful to the various Support Astronomers and Observing Assistants who helped us over the many observing runs for this project. We are indebted to Hai Fu for his IRAF modification that enabled us to measure equivalent widths quickly and easily. We thank Gabriel Dima for determining Li abundances in six of our stars. We acknowledge support from NSF through grant AST 05-05899 to A.M.B.

## REFERENCES

- Allen, C., Poveda, A. & Schuster, W.J. 1991, *A&A*, 244, 280
- Anders, E., & Grevesse, N. 1989, *Geochim. Cosmochim. Acta*, 53, 197
- Aoki, W., Norris, J.E., Ryan, S.G., Beers, T.C. & Ando, H. 2002 *PASJ*, 54, 933
- Asplund, M. & García Pérez, 2001, *A&A*, 372, 601
- Asplund, M., Grevesse, N., Sauval, A.J. & Scott, P. 2009, *ARA&A*, 47, 481
- Asplund, M., Lambert, D.L., Nissen, P.E., Primas, F. & Smith, V.V., 2006, *ApJ*, 644, 229
- Balachandran, S. 1990, *ApJ*, 354, 310
- Boesgaard, A. M., Deliyannis, C. P., King, J. R., Ryan, S. G., Vogt, S. S., & Beers, T. C. 1999a, *AJ*, 117, 1549
- Boesgaard, A. M., & King, J. R. 1993, *AJ*, 106, 2309
- Boesgaard, A. M., & Hollek, J.K. 2009, *ApJ*, 691, 1412
- Boesgaard, A. M. & Novicki, M. C. 2006, *ApJ*, 641, 1122
- Boesgaard, A. M., Rich, J.A., Levesque, E. & Bowler, B.P. 2010, *IAUS 268*, “Light Elements in the Universe” ed. C. Charbonnel, M. Tosi, F. Primas & C. Chiappini, (University Press: Cambridge) p. 231
- Boesgaard, A. M., Stephens, A. & Deliyannis, C. P. 2005, *ApJ*, 633, 398
- Borkova, T. V. & Marsakov, V. A. 2004, *Astron. Zh.* 30, 173
- Borkova, T. V. & Marsakov, V. A. 2005, *Astron. Zh.*, 82, 453
- Bobylev, V. V., Goncharov, G.A. & Bajkova, A.T. 2006, *A. Rep.*, 50, 733
- Carney, B.W., Latham, D.W., Laird, J.B. & Aguilar, L.A. 1994, *AJ*, 107, 2240
- Casagrande, L., Ramírez, I., Meléndez, J., Bessell, M. & Asplund, M. 2010, *A&A*, 512, A54
- Casella, G. & Berger, R. 2002, *Statistical Inference* (2nd ed.), (Pacific Grove, CA: Duxbury Press), p. 558
- Charbonnel, C. & Primas, F. 2005, *A&A*, 442, 961
- Chen, Y. Q., Nissen, P. E., Zhao, G., Zhang, H. W. & Benoni, T. 2000, *A&AS*, 141, 491
- Chen, Y. Q., Nissen, P. E., Benoni, T. & Zhao, G. 2001, *A&A*, 371, 943
- Duncan, D. K., Primas, F., Rebull, L. M., Boesgaard, A. M., Deliyannis, C. P., Hobbs, L. M., King, J. R., & Ryan, S. G. 1997, *ApJ*, 488, 338
- Duncan, D. K., Rebull, L. M., Primas, F., Boesgaard, A. M., Deliyannis, C. P., Hobbs, L. M., King, J. R., & Ryan, S. G. 1998, *A&A*, 332, 1017



- Eggen, O. J., 1996, *AJ*, 112, 2661
- Eggen, O. J., Lynden-Bell, D., & Sandage, A. R. 1962, *ApJ*, 136, 748
- Fields, B. D., and Daigne, F., Casse, M., and Vangioni-Flam, E., 2002, *ApJ*, 581, 389
- Fulbright, J. P. 2002, *AJ*, 123, 404
- Gilmore, G., Gustafsson, B., Edvardsson, B., & Nissen, P. E. 1992, *Nature*, 357, 379
- Gilmore, G., Edvardsson, B., & Nissen, P. E. 1991, *ApJ*, 378, 17
- Gratton, R. G., Carretta, E., Desidera, S., Lucatello, S., Mazzei, S., & Barbieri, M. 2003, *A&A*, 406, 131
- Grevesse, N. & Sauval, A.J. 1998, *SSRv*, 85, 161
- Holmberg, J., Nordstrom, B. & Andersen, J. 2007, *A&A*, 475, 519
- Ito, H., Aoki, W., Honda, S. & Beers, T.C. 2009, *ApJ*, 698, 371
- Kurucz, R. L. 1993, CD-ROM 13 (Cambridge: Smithsonian Astrophys. Obs.)
- Lemoine, M., Vangioni-Flam, E., & Cass, M. 1998, *ApJ*, 499, 735
- Lodders, K. 2003, *ApJ*, 591, 1230
- Magain, P. 1984, *A&A*, 132, 208
- Meléndez, J., Casagrande, L., Ramirez, I., Asplund, M., & Schuster, W. J. 2010, *A&A*, 515, 3
- Meneguzzi, M., Audouze, J., and Reeves, H. 1971, *A&A*, 15, 337
- Mishenina, T.V., Soubiran, C., Kovtyukh, V.V. & Korotin, S.A. 2004, *A&A*, 418, 551
- Molaro, P., Bonifacio, P., Castelli, F., & Pasquini, L. 1997, *A&A*, 319, 593
- Nissen, P.E., Chen, Y.Q., Schuster, W.J., & Zhao, G. 2000, *A&A*, 353, 722
- Nissen, P.E. & Schuster, W.J. 1997, *A&A*, 326, 751
- Nissen, P.E. & Schuster, W.J. 2010, *A&A*, 511, L10
- Nakamura, K., Inoue, S., Wanajo, S., and Shigeyama, T., 2006, *ApJ*, 643, 115
- Nordstrom, B., Mayor, M., Andersen, J., Holmberg, J., Pont, F., Jrgensen, B. R., Olsen, E. H., Udry, S., & Mowlavi, N. 2004, *A&A*, 418, 989
- Novicki, M. 2005, Ph.D. Thesis, University of Hawaii
- Parizot, E. 2000, *A&A*, 362, 786
- Pasquini, L., Galli, D., Gratton, R. G., Bonifacio, P., Randich, S., & Valle, G. 2005, *A&A*, 436, L57

- Prantzos, N., Cassé, M., & Vangioni-Flam, E. 1993, *ApJ*, 403, 630
- Primas, F., Asplund, M., Nissen, P. E., & Hill, V. 2000a, *A&A*, 364, L42
- Primas, F., Molaro, P., Bonifacio, P., & Hill, V. 2000b, *A&A*, 362, 666
- Ramaty, R., Kozlovsky, B., Lingenfelter, R.E., & Reeves, H. 1997, *ApJ*, 488, 730
- Rebolo, R., Molaro, P., Abia, C., & Beckman, J. E. 1988, *A&A*, 193, 193
- Reddy, B.E., Lambert, D.L. & Allende Prieto, C. 2006, *MNRAS*, 367, 1329
- Reeves, H., Fowler, W. A., & Hoyle, F. 1970, *Nature*, 226, 727
- Rich, J.A. & Boesgaard, A.M. 2009, *ApJ*, 701, 1519
- Ryan, S. G., Beers, T.C., Deliyannis, C.P. & Thorburn, J.A. 1996, *ApJ*, 543
- Ryan, S. G., Bessell, M. S., Sutherland, R. S., & Norris, J. E. 1990, *ApJ*, 348, L57
- Ryan, S.G. & Deliyannis, C.P. 1998, *ApJ*, 500, 398
- Ryan, S. G. & Norris, J. E. 1991, *AJ*, 101, 1865
- Ryan, S. G., Norris, J. E. & Beers, T.C. 1999 *ApJ*, 523, 654
- Ryan, S. G., Norris, J. E., Bessell, M. S., & Deliyannis, C. P. 1992, *ApJ*, 388, 184
- Searle, L., & Zinn, R. 1978, *ApJ*, 225, 357
- Schuster, W.J., Moitinho, A., Mrquez, A., Parrao, L. & Covarrubias, E. 2006, *A&A*, 445, 939
- Shi, J. R., Gehren, T., Zhang, H. W., Zeng, J. L. & Zhao, G. 2007, *A&A*, 465, 587
- Smiljanic, R., Pasquini, L., Bonifacio, P., Galli, D., Gratton, R. G., Randich, S., & Wolff, B. 2009, *A&A*, 499, 103
- Smiljanic, R., Pasquini, L., Primas, F., Mazzali, P.A., Galli, D. & Valle, G. 2008, *MNRAS*, 385, L93
- Snedden, C. A. 1973, PhD thesis, Univ. of Texas, Austin
- Soubiran, C. & Girard, P. 2005, *A&A*, 438, 139
- Stephens, A. & Boesgaard, A.M. 2002, *AJ*, 123, 1647
- Suzuki, T.K & Yoshii, Y. 2001, *ApJ*, 549, 303
- Suzuki, T.K, Yoshii, Y., & Kajino, T. 1999, *ApJ*, 522, L125
- Tan, K. F., Shi, J. R., & Zhao, G. 2009, *MNRAS*, 392, 205
- Tan, K. & Zhao, G. 2011, *ApJ*, 738, L33
- Thielemann, F.-K., Nomoto, K. & Hashimoto, M. 1996, *ApJ*, 460

- Thorburn, J. 1994, ApJ, 421, 318
- Travaglio, C., Galli, D., Gallino, et al. 1999, ApJ, 521, 691
- Tsujimoto, T., Nomoto, K., Yoshii, Y., Hashimoto, M., Yanagida, S. & Thielemann, F-K. 1995, MNRAS, 277, 945
- Valle, G., Ferrini, F., Galli, D. & Shore, S.N. 2002, ApJ, 566, 252
- Venn, K.A., Erwin, M., Shetrone, M.D., Tout, C.A., Hill, V. & Tolstoy, E. 2004, AJ, 128, 1177
- Vogt, S. S., Allen, S. L., Bigelow, B. C., Bresee, L., Brown, B., Cantrall, T., Conrad, A., Couture, M., Delaney, C., Epps, H. W., and 17 coauthors 1994, SPIE, 2198, 362
- Woosley, S.E., Hartmann, D.H., Hoffman, R.D., & Haxton, W.C. 1990, ApJ, 356, 272
- Woosley, S.E. & Weaver, T.A. 1995, ApJS, 101, 181
- Yoshii, Y., Kajino, T., & Ryan, S.G. 1997, ApJ, 485, 605

Table 1. Log of the Beryllium Observations

Star	HIP	Other	Code <sup>a</sup>	R.A.	Dec.	V	Date U.T.	Exp.	S/N
G 130-65	...	LP 349-6	1	00 22	+23 54	11.64	2004 Nov 18	60	59
G 268-32	3446	LP 706-7	2	00 44	−13 55	12.10	2004 Sep 2 2004 Nov 18 2006 Jan 2	270	113
BD +4 302	...	G 3-16	3	01 43	+04 51	10.47	2007 Nov 7 2005 Sep 27	90	151
BD +2 263	...	G 71-33	4	01 45	+03 30	10.63	2005 Sep 27	50	108
BD −10 388	8572	G 271-162	5	01 50	−09 21	10.37	2004 Nov 7	55	123
G 74-5	10140	BD +29 366	6	02 10	+29 48	8.77	2008 Jan 16	10	137
BD −1 306	10449	G 159-50	7	02 14	−01 12	9.09	2008 Jan 16	15	135
BD −9 466	...	NLTT 8103	8	02 28	−08 59	11.19	2006 Jan 2	30	89
BD −17 484	11729	LTT 1242	9	02 31	−16 59	10.43	2008 Jan 16	45	108
HD 16031	11952	BD −13 482	10	02 34	−12 23	9.78	2006 Jan 2	20	135
BD +9 352	12529	G 76-21	...	02 41	+09 46	10.17	2004 Nov 18	50	115
G 4-37	12807	G 76-26	11	02 44	+08 28	11.43	2005 Sep 27	90	104
BD +22 396	13111	G 5-1	12	02 48	+22 35	10.10	2007 Nov 19	20	69
G 5-19	...	LHS 6057	13	03 11	+12 37	11.12	2005 Sep 27	60	90
LTT 1566	15396	Ross 570	14	03 18	−07 08	11.22	2004 Nov 18	90	86
CD −24 1656	16063	NLTT 10967	15	03 26	−23 43	10.89	2005 Jan 31 2006 Jan 2	79	82
HD 24289	18082	BD −4 680	16	03 51	−03 49	9.96	2007 Nov 7	50	126
BD +21 607	19797	HD 284248	17	04 14	+22 21	9.22	2004 Nov 18	15	98
HD 31128	22632	CD −27 1935	18	04 52	−27 03	9.14	2008 Jan 16	30	76
HD 241253	24030	G 97-22	19	05 09	+05 33	9.72	2004 Nov 18	25	95
HD 247168	27111	BD +9 946	20	05 44	+09 14	11.82	2004 Nov 18	90	68
HD 247297	27182	BD +14 1018	21	05 45	+14 41	9.11	2005 Sep 27	12	99
Ross 797	27880	LTT 2402	22	05 53	−14 22	11.47	2006 Jan 2	60	89
G 191-55	...	BD +58 876	23	05 57	+58 40	10.47	2005 Jan 31	90	98
BD +19 1185	28671	HD 250792	24	06 03	+19 21	9.32	2005 Sep 27	14	108
BD +37 1458	29759	G 101-29	25	06 16	+37 43	8.92	2005 Jan 31	30	145
G 192-43	32567	G 193-4	26	06 47	+58 38	10.32	2007 Nov 19	60	106
G 88-10	34630	LTT 11991	27	07 10	+24 20	11.86	2007 Nov 19 2008 Jan 16	150	121
G 108-58	...	LP 708-12	28	07 10	−01 17	11.82	2008 Jan 16	90	91

Table 1—Continued

Star	HIP	Other	Code <sup>a</sup>	R.A.	Dec.	V	Date U.T.	Exp.	S/N
G 90-3	36430	LTT 17974	29	07 29	+32 51	10.50	2004 Nov 7	56	123
BD +24 1676	36513	G 88-32	30	07 30	+24 05	10.80	2004 Nov 18	125	140
Ross 390	36878	LTT 2886	31	07 34	−10 23	11.10	2006 Jan 2	60	96
G 113-9	...	NLTT 18799	32	08 00	−04 05	11.00	2008 Jan 16	60	100
G 113-22	...	BD +0 2245	33	08 16	+00 01	9.69	2006 Jan 2	30	140
HD 233511	40778	BD +54 1216	34	08 19	+54 05	9.71	2005 Jan 31	30	108
BD +39 2173	...	G 115-34	35	08 55	+38 39	11.22	2007 Nov 19	60	89
BD −3 2525	44124	G 114-26	36	08 59	−04 01	9.67	2004 Nov 7	30	130
G 115-49	44605	LTT 12383	37	09 05	+38 47	11.60	2007 Nov 19	60	81
G 10-4	54639	G 45-38	38	11 11	+06 25	11.41	2005 May 15		
							2006 Jan 2	120	99
BD +36 2165	54772	LTT 13019	39	11 12	+35 43	9.75	2005 Jan 31	35	110
BD +51 1696	57450	LTT 13244	40	11 46	+50 52	9.90	2005 Jan 31		
							2005 Apr 1	43	117
HD 104056	58443	BD −3 3216	41	11 59	−04 46	9.01	2006 Jan 2	12	139
BD −4 3208	59109	G 13-9	42	12 07	−05 44	9.99	2005 Apr 1	60	109
HD 106038	59490	BD +14 2481	43	12 12	+13 15	10.16	2008 Jan 16	25	107
HD 106516	59750	BD −9 3468	...	12 15	−10 18	6.11	2007 Jan 12	17	276
HD 108177	60632	BD +2 2538	44	12 25	+01 17	9.66	2005 Jan 31	30	93
HD 109303	61264	BD +50 1929	45	12 33	+49 18	8.15	2010 Jul 4	6	110
BD +28 2137	61545	G 59-27	46	12 36	+27 28	10.86	2007 Jun 10	30	100
G 63-46	66665	BD +13 2698	47	13 39	+12 35	9.37	2006 Jun 19	20	93
BD +34 2476	68321	G 165-39	48	13 59	+33 51	10.06	2006 Jun 19	55	123
G 64-37	68592	LTT 5476	49	14 02	−05 39	11.14	2010 Jul 4	150	139
BD +26 2606	72461	G 166-45	...	14 49	+25 42	9.72	2006 Jun 19	25	104
BD +26 2621	72920	G 166-54	50	14 54	+25 34	10.99	2005 Jan 31	60	125
G 153-21	78620	BD −6 4346	51	16 03	−06 27	10.20	2007 Jun 10	30	94
G 180-24	78640	BD +42 2667	52	16 03	+42 14	9.85	2006 Jun 19	30	86
G 181-28	...	LTT 15067	53	17 07	+34 21	12.02	2010 Jul 4	150	107
BD +2 3375	86443	G 20-8	54	17 39	+02 24	9.93	2006 Jun 19	45	115
BD −8 4501	87062	G 20-15	55	17 47	−08 46	10.59	2004 Sep 7	55	77
HD 161770	87101	BD −9 4604	56	17 47	−09 36	9.66	2004 Sep 7	25	78
BD +36 2964	87467	G 182-31	57	17 52	+36 24	10.37	2004 Sep 7	40	87
BD +20 3603	87693	G 183-11	58	17 54	+20 16	9.69	2006 Jun 19	30	102
G 20-24	88827	BD +1 3579	59	18 07	+01 52	11.09	2007 Jun 10	60	110

Table 1—Continued

Star	HIP	Other	Code <sup>a</sup>	R.A.	Dec.	V	Date U.T.	Exp.	S/N
BD +13 3683	90957	G 141-19	60	18 33	+13 09	10.55	2005 Jul 5 2006 Jun 19	80	93
HD 179626	94449	BD −0 3676	61	19 13	−00 35	9.14	2005 Jul 6	25	70
HD 188510	98020	BD +10 4091	62	19 55	+10 44	8.82	2010 Jul 4	15	132
G 24-3	98989	G 92-52	63	20 05	+04 02	10.44	2005 Jul 5	50	95
BD +42 3607	99267	G 125-64	64	20 09	+42 51	10.11	2007 Jun 10	30	120
BD +23 3912	...	HD 345957	65	20 10	+23 57	8.93	2004 Nov 7	25	113
HD 194598	100792	BD +9 4529	...	20 26	+09 27	8.36	2004 Nov 7	10	132
G 24-25	...	LTT 16036	66	20 40	+00 33	10.61	2010 Jul 4	15	56
BD −14 5850	102602	Ross 190	67	20 47	−14 25	10.96	2004 Nov 18 2005 Sep 27	140	103
BD +4 4551	102718	SAO 126242	68	20 48	+05 11	9.69	2004 Nov 7	20	90
G 26-12	106447	LP 638-7	69	21 33	+00 23	12.15	2010 Jul 4	150	96
G 188-22	107294	BD +26 4251	70	21 43	+27 23	10.05	2006 Jun 19	30	121
BD +19 4788	...	G 126-36	71	21 48	+19 58	9.93	2010 Jul 4	30	106
G 126-52	...	LTT 16447	72	22 04	+19 32	11.02	2004 Sep 7 2006 Jun 19	110	121
BD +17 4708	109558	LTT 16493	73	22 11	+18 05	9.47	2004 Nov 7 2005 Jul 5	40	122
BD +7 4841	110140	G 18-39	74	22 18	+08 26	10.38	2004 Nov 7	35	75
HD 218502	114271	BD −15 6355	75	23 08	−15 03	8.50	2010 Jul 4	12	125
BD +2 4651	115167	G29-23	76	23 19	+03 22	10.19	2004 Nov 7 2005 Sep 27	75	134
BD +59 2723	115704	Ross 233	77	23 26	+60 37	10.47	2004 Nov 7	75	61
HD 221377	116082	BD +51 3630	...	23 31	+52 24	7.57	2005 Jul 6	9	116
Moon							2005 May 15	10	470

<sup>a</sup>Code is an ID number for the star in the Appendix Table of equivalent widths.

Table 2. Stellar Parameters and Abundances

Star	$T_{\text{eff}}$	[Fe/H]	log g	$\xi$	A(Be)	[O/H]	[Be/Fe]	[O/Fe]
HD 16031	6162	-1.81	3.89	1.55	-0.38	-0.97	+0.01	+0.84
HD 19445	5853	-2.10	4.41	1.5	-0.48	-1.53	+0.20	+0.57
HD 24289	5700	-2.22	3.50	1.5	-0.83	-1.67	-0.03	+0.55
HD 30743	6222	-0.62	4.15	1.88	+0.78	-0.73	-0.02	+0.11
HD 31128	5882	-1.56	3.94	1.27	-0.13	-0.83	+0.01	+0.74
HD 64090	5500	-1.77	4.73	1.5	-0.09	-1.36	+0.26	+0.41
HD 74000	6134	-2.05	4.26	1.5	-0.49	-1.56	+0.14	+0.49
HD 76932	5807	-0.95	4.00	1.5	+0.77	-0.65	+0.30	+0.30
HD 84937	6206	-2.20	3.89	1.5	-0.83	-1.49	-0.05	+0.71
HD 94028	5907	-1.54	4.44	1.5	+0.45	-1.15	+0.57	+0.39
HD 104056	6085	-0.66	4.43	1.50	+0.44	-0.34	-0.32	+0.32
HD 106038	6085	-1.34	4.63	1.46	+1.47	-0.93	+1.39	+0.41
HD 108177	6105	-1.72	3.91	1.47	-0.41	-1.06	-0.11	+0.66
HD 109303	6230	-0.47	4.04	1.5	+0.80	-0.20	-0.15	+0.27
HD 118244	6234	-0.53	4.13	1.92	+0.76	-0.65	-0.13	-0.12
HD 132475	5765	-1.50	3.60	1.5	+0.78	-0.78	+0.86	+0.72
HD 134169	5759	-0.94	3.68	1.5	+0.55	-0.66	+0.07	+0.28
HD 140283	5692	-2.56	3.47	1.5	-1.18	-1.72	-0.04	+0.84
HD 161770	5708	-1.50	3.32	1.32	-0.20	-0.62	-0.12	+0.66
HD 179626	5882	-1.01	3.74	1.08	+0.47	-0.59	+0.06	+0.42
HD 184499	5670	-0.51	4.00	1.5	+1.12	-0.41	+0.21	+0.10
HD 188510	5600	-1.49	4.43	1.46	-0.41	-0.93	-0.34	0.56
HD 194598	5875	-1.23	4.20	1.5	+0.12	-1.00	-0.07	+0.23
HD 195633	5986	-0.88	3.89	1.5	+0.66	-0.76	+0.12	+0.12
HD 200580	5853	-0.54	4.04	1.72	+0.62	-0.77	-0.26	-0.23
HD 201889	5553	-0.95	3.74	1.5	+0.58	-1.02	+0.11	-0.07
HD 201891	5806	-1.07	4.42	1.5	+0.56	-0.87	+0.21	+0.20
HD 208906	5929	-0.73	4.39	1.34	+0.72	-0.79	+0.03	-0.06
HD 218502	6155	-1.86	3.73	1.37	-0.46	-1.17	-0.02	+0.69
HD 219617	5872	-1.58	4.52	1.5	-0.23	-1.27	-0.07	+0.31
HD 233511	6075	-1.62	4.17	1.5	-0.16	-0.86	+0.04	+0.76
HD 241253	6055	-1.07	4.13	1.42	+0.60	-0.38	+0.25	+0.69
HD 247168	5620	-1.74	4.33	1.14	-0.84	-1.47	-0.52	+0.27
HD 247297	5758	-0.55	4.07	1.5	-0.08	-0.52	-0.95	+0.03

Table 2—Continued

Star	$T_{\text{eff}}$	[Fe/H]	log g	$\xi$	A(Be)	[O/H]	[Be/Fe]	[O/Fe]
CD –24 1656	6172	–2.03	3.85	1.46	–0.56	–1.21	+0.05	+0.82
BD –17 484	6110	–1.56	3.63	1.32	–0.37	–0.95	–0.23	+0.61
BD –14 5850	5777	–2.18	4.12	1.5	–0.79	–1.38	–0.03	+0.80
BD –13 3442	6090	–2.91	4.11	1.5	–1.12	–2.15	+0.37	+0.76
BD –10 388	5768	–2.79	3.04	1.54	–1.30	–1.98	+0.07	+0.81
BD –9 466	5990	–1.89	3.79	1.54	–0.61	–1.12	–0.14	+0.77
BD –8 4501	6392	–1.28	4.39	1.46	–0.18	–0.40	–0.32	+0.88
BD –4 3208	6210	–2.35	4.03	1.5	–0.73	–1.68	+0.20	+0.67
BD –3 2525	6115	–1.91	4.04	1.5	–0.19	–1.07	+0.30	+0.84
BD –1 306	6060	–0.78	4.77	1.5	+0.87	–0.35	+0.23	+0.43
BD +1 2341p	6402	–2.67	4.24	1.5	–1.00	–1.76	+0.25	+0.91
BD +2 263	5842	–1.92	3.95	1.10	–0.73	–1.56	–0.23	+0.36
BD +2 3375	6008	–2.22	4.04	1.28	–0.68	–1.48	+0.12	+0.74
BD +2 4651	5992	–1.90	3.33	1.44	–0.58	–1.18	–0.10	+0.72
BD +3 740	6030	–2.95	3.83	1.5	–1.40	–2.26	+0.13	+0.69
BD +4 302	6095	–2.17	3.71	1.48	–0.76	–1.34	–0.01	+0.83
BD +4 4551	5990	–1.43	3.85	1.41	+0.22	–0.89	+0.23	+0.54
BD +7 4841	6018	–1.56	3.60	1.50	–0.18	–0.93	–0.04	+0.63
BD +9 2190	6008	–3.00	3.85	1.5	–1.22	–2.38	+0.36	+0.62
BD +13 3683	5502	–2.38	3.06	1.47	–1.23	–1.46	–0.27	+0.92
BD +17 4708	5992	–1.70	3.54	1.36	–0.45	–1.09	–0.17	+0.61
BD +19 1185	5835	–0.92	4.62	1.50	+0.17	–0.78	–0.33	+0.14
BD +19 4788	6020	–0.78	4.92	1.5	+0.72	–0.23	+0.08	+0.55
BD +20 2030	5978	–2.77	3.61	1.5	–1.23	–2.06	+0.12	+0.71
BD +20 3603	5908	–2.18	3.61	1.01	–0.93	–1.85	–0.17	+0.33
BD +21 607	6097	–1.72	4.11	1.5	–0.35	–1.17	–0.05	+0.55
BD +22 396	6050	–0.88	4.89	1.05	+0.65	–0.48	+0.11	+0.40
BD +23 3912	5815	–1.46	3.36	1.44	–0.16	–1.09	–0.12	+0.37
BD +24 1676	6125	–2.55	3.74	1.45	–1.28	–1.94	–0.15	+0.61
BD +26 2621	6266	–2.69	4.50	1.5	–0.94	–1.96	+0.33	+0.73
BD +26 3578	6158	–2.32	3.94	1.5	–0.90	–1.69	+0.00	+0.63
BD +28 2137	6110	–1.97	3.83	1.07	–0.68	–1.33	–0.13	+0.64
BD +34 2476	6248	–1.94	3.72	1.23	–0.76	–1.25	–0.24	+0.69
BD +36 2165	6052	–1.71	3.78	1.5	–0.45	–1.28	–0.16	+0.43



Table 2—Continued

Star	$T_{\text{eff}}$	[Fe/H]	log g	$\xi$	A(Be)	[O/H]	[Be/Fe]	[O/Fe]
BD +36 2964	6152	-2.20	3.85	1.39	-0.47	-1.18	+0.31	+1.02
BD +37 1458	5492	-2.02	3.85	1.5	-0.95	-1.37	-0.35	+0.65
BD +39 2173	6200	-1.99	3.76	1.13	-0.58	-1.33	-0.01	+0.66
BD +42 3607	5655	-2.29	3.81	1.43	-1.10	-1.48	-0.23	+0.81
BD +44 1910	5878	-2.64	3.56	1.5	-1.11	-1.96	+0.11	+0.68
BD +51 1696	5852	-1.21	4.19	1.5	-0.33	-0.53	-0.54	+0.68
BD +59 2723	5945	-2.20	4.50	1.02	-0.35	-1.70	+0.43	+0.50
G 4-37	6120	-2.50	3.82	1.33	-0.75	-1.62	+0.33	+0.88
G 5-19	5975	-1.13	3.93	1.34	-0.08	-0.62	-0.37	+0.51
G 11-44	5820	-2.29	3.58	1.5	-1.04	-1.63	-0.17	+0.66
G 20-24	6222	-1.89	4.07	1.14	-0.57	-1.41	-0.10	+0.48
G 21-22	5916	-1.02	4.59	1.5	+0.31	-1.02	-0.09	+0.00
G 24-3	6000	-1.62	3.98	1.47	-0.28	-1.21	-0.08	+0.41
G 24-25	5752	-1.56	3.69	1.43	-0.73	-0.98	-0.59	+0.58
G 26-12	6135	-2.33	3.84	1.39	-0.88	-1.35	+0.03	+0.98
G 59-24	6112	-2.32	4.10	1.5	-0.69	-1.32	+0.21	+1.00
G 63-46	6125	-0.60	4.70	1.50	+0.98	-0.04	+0.16	+0.56
G 64-12	6074	-3.45	3.72	1.5	-1.43	-2.24	+0.60	+1.21
G 64-37	6122	-3.28	3.87	1.5	-1.40	-2.32	+0.46	+0.96
G 74-5	6025	-0.84	4.77	1.50	+0.81	-0.21	+0.23	+0.63
G 75-56	5890	-2.38	3.83	1.5	-0.84	-1.74	+0.12	+0.64
G 88-10	5945	-2.61	4.00	1.5	-1.08	-1.86	+0.11	+0.75
G 90-3	5710	-2.28	3.19	1.48	-0.88	-1.79	-0.02	+0.49
G 92-6	6115	-2.70	4.79	1.5	-0.91	-2.28	+0.37	+0.42
G 108-58	5865	-2.37	4.03	1.5	-1.12	-1.33	-0.17	+1.04
G 113-9	5998	-1.75	3.68	1.27	-0.26	-1.01	+0.07	+0.74
G 113-22	5802	-1.01	3.95	1.50	+0.70	-0.40	+0.29	+0.61
G 115-49	5605	-2.23	3.78	1.16	-1.03	-1.47	-0.22	+0.76
G 126-52	6182	-2.36	3.95	1.47	-0.81	-1.67	+0.13	+0.69
G 130-65	6018	-2.21	3.65	1.54	-0.70	-1.24	+0.09	+0.97
G 153-21	6142	-0.39	4.55	1.50	+1.03	-0.05	+0.00	+0.34
G 180-24	6008	-1.44	3.77	1.31	-0.18	-0.88	-0.16	+0.56
G 181-28	5965	-2.42	3.98	1.33	-1.20	-1.62	-0.20	+0.80
G 188-22	5975	-1.35	3.72	1.31	+0.22	-0.78	+0.15	+0.57

Table 2—Continued

Star	$T_{\text{eff}}$	[Fe/H]	log g	$\xi$	A(Be)	[O/H]	[Be/Fe]	[O/Fe]
G 191-55	5828	-1.81	4.11	1.06	-0.80	-1.37	-0.41	+0.44
G 192-43	6140	-1.42	3.78	1.28	-0.38	-0.93	-0.38	+0.49
G 201-5	5950	-2.54	4.00	1.5	-1.27	-1.97	-0.15	+0.57
G 206-34	5825	-3.12	3.99	1.5	-1.20	-2.37	+0.50	+0.75
G 268-32	6230	-2.51	4.60	1.46	< -1.50	...	< -0.41	...
G 275-4	5942	-3.42	4.05	1.5	-1.53	-2.48	+0.47	+0.94
LP 553-62	6128	-2.73	3.93	1.5	-1.00	-2.02	+0.31	+0.71
LP 635-14	5932	-2.71	3.57	1.5	-1.17	-2.00	+0.12	+0.71
LP 651-4	6030	-2.89	4.26	1.5	-1.12	-2.04	+0.35	+0.85
LP 752-17	5738	-2.38	3.20	1.5	-0.86	-1.80	+0.10	+0.58
LP 815-43	6405	-2.76	4.37	1.5	-0.95	-1.86	+0.39	+0.90
LP 831-70	6005	-3.05	3.40	1.47	< -1.10	-1.85	<0.53	+1.20
LTT 1566	6025	-2.36	3.93	1.49	-0.90	-1.71	+0.04	+0.65
Ross 390	5920	-0.78	4.71	1.50	+0.07	-0.13	-0.57	+0.75
Ross 797	5838	-1.17	4.17	1.21	-0.24	-0.71	-0.49	+0.46

Table 3. Stellar Abundances of Ti, Mg, and Li

Star	$T_{\text{eff}}$	[Fe/H]	[Ti/H]	[Mg/H]	A(Li)	Li ref. <sup>1</sup>
HD 16031	6162	−1.81	−1.39	−1.32	2.18	CP05
HD 19445	5853	−2.10	...	...	2.18	CP05
HD 24289	5700	−2.22	−1.94	−1.91	2.38	CP05
HD 30743	6222	−0.62	...	...	2.35	B90
HD 31128	5882	−1.56	−1.30	−1.14	2.16	CP05
HD 64090	5500	−1.77	...	...	1.21	CP05
HD 74000	6134	−2.05	...	...	2.14	CP05
HD 76932	5807	−0.95	...	...	2.03	C01
HD 84937	6206	−2.20	...	...	2.28	CP05
HD 94028	5907	−1.54	...	...	2.21	CP05
HD 104056	6085	−0.66	−0.37	−0.14	...	...
HD 106038	6085	−1.34	−1.06	−0.82	2.48	A06
HD 108177	6105	−1.72	−1.42	−1.29	2.20	CP05
HD 109303	6230	−0.47	−0.33	−0.22	<1.65	C01
HD 118244	6234	−0.53	...	...	2.07	C01
HD 132475	5765	−1.50	...	...	2.39	MN05
HD 134169	5759	−0.94	...	...	2.22	CP05
HD 140283	5692	−2.56	...	...	2.26	CP05
HD 161770	5708	−1.50	−1.27	−1.05	2.12	CP05
HD 179626	5882	−1.01	−0.76	−0.67	1.81	CP05
HD 184499	5670	−0.51	...	...	...	...
HD 188510	5600	−1.49	−1.29	−1.09	1.61	S07
HD 194598	5875	−1.23	...	...	2.00	CP05
HD 195633	5986	−0.88	...	...	2.15	R88
HD 200580	5853	−0.54	...	...	2.08	C01
HD 201889	5553	−0.95	...	...	1.04	CP05
HD 201891	5806	−1.07	...	...	1.98	MN05
HD 208906	5929	−0.73	...	...	2.31	C01
HD 218502	6155	−1.86	−1.46	−1.58	2.31	M10
HD 219617	5872	−1.58	...	...	2.23	CP05
HD 233511	6075	−1.62	−1.30	−1.16	2.12	CP05
HD 241253	6055	−1.07	−0.81	−0.66	1.98	M10
HD 247168	5620	−1.74	−1.60	−1.58	2.18	GD
HD 247297	5758	−0.55	−0.21	−0.24	...	...

Table 3—Continued

Star	$T_{\text{eff}}$	[Fe/H]	[Ti/H]	[Mg/H]	A(Li)	Li ref. <sup>1</sup>
CD –24 1656	6172	–2.03	–1.61	–1.65	...	...
BD –17 484	6110	–1.57	–1.29	–1.19	...	...
BD –14 5850	5777	–2.18	–1.95	–1.74	...	...
BD –13 3442	6090	–2.91	–2.16	–2.31	2.18	R99
BD –10 388	5768	–2.79	–2.33	–2.16	2.26	CP05
BD –9 466	5990	–1.89	–1.55	–1.47	2.20	GD
BD –8 4501	6392	–1.28	–1.05	–1.05	2.11	CP05
BD –4 3208	6210	–2.35	–1.92	–1.89	2.30	CP05
BD –3 2525	6115	–1.91	–1.59	–1.55	...	...
BD –1 306	6060	–0.78	–0.45	–0.33	...	...
BD +1 2341p	6402	–2.67	–2.09	–2.30	2.19	MN05
BD +2 263	5842	–1.92	–1.62	–1.64	2.12	R96
BD +2 3375	6008	–2.22	–1.94	–1.85	2.06	CP05
BD +2 4651	5992	–1.90	–1.57	–1.48	2.18	CP05
BD +3 740	6030	–2.95	–2.27	–2.45	2.16	CP05
BD +4 302	6095	–2.17	–1.71	–1.73	2.33	GD
BD +4 4551	5990	–1.43	–1.17	–0.97	1.97	CP05
BD +7 4841	6018	–1.56	–1.24	–1.06	2.22	CP05
BD +9 2190	6008	–3.00	–2.41	–2.41	2.18	CP05
BD +13 3683	5502	–2.38	–2.14	–1.94	1.94	T94
BD +17 4708	5992	–1.70	–1.42	–1.31	2.10	CP05
BD +19 1185	5835	–0.92	–0.68	–0.62	...	...
BD +19 4788	6020	–0.78	–0.43	–0.33	...	...
BD +20 2030	5978	–2.77	–2.24	–2.29	2.16	R96
BD +20 3603	5908	–2.18	–1.72	–1.72	2.22	CP05
BD +21 607	6097	–1.72	–1.44	–1.40	2.14	CP05
BD +22 396	6050	–0.88	–0.60	–0.42	...	...
BD +23 3912	5815	–1.46	–1.18	–0.97	2.51	MN05
BD +24 1676	6125	–2.55	–2.06	–2.11	2.16	CP05
BD +26 2621	6266	–2.69	–2.15	–2.31	2.21	CP05
BD +26 3578	6158	–2.32	...	...	2.25	CP05
BD +28 2137	6110	–1.97	–1.59	–1.67	2.16	CP05
BD +34 2476	6248	–1.94	–1.45	–1.71	2.17	CP05
BD +36 2165	6052	–1.71	–1.39	–1.39	2.42	M10

Table 3—Continued

Star	$T_{\text{eff}}$	[Fe/H]	[Ti/H]	[Mg/H]	A(Li)	Li ref. <sup>1</sup>
BD +36 2964	6152	-2.20	-1.82	-1.90	2.27	R96
BD +37 1458	5492	-2.02	-1.72	-1.54	1.37	CP05
BD +39 2173	6200	-1.99	-1.56	-1.70	2.21	R96
BD +42 3607	5655	-2.29	-2.04	-1.83	2.33	R96
BD +44 1910	5878	-2.64	-2.14	-2.25	...	...
BD +51 1696	5852	-1.21	-1.02	-0.87	1.80	M10
BD +59 2723	5945	-2.20	-1.65	-1.89	2.16	CP05
G 4-37	6120	-2.50	-2.03	-2.11	1.92	CP05
G 5-19	5975	-1.13	-1.02	-0.88	2.26	B05
G 11-44	5820	-2.29	-1.97	-1.90	2.12	CP05
G 20-24	6222	-1.89	-1.42	-1.61	2.35	CP05
G 21-22	5916	-1.02	...	...	2.48	MN05
G 24-3	6000	-1.62	-1.31	-1.24	2.09	CP05
G 24-25	5752	-1.56	-1.33	-1.22	...	...
G 26-12	6135	-2.33	-1.99	-1.95	2.24	B05
G 59-24	6112	-2.32	-1.97	-1.89	2.25	CP05
G 63-46	6125	-0.60	-0.24	-0.15	...	...
G 64-12	6074	-3.45	-2.80	-2.76	2.35	CP05
G 64-37	6122	-3.28	-2.83	-2.71	2.06	MN05
G 74-5	6025	-0.84	-0.53	-0.45	1.48	CP05
G 75-56	5890	-2.38	-1.89	-1.96	2.06	R96
G 88-10	5945	-2.61	-2.09	-2.08	2.13	CP05
G 90-3	5710	-2.28	-2.00	-1.96	2.36	CP05
G 92-6	6115	-2.70	-1.99	-2.36	2.43	MN05
G 108-58	5865	-2.37	-2.10	-2.04	...	...
G 113-9	5998	-1.75	-1.43	-1.26	...	...
G 113-22	5802	-1.01	-0.71	-0.52	...	...
G 115-49	5605	-2.23	-1.99	-1.79	2.09	CP05
G 126-52	6182	-2.36	-1.91	-1.95	2.14	R99
G 130-65	6018	-2.21	-1.86	-1.69	2.15	GD
G 153-21	6142	-0.39	-0.14	+0.02	...	...
G 180-24	6008	-1.44	-1.16	-1.06	2.08	CP05
G 181-28	5965	-2.42	-2.16	-2.10	2.22	R96
G 188-22	5975	-1.35	-1.11	-0.97	...	...

Table 3—Continued

Star	$T_{\text{eff}}$	[Fe/H]	[Ti/H]	[Mg/H]	A(Li)	Li ref. <sup>1</sup>
G 191-55	5828	−1.81	−1.54	−1.49	...	...
G 192-43	6140	−1.42	−1.15	−1.11	2.32	CP05
G 201-5	5950	−2.54	−2.09	−2.13	2.27	MN05
G 206-34	5825	−3.12	−2.65	−2.55	2.27	R96
G 268-32	6230	−2.51	−2.38	−2.18	1.97	CP05
G 275-4	5942	−3.42	−2.84	−2.82	2.21	T94
LP 553-62	6128	−2.73	−2.05	−2.17	1.97	R96
LP 635-14	5932	−2.71	−2.20	−2.21	2.35	M10
LP 651-4	6030	−2.89	−2.24	−2.33	2.18	R99
LP 752-17	5738	−2.38	−1.98	−1.93	...	...
LP 815-43	6405	−2.76	−2.06	−2.45	2.26	M10
LP 831-70	6005	−3.05	−2.53	−2.50	2.28	M10
LTT 1566	6025	−2.36	−1.98	−2.00	2.26	GD
Ross 390	5920	−0.78	−0.55	−0.53	1.15	RD98
Ross 797	5838	−1.17	−1.05	−0.84	2.32	GD

<sup>1</sup>A06 = Asplund et al. (2006), B90 = Balachandran (1990), B05 = Boesgaard et al. (2005), C01 = Chen et al. (2001), CP05 = Charbonnel & Primas (2005) compilation, GD = private communication from G. Dima, M10 = Melendez et al. (2010), MN05 = Novicki (2005), T94 = Thorburn (1994), R88 = Rebolo et al. (1988), R96 = Ryan et al. (1996), R99 = Ryan et al. (1999), RD98 = Ryan & Deliyannis (1998) S07 = Shi et al. (2007).

Table 4. Abundance Uncertainties for Three Representative Stars

Element	Abundance	T: $\pm 100$ K	$\log g$ : $\pm 0.2$	[Fe/H]: $\pm 0.1$	$\xi$ : $\pm 0.2$
BD –10 388: T = 5768 K, $\log g = 3.04$ , [Fe/H] = –2.79, $\xi = 1.54$					
[Fe/H]	–2.79	$\pm 0.07$	$\mp 0.02$	$\mp 0.01$	$\mp 0.02$
[Ti/H]	–2.23	$\pm 0.09$	$\mp 0.01$	0.00	0.00
[Mg/H]	–2.16	$\pm 0.04$	$\mp 0.01$	0.00	$\mp 0.01$
A(Be)	–1.30	$\pm 0.03$	$\pm 0.06$	$\mp 0.01$	0.00
[O/H]	–2.00	$\pm 0.20$	$\mp 0.10$	$\pm 0.01$	0.00
G 188-22: T = 5975 K, $\log g = 3.72$ , [Fe/H] = –1.35, $\xi = 1.31$					
[Fe/H]	–1.35	$\pm 0.06$	$\mp 0.02$	$\mp 0.01$	$\mp 0.05$
[Ti/H]	–1.11	$\pm 0.09$	0.00	0.00	$\mp 0.02$
[Mg/H]	–0.97	$\pm 0.07$	$\mp 0.03$	0.00	$\mp 0.02$
A(Be)	+0.22	$\pm 0.05$	$\pm 0.08$	$\pm 0.01$	$\pm 0.01$
[O/H]	–0.80	$\pm 0.19$	$\mp 0.05$	$\pm 0.01$	$\mp 0.01$
G 20-24: T = 6222 K, $\log g = 4.07$ , [Fe/H] = –1.89, $\xi = 1.14$					
[Fe/H]	–1.89	$\pm 0.06$	$\mp 0.02$	0.00	$\mp 0.03$
[Ti/H]	–1.42	$\pm 0.07$	$\mp 0.01$	0.00	$\mp 0.01$
[Mg/H]	–1.61	$\pm 0.07$	$\mp 0.02$	0.00	$\mp 0.01$
A(Be)	–0.57	$\pm 0.06$	$\pm 0.08$	$\mp 0.01$	0.00
[O/H]	–1.46	$\pm 0.19$	$\mp 0.08$	0.00	0.00

Table 5. Kinematic Properties

Star	Rad.Vel.	$U_{lsr}$	$V_{lsr}$	$W_{lsr}$	$R_{apo}$	$Z_{max}$	ref. <sup>1</sup>	$v_{RF}$	D or A
HD 16031	23.6	−31	−49	−27	8.2	0.3	C	175.9	D
HD 19445	−139.3	−159	−94	−35	11.1	0.4	C	205.9	D
HD 24289	143	140	−90	−9	...	...	RN, Be	190.7	?
HD 30743	−3.0	−25.8	−5.4	−23.6	9.9	...	Bk05	217.4	D
HD 31128	105	−63	−100	−31	8.4	0.4	GC	139.0	D
HD 64090	−240	−265	−178	−84	17.3	2.9	C	281.1	A
HD 74000	204.2	−112	−267	69	9.2	0.9	C	139.7	A,R
HD 76932	120.8	40	−80	77	8.8	0.8	F	164.7	D
HD 84937	−16.7	−139	−117	−3	10.0	0.0	C	173.0	D
HD 94028	61.9	23	−96	29	8.1	0.3	C	129.4	D
HD 104056	−22.8	−68	−1	−37	9.8	0.5	C	232.3	D
HD 106038	95	13	−270	19	8.6	0.6	G	55.0	A,R
HD 108177	159	−111	−184	70	8.8	1.9	C	136.1	D
HD 109303	23.8	20.7	−22.7	34.7	8.79	0.48	N, Bk05,Bo	246.0	D
HD 118244	−11.1	48.8	−5.7	6.8	9.8	...	Ch,So	219.9	D
HD 132475	167	−51	−354	62	8.8	0.6	F	156.2	A,R
HD 134169	18.8	−24	10	20	9.2	0.2	F	232.1	D
HD 140283	7.2	240	−239	48	14.7	0.6	F	245.5	A,R
HD 161770	−129	−54	−273	−1	9.2	0.2	GC	75.7	A,R
HD 179626	−70.8	−58	−162	45	8.0	0.9	C	93.6	D
HD 184499	−163.3	53	−144	39	8.2	0.4	C	100.5	D
HD 188510	−192.2	143	−102	69	6.77	0.87	V,Bo,Re06	128.6	D
HD 194598	−246.3	68	−264	−22	8.9	0.2	F	83.9	A,R
HD 195633	−46.1	63	−26	3	9.4	0.0	F	204.0	D
HD 200580	−6.4	−106	−69.6	16.4	10.5	...	V,So	184.7	D
HD 201889	−102.5	119	−69	−30	10.5	0.3	F	194.6	D
HD 201891	−45.1	−100	−102	−51	9.6	0.5	F	162.9	D
HD 208906	8.4	−63.5	−0.8	−11.4	11.6	...	V,M	228.5	D
HD 218502	−32	−12	−92	1	8.5	0.06	V,G03, Bk05	128.6	D
HD 219617	10.1	−183	−125	−23	11.6	0.3	C	207.5	D
HD 233511	59	108	−191	41	8.8	0.9	C	119.1	A
HD 241253	−16.0	−19	−61	88	8.2	1.8	C	182.7	D
HD 247168	−4	−196	−433	−175	24.1	7.8	C	338.2	A,R
HD 247297	38.3	18	−31	−5	8.1	0.1	C	189.9	D



Table 5—Continued

Star	Rad.Vel.	$U_{lsr}$	$V_{lsr}$	$W_{lsr}$	$R_{apo}$	$Z_{max}$	ref. <sup>1</sup>	$v_{RF}$	D or A
CD –24 1656	66	–73	–188	–27	...	...	RN,Sc	84.2	A
BD –17 484	234.7	226	–189	–134	...	...	Eg	264.6	A
BD –14 5850	0.0	–140	–136	71.8	14.6	...	Bo,IDL	178.4	D
BD –13 3442	159	–246	–102	21	...	...	RN	273.6	?
BD –10 388	36.2	100	–24	8	10.2	0.1	C	220.2	D
BD –9 466	–164	–193	–226	90	...	...	RN	213.0	A,R
BD –8 4501	91	–136	–16	–136	14.2	4.2	C	280.4	D
BD –4 3208	56	38	–146	–23	8.1	0.2	C	86.3	D
BD –3 2525	25	–246	–192	48	14.6	2.6	C	252.2	A
BD –1 306	19.2	166	–157	53	10.8	0.7	C	185.3	D
BD +1 2341p	–59	–234	–168	–112	15.5	3.6	C	264.6	A
BD +2 263	–12.5	67	–36	45	9.0	0.6	C	200.9	D
BD +2 3375	–397.8	375	–208	14	21.7	3.2	C	375.5	A
BD +2 4651	–253	140	–264	98	...	...	RN,Bo	176.5	A,R
BD +3 740	173.9	131	–110	–36	9.9	0.4	C	174.8	D
BD +4 302	–70	65	–201	53	...	...	RN	86.0	A
BD +4 4551	–119.2	–75	–46	76	10.3	...	Sc,IDL,Ka	204.1	D
BD +7 4841	–234.8	115	–225	49	8.6	2.1	C	125.1	A,R
BD +9 2190	266.1	–67	–319	193	9.5	6.5	C	227.0	A,R
BD +13 3683	101.2	136	7	–10	13.9	0.1	GC	264.8	D
BD +17 4708	–291.3	178	–248	80	11.1	2.2	C	197.2	A,R
BD +19 1185	–190	–227	–115	64	14.8	1.2	C	258.2	D
BD +19 4788	–87	–83	–102	12	8.7	0.1	C	144.8	D
BD +20 2030	–65.7	–169	–229	–42	10.4	1.5	C	174.4	A,R
BD +20 3603	–242.7	37	–273	–49	8.0	1.0	C	81.1	A,R
BD +21 607	339	349	–130	–76	30.9	1.8	F	368.3	A
BD +22 396	–22.4	–55	–93	–84	8.5	1.6	C	161.9	D
BD +23 3912	–115.2	21	–92	107	8.6	1.4	F,Ka	168.1	D
BD +24 1676	–238.6	–283	–92	–39	21.4	1.3	C	313.0	A
BD +26 2621	–63	–63	–201	–18	7.7	1.3	C	68.2	A
BD +26 3578	–129.1	–40	–143	–57	8.6	0.5	F	103.8	D
BD +28 2137	–132.5	–132	–426	–148	8.6	7.2	GC	285.9	A,R
BD +34 2476	–162	–146	–130	–153	11.7	4.8	C	229.8	D
BD +36 2165	–198	–184	–156	–139	12.8	5.2	C	239.3	D

Table 5—Continued

Star	Rad.Vel.	$U_{lsr}$	$V_{lsr}$	$W_{lsr}$	$R_{apo}$	$Z_{max}$	ref. <sup>1</sup>	$v_{RF}$	D or A
BD +36 2964	−60.5	−81	−96	1	8.7	0.0	C	148.1	D
BD +37 1458	242.2	264	−251	−28	17.0	0.3	F	267.3	A,R
BD +39 2173	−79.5	−117	−183	−6	9.3	0.1	C	122.9	D
BD +42 3607	−196.1	147	−156	19	10.0	0.2	C	161.5	D
BD +44 1910	−86	74	−211	−40	8.8	0.6	APS	84.6	A
BD +51 1696	64.3	202	−234	61	11.8	2.6	C	211.5	A
BD +59 2723	−105.8	157	−168	−42	10.1	1.4	C	170.6	D
G 4-37	−108.4	−170	−87	−21	11.8	0.3	C	216.9	D
G 5-19	−216.7	−254	−169	4	15.6	0.1	C	259.1	A
G 11-44	98.4	−135	−266	−42	9.7	0.3	C	148.7	A,R
G 20-24	34.4	−122	−129	56	9.4	0.8	C	162.2	D
G 21-22	59.4	−232	−228	−26	12.4	4.8	C	233.6	A,R
G 24-3	−208.9	53	−201	75	7.9	1.8	C	93.8	A
G 24-25	−307.2	191	−225	61	11.2	1.9	C	201	D
G 26-12	−239.3	299	−164	−39	19.9	10.87	V, Sc, Bk05	306.7	A
G 59-24	−57	217	−234	−109	13.8	3.2	C	243.2	A,R
G 63-46	−24.8	−77	−24	−44	9.4	0.6	C	215.1	D
G 64-12	442.5	−77	−272	398	44.7	25.0	C	408.7	A,R
G 64-37	91	−165	−252	−86	10.6	1.7	C	188.8	A,R
G 74-5	24.2	46	−45	−32	8.4	0.3	C	183.8	D
G 75-56	23.8	−62	−246	−47	8.0	1.5	C	82.0	A,R
G 88-10	83	56	−218	−69	8.0	2.3	C,Be	88.9	A
G 90-3	29.1	19	−86	−13	8.1	0.1	C	136.0	D
G 92-6	49.2	−173	−97	65	11.6	11.6	C	222.0	D
G 108-58	143.0	8	−209	−61	7.9	1.2	C	62.5	A
G 113-9	191	−31	−291	−2	...	...	RN	77.5	A,R
G 113-22	53.8	−29	−63	59	8.2	0.9	C	170.2	D
G 115-49	−51	−81	−308	−36	8.7	0.4	C	124.9	A,R
G 126-52	−241.9	−79	−290	−8	8.5	0.1	C	105.9	A,R
G 130-65	−271.0	−143	−300	14	10.1	0.2	C	164.5	A,R
G 153-21	−64.3	72	−28	21	9.1	0.2	C	206.1	D
G 180-24	−157	−64	−192	−46	7.9	1.3	C	83.6	A
G 181-28	−169.8	12	−263	60	8.0	0.5	C	74.8	A,R
G 188-22	−94.9	−112	−86	63	9.6	1.0	C	185.7	D

Table 5—Continued

Star	Rad.Vel.	$U_{lsr}$	$V_{lsr}$	$W_{lsr}$	$R_{apo}$	$Z_{max}$	ref. <sup>1</sup>	$v_{RF}$	D or A
G 191-55	–258.2	–224	–168	16	13.4	0.2	C	230.5	D
G 192-43	189	265	–128	29	17.5	0.3	C	282.0	A
G 201-5	–35.7	–262	–51	28	20.6	0.9	C	313.0	A
G 206-34	–72	–140	–144	–89	9.9	2.0	C	182.5	D
G 268-32	80.8	194	–241	156	...	...	Sc	249.8	A,R
G 275-4	135	114	–293	–261	...	...	RN,Sc	294.0	A,R
LP 553-62	177	–1	–314	35	...	...	RN,Sc	100.3	A,R
LP 635-14	–106	–83	–211	41	...	...	RN	93.0	A
LP 651-4	34	–157	–211	–138	...	...	RN,Sc	209.2	A
LP 752-17	–225	73	–382	25	...	...	RN,Sc	179.4	A,R
LP 815-43	15	–128	–195	13	...	...	RN,Sc	131.1	A
LP 831-70	–33	–16	–175	100	6.5	...	RN,Sc	110.8	D
LTT 1566	154	13	–336	–123	...	...	RN	169.6	A,R
Ross 390	89	–152	–228	52	...	...	RN	160.8	A,R
Ross 797	12	–260	–262	–81	...	...	RN	275.5	A,R

<sup>1</sup>APS = Allen et al. (1991), Bk04 = Borkova et al. (2004), Bk05 = Borkova et al. (2005), Bo = Bobylev et al. (2006), C = Carney et al. (1994), Ch = Chen et al. (2000), Eg = Eggen (1996), F = Fulbright (2002), GC = Geneva-Copenhagen (Nordstrom et al. (2004) as recalibrated Holmberg et al. (2007), Gr03 = Gratton et al. (2003), M = Mishenina et al. (2004), N = Nissen et al. (2000), R06 = Reddy et al. (2006), RN = Ryan & Norris (1991), Sc = Schuster et al. (2006), So = Soubiran & Girard (2005), V = Venn et al. (2004),

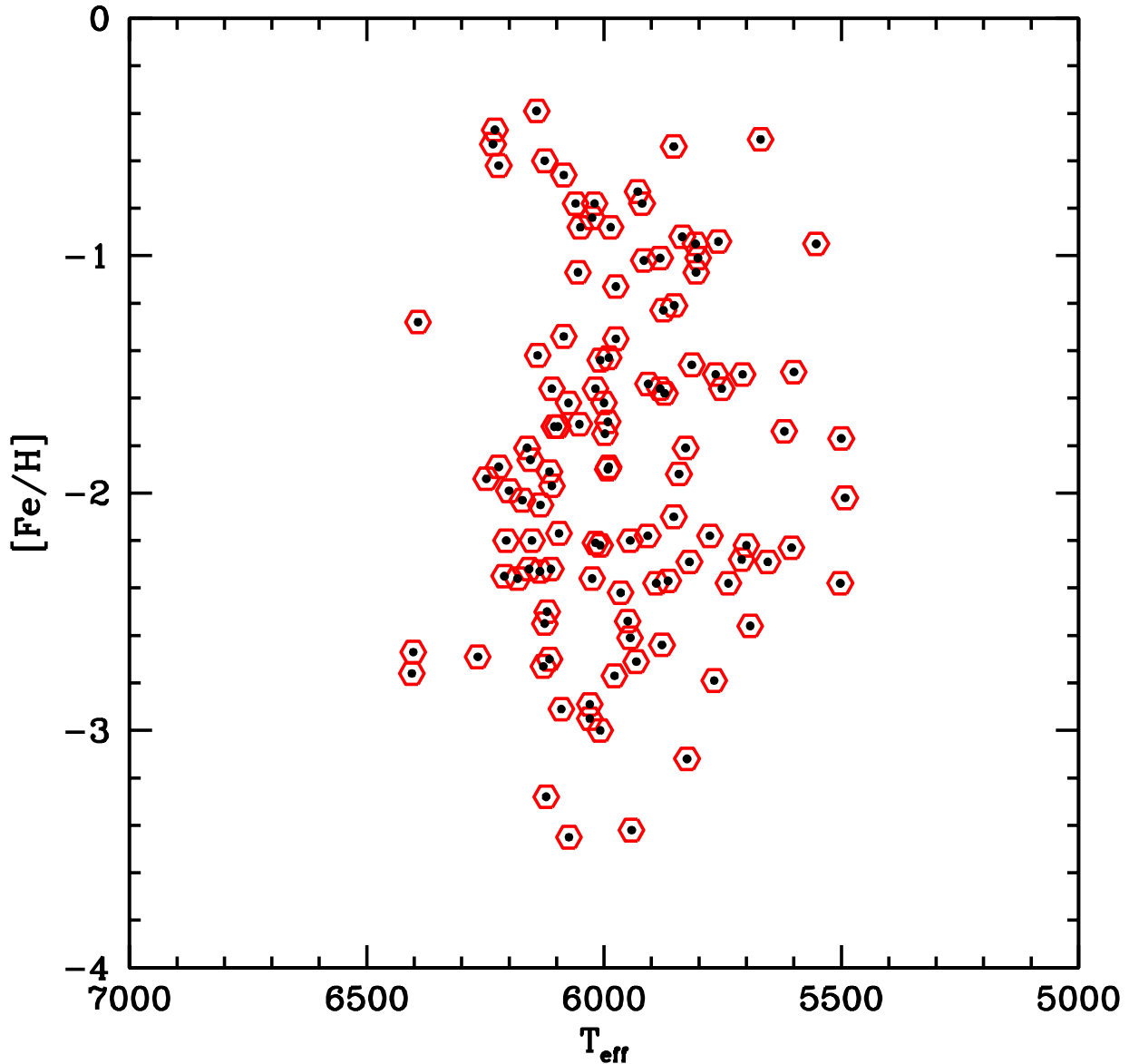


Fig. 1.— Distribution of our sample of stars in the  $T_{\text{eff}} - [\text{Fe}/\text{H}]$  plane. Our stars cover more than 3 orders of magnitude in  $[\text{Fe}/\text{H}]$ . We set a limit on  $T_{\text{eff}}$  of  $> 5500$  K due to the growing weakness of the Be II lines and increasing strengths of the blending features below that temperature. There are six stars with  $[\text{Fe}/\text{H}] \leq -3.0$ . The parameters plotted are those derived in section 3.

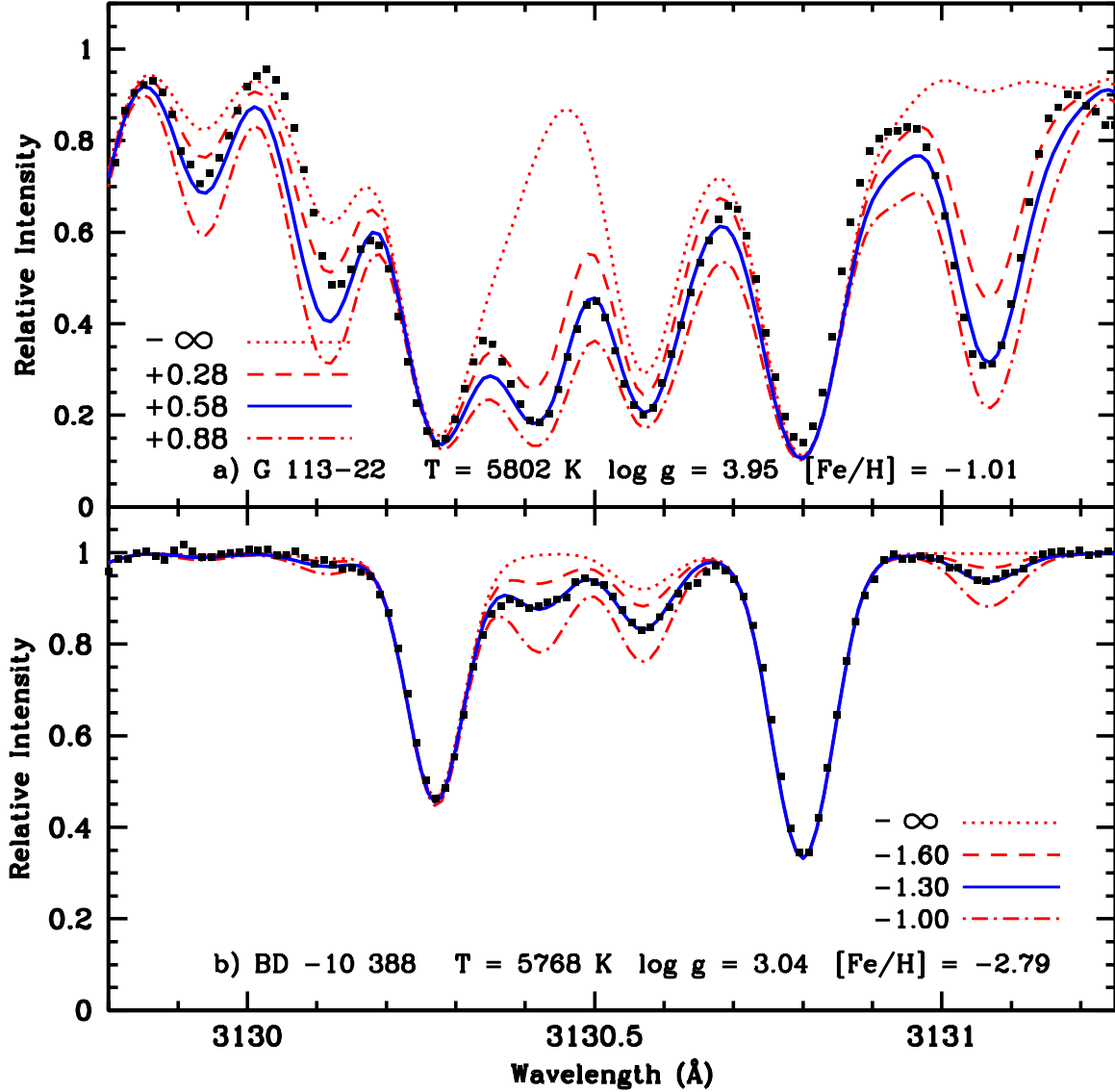


Fig. 2.— Spectrum synthesis in the Be region of stars with similar  $T_{\text{eff}}$  but very different metallicities. The Be II lines are at 3130.421 and 3131.065 Å. The filled squares are the observational data points and the solid line is the best fit. The dotted line contains no Be. The dashed and dot-dash lines are a factor of two lower and higher in Be abundance. For G 113-22, with a value for  $[\text{Fe}/\text{H}]$  of  $-1.01$ , the spectrum is full of line blends and has strong lines. For BD  $-10^\circ$  388 at  $[\text{Fe}/\text{H}] = -2.79$  the synthesis is much more straight-forward and both the Be II lines and the OH features are well-fit. In this example the solid line is also for the best fit for OH and the other syntheses differ in  $[\text{O}/\text{H}]$  by 0.20 dex. The best fit for this OH feature gives  $[\text{O}/\text{H}]$  of  $-0.53$  in G 113-22 and  $-2.00$  in BD  $-10^\circ$  388. It is clearly easier to derive good Be abundances in metal-poor stars.

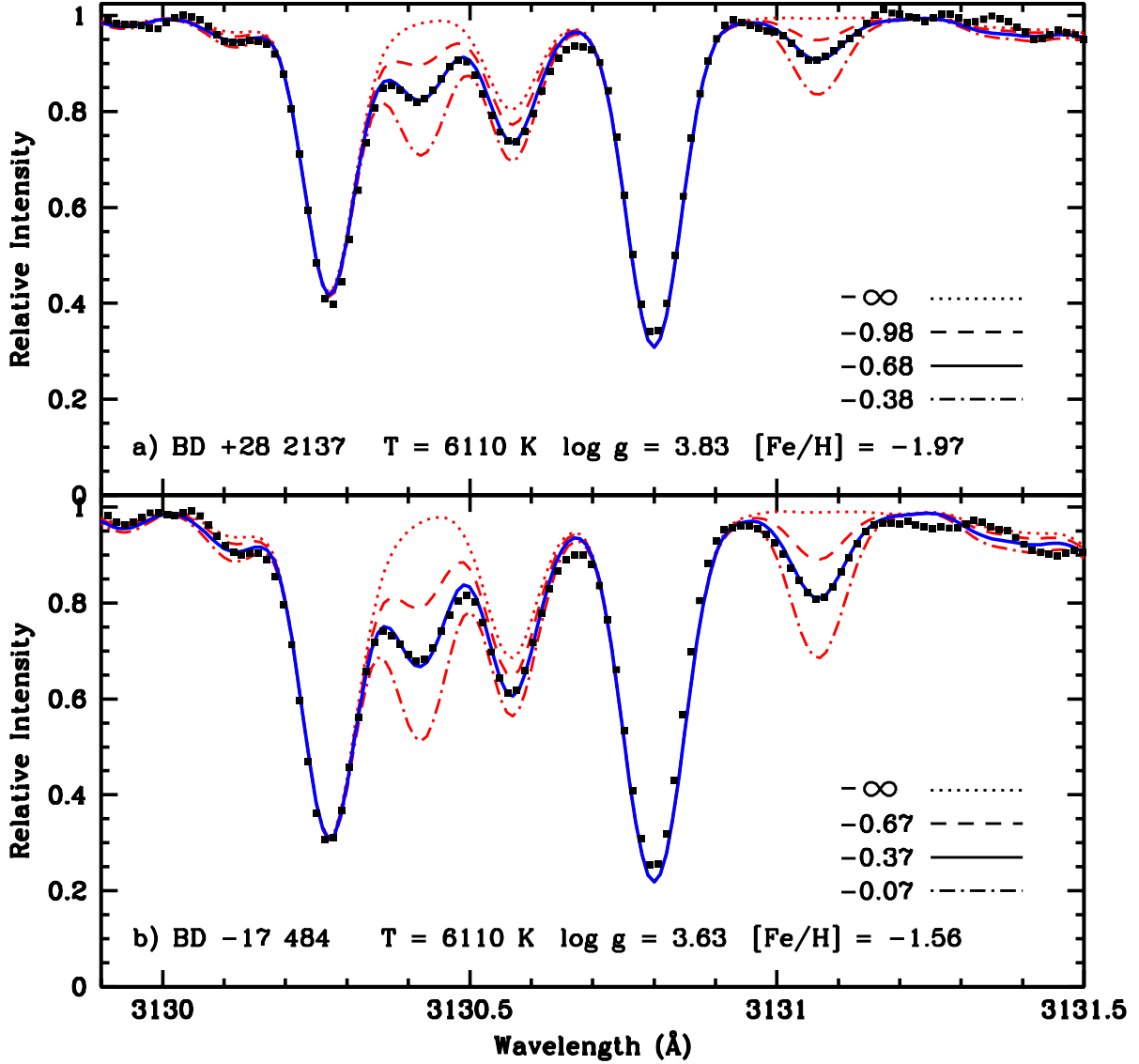


Fig. 3.— Spectrum synthesis in the Be region of two stars with the same  $T_{\text{eff}}$ . The metallicities differ by a factor of 2.6 and the Be abundances by a factor of 2.0. The lower metallicity star has the lower Be abundance. The points and the lines are as in Figure 2, but the O abundances differ by 0.10 dex in this figure. The best fit for this OH feature gives  $[\text{O}/\text{H}]$  of  $-1.37$  in BD +28° 2137 and  $-0.98$  in BD -17° 484.

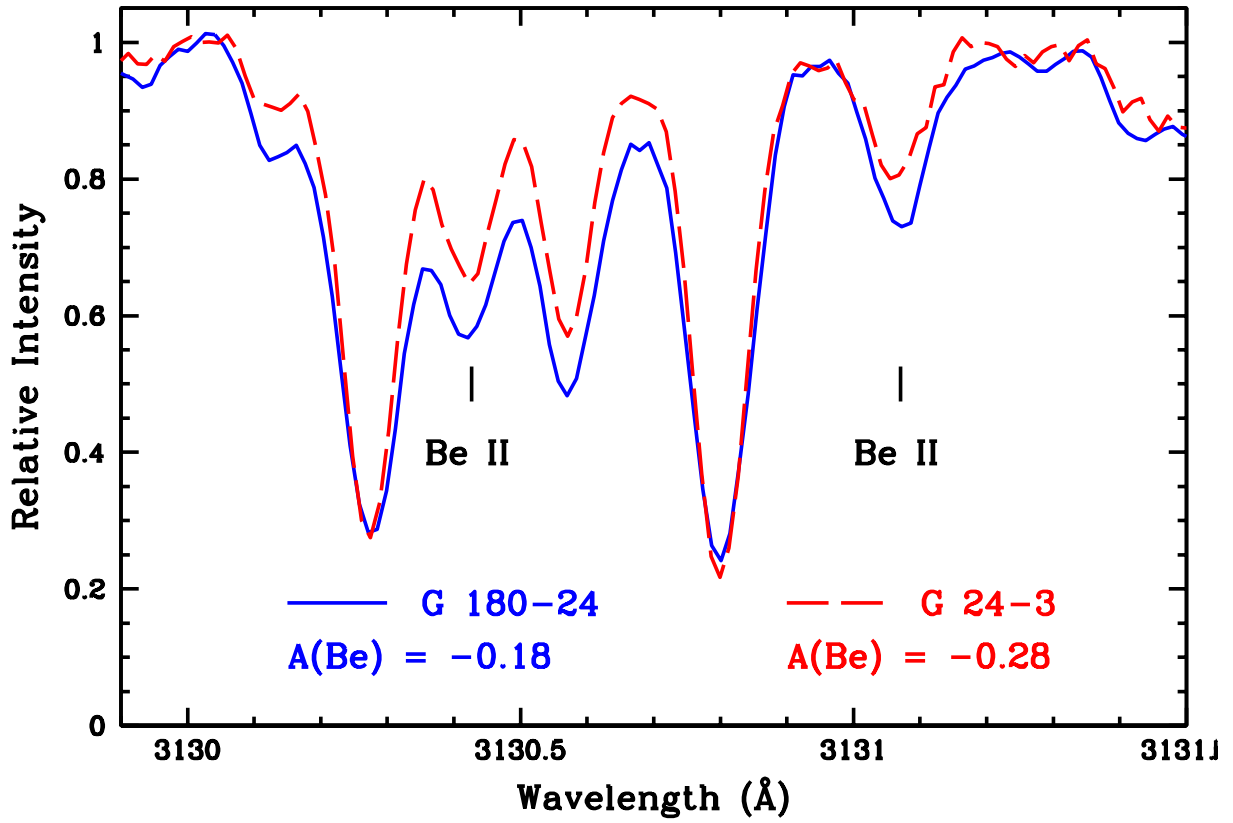


Fig. 4.— The observed spectra of two similar stars. The star with the broader lines and the stronger Be lines, G 180-24, has a lower  $\log g$  by 0.21 dex. This comparison shows the effect of  $\log g$  on  $A(\text{Be})$ : the Be II lines are stronger for a given Be abundance in subgiants than in dwarf stars with similar parameters.

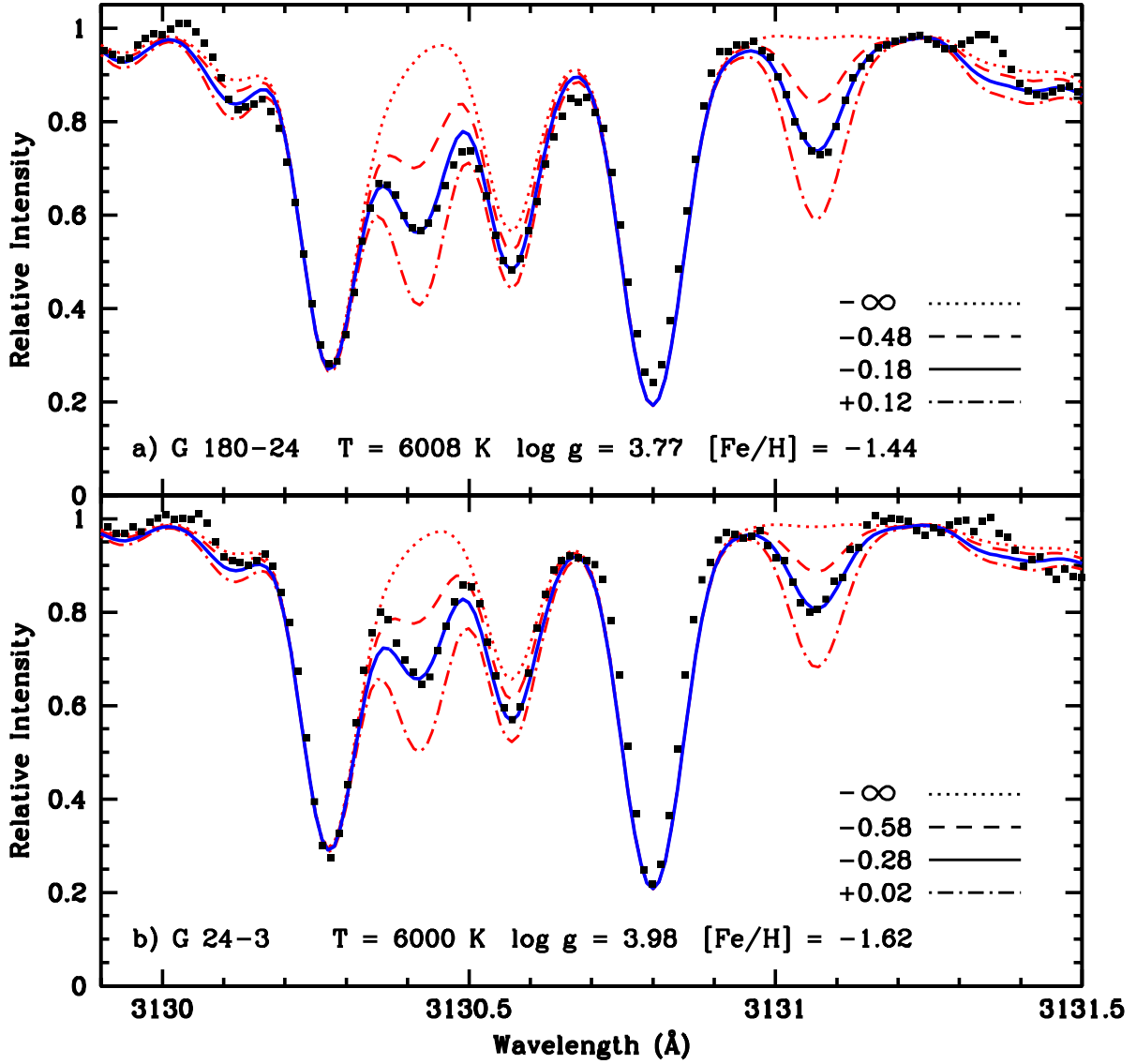


Fig. 5.— The spectrum syntheses for the two stars in Figure 4. The best fit to the data points is the solid line. The dotted line contains no Be. The dashed and dot-dash lines are a factor of two lower and higher in Be abundance. The solid line is also for the best fit for OH and the other syntheses differ in  $[\text{O}/\text{H}]$  by 0.10 dex, with the best fit for this OH feature of  $[\text{O}/\text{H}] = -0.92$  in G 180-24 and  $-1.20$  in G 24-3.



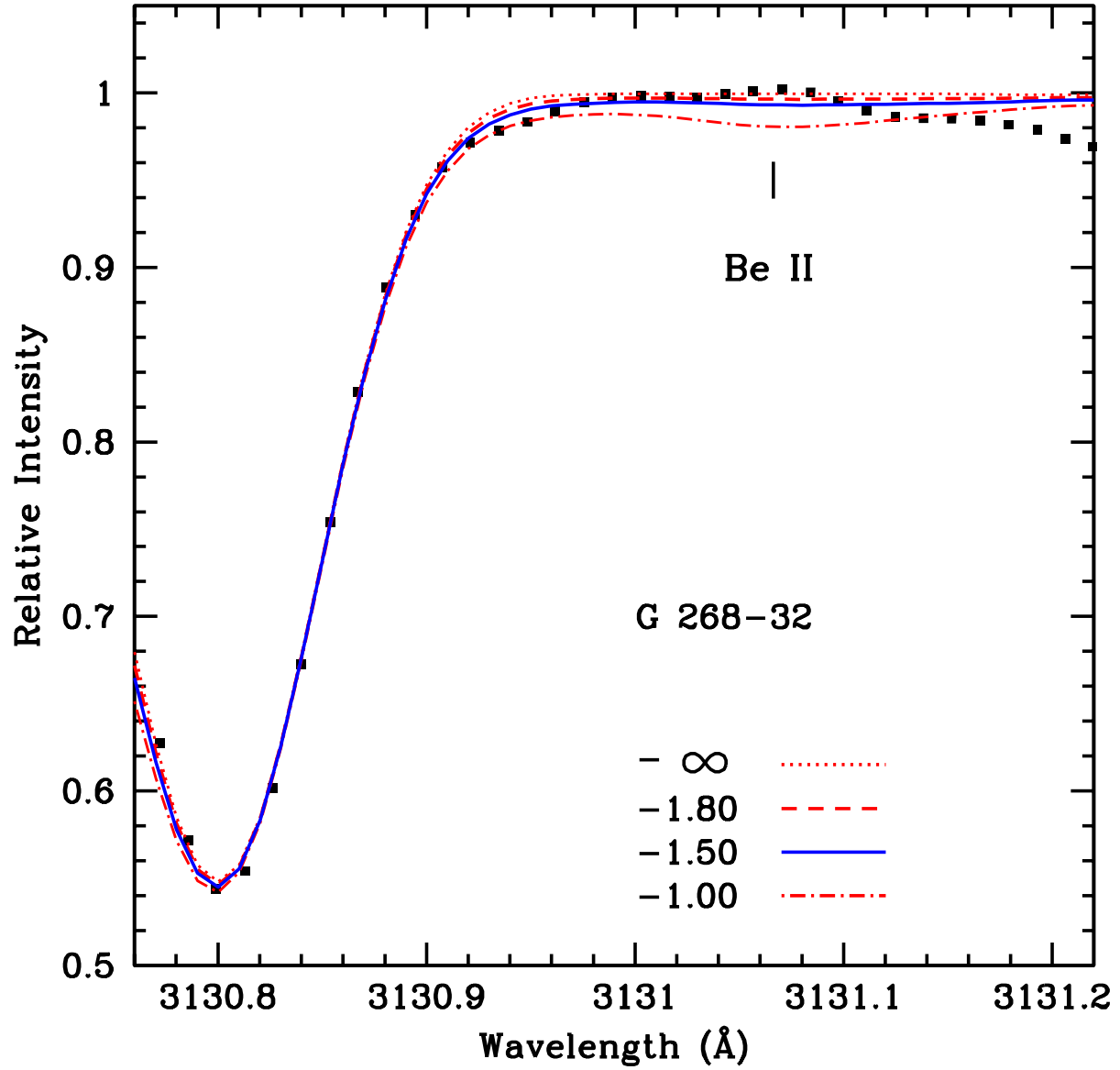


Fig. 6.— An expanded view of the 3131 Å line of the Be II in the CEMP star, G 268-32. The CH lines were removed from the line list in order to get an upper limit for  $A(\text{Be})$ . The feature at 3130.8, mostly Ti II, is well-fit.

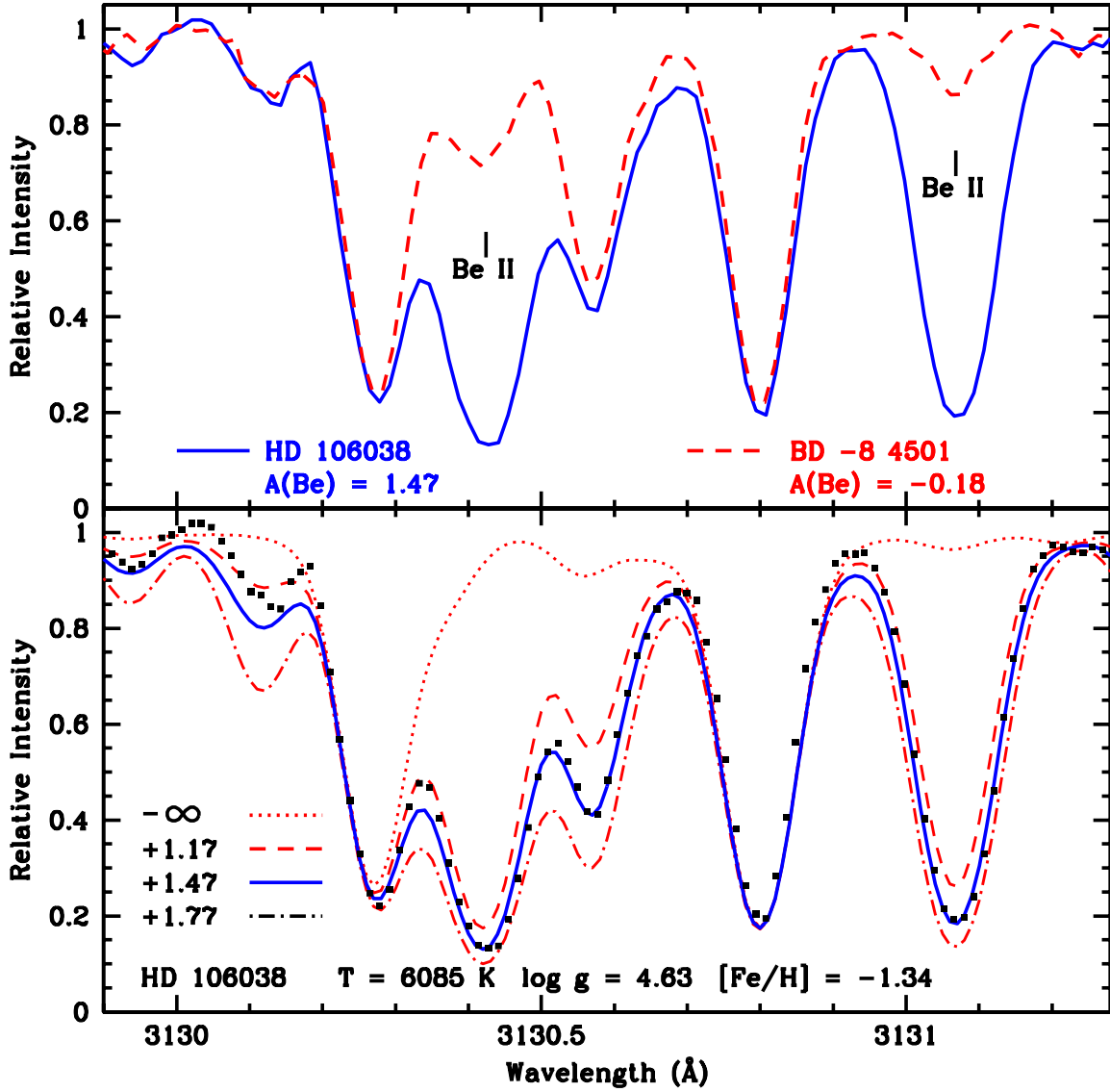


Fig. 7.— Top panel: Our Keck spectrum of the Be-rich star, HD 106038 discovered by Smiljanic et al (2008) compared to BD  $-8^\circ$  4801, a star of similar metallicity ( $[\text{Fe}/\text{H}] = -1.23$ ) and  $\log g$  (4.39). Lower panel: The spectrum synthesis for HD 106038 with our spectroscopically determined parameters. The solid line is the best fit with  $A(\text{Be}) = 1.47$  and  $[\text{O}/\text{H}] = -0.95$ .

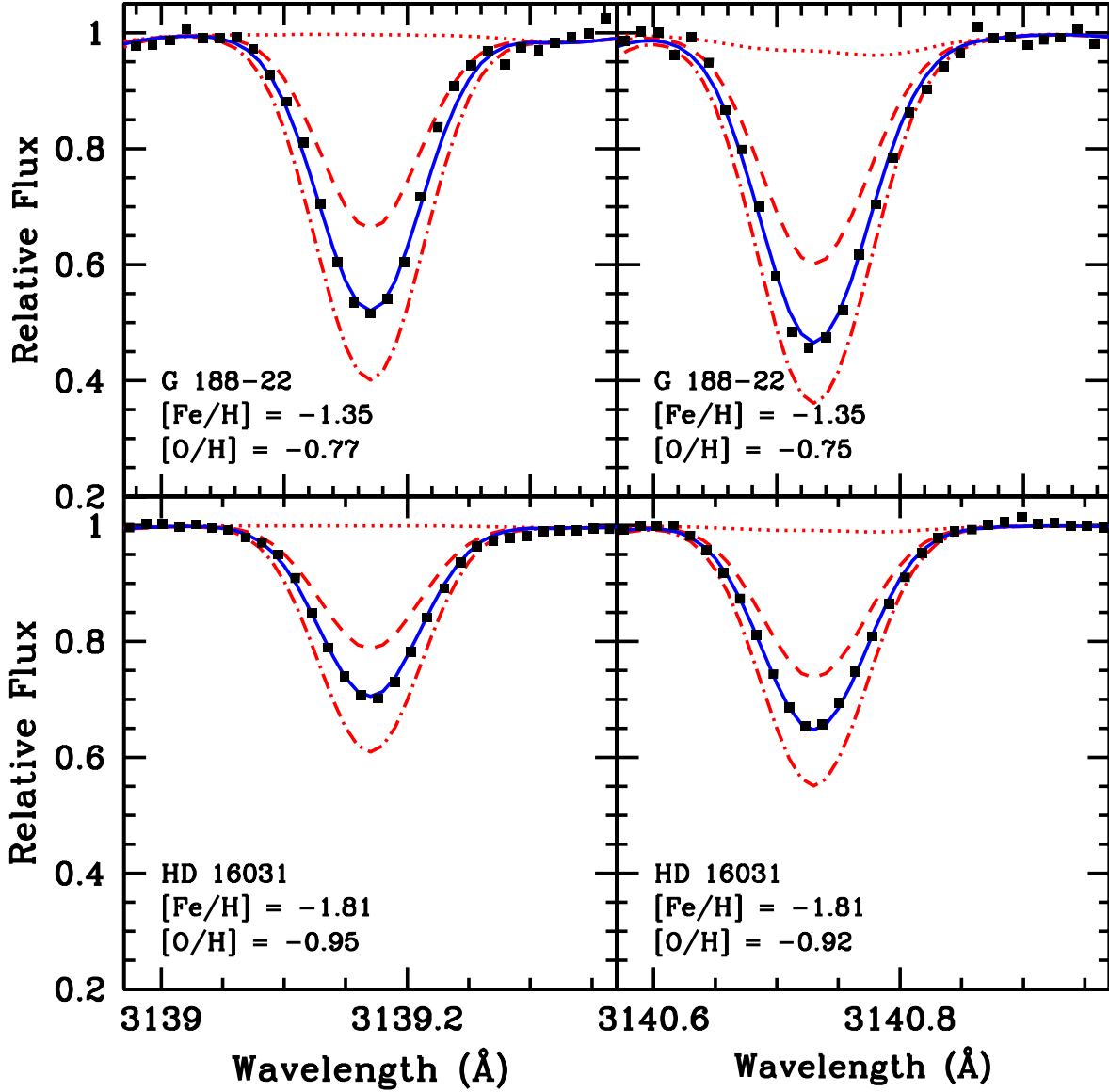


Fig. 8.— Spectrum syntheses for the other two OH features used to find O abundances in two of our stars. The observations are the solid squares and the solid line is the best fit O abundance. The dotted line corresponds to no oxygen. The dashed and dot-dash lines are 0.2 dex less and 0.2 dex more O. The final  $[O/H]$  abundance for G 188-22 is  $-0.78$  and for HD 16031 is  $-0.97$ , showing good agreement among the three features.

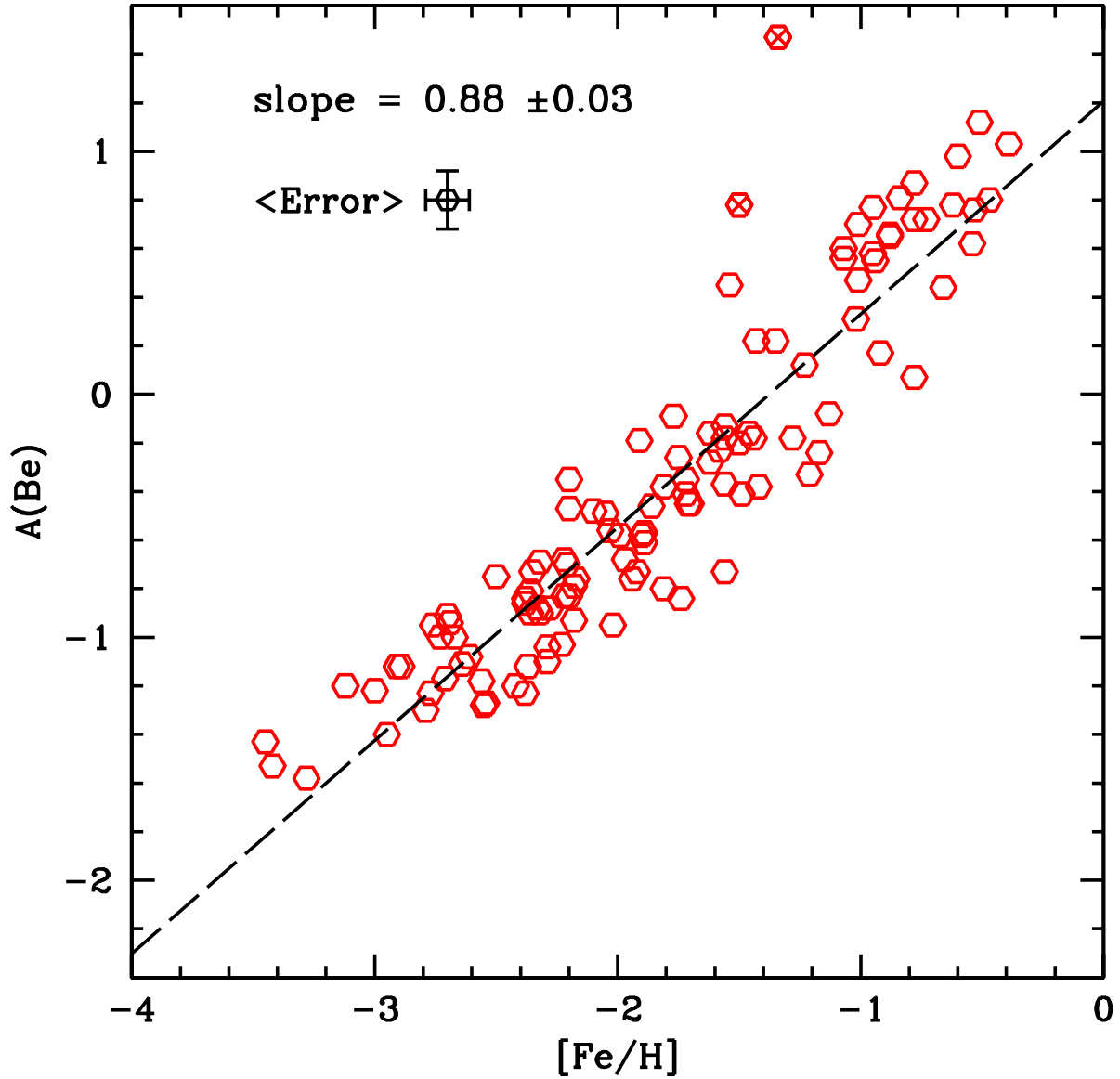


Fig. 9.— Our Be abundances for the stars in Table 2 plotted against our derived Fe abundances. The slope of +0.89 was calculated excluding the two points that are indicated by a cross within the hexagon. Those two high points are the Be-rich stars, HD 106038 and HD 132475. The mean  $1\sigma$  error bar is shown in the upper left in this figure and in subsequent figures.

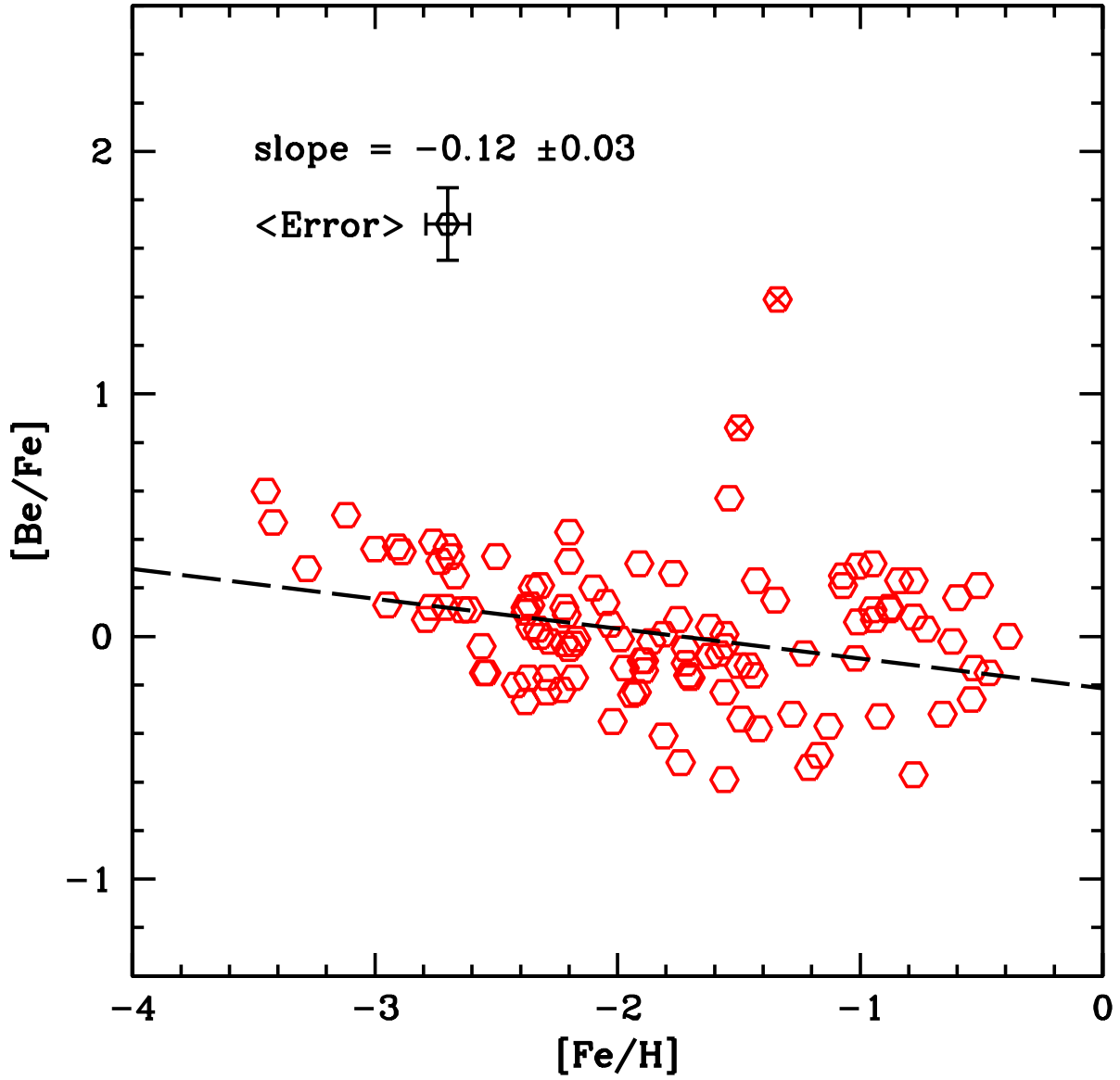


Fig. 10.— This plot shows Be values as normalized to the Fe values compared to Fe. Again the two Be-rich stars were not used in the calculation of the slope and are indicated by a cross within the hexagon.

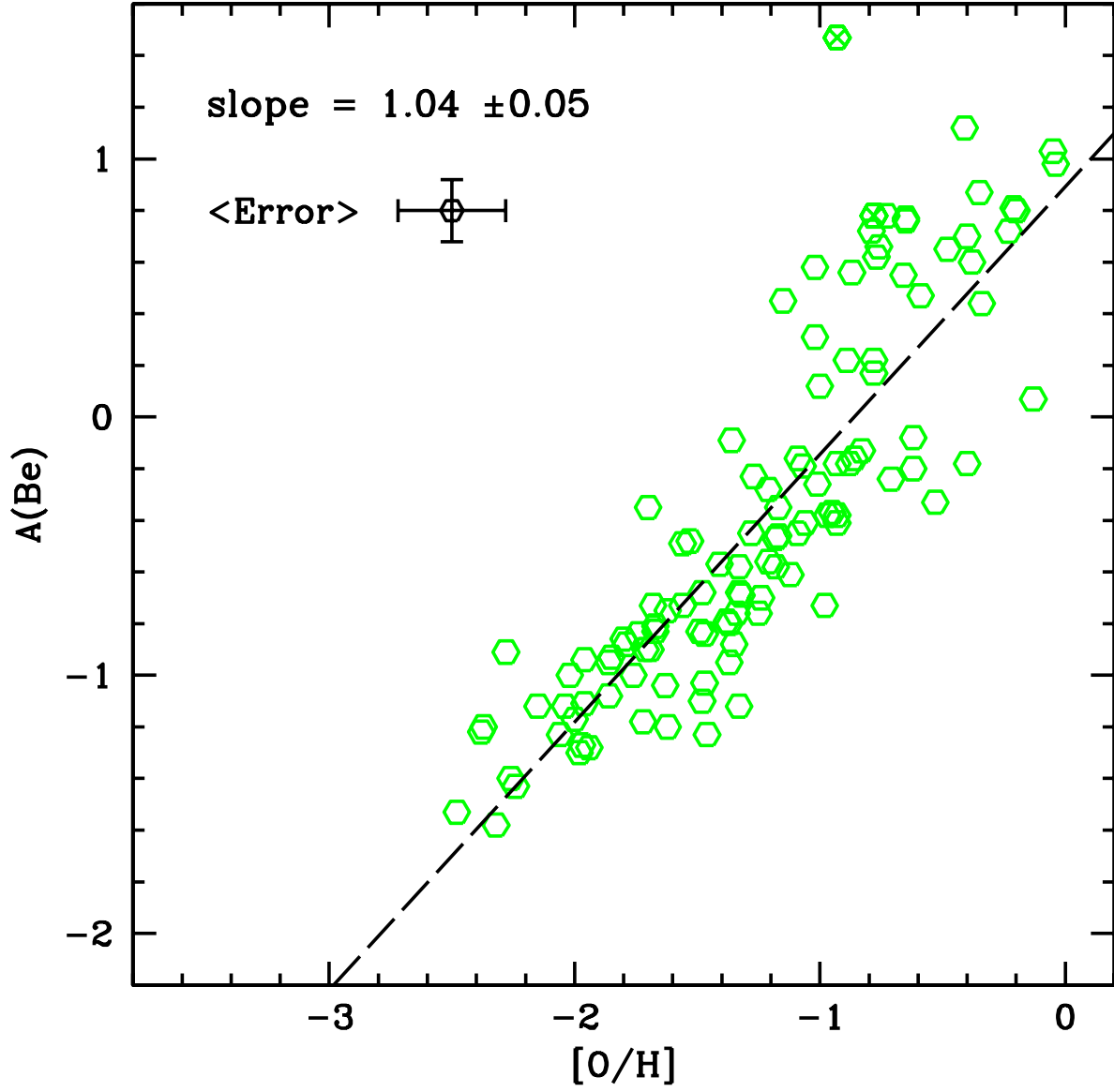


Fig. 11.— Our Be abundances for the stars in Table 2 plotted against our derived O abundances. Both the Be-rich and the Be-poor stars lie above the best fitting straight line indicating that a polynomial fit might be better.

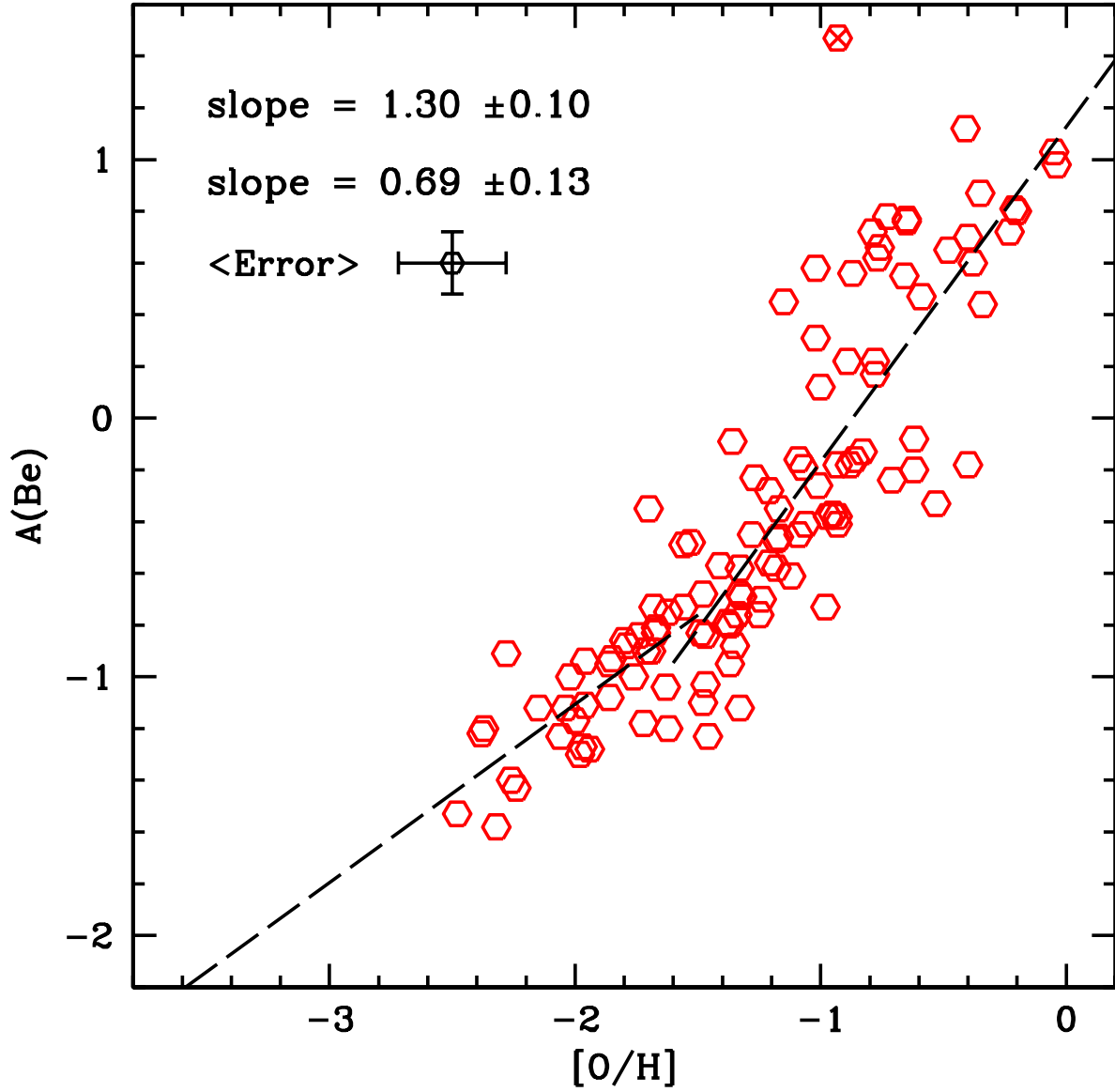


Fig. 12.— A fit for the  $A(\text{Be})$  with  $[\text{O}/\text{H}]$  with 2 lines. We have separated the stars into high-O and low-O groups. See the text in §4.2 for discussion.

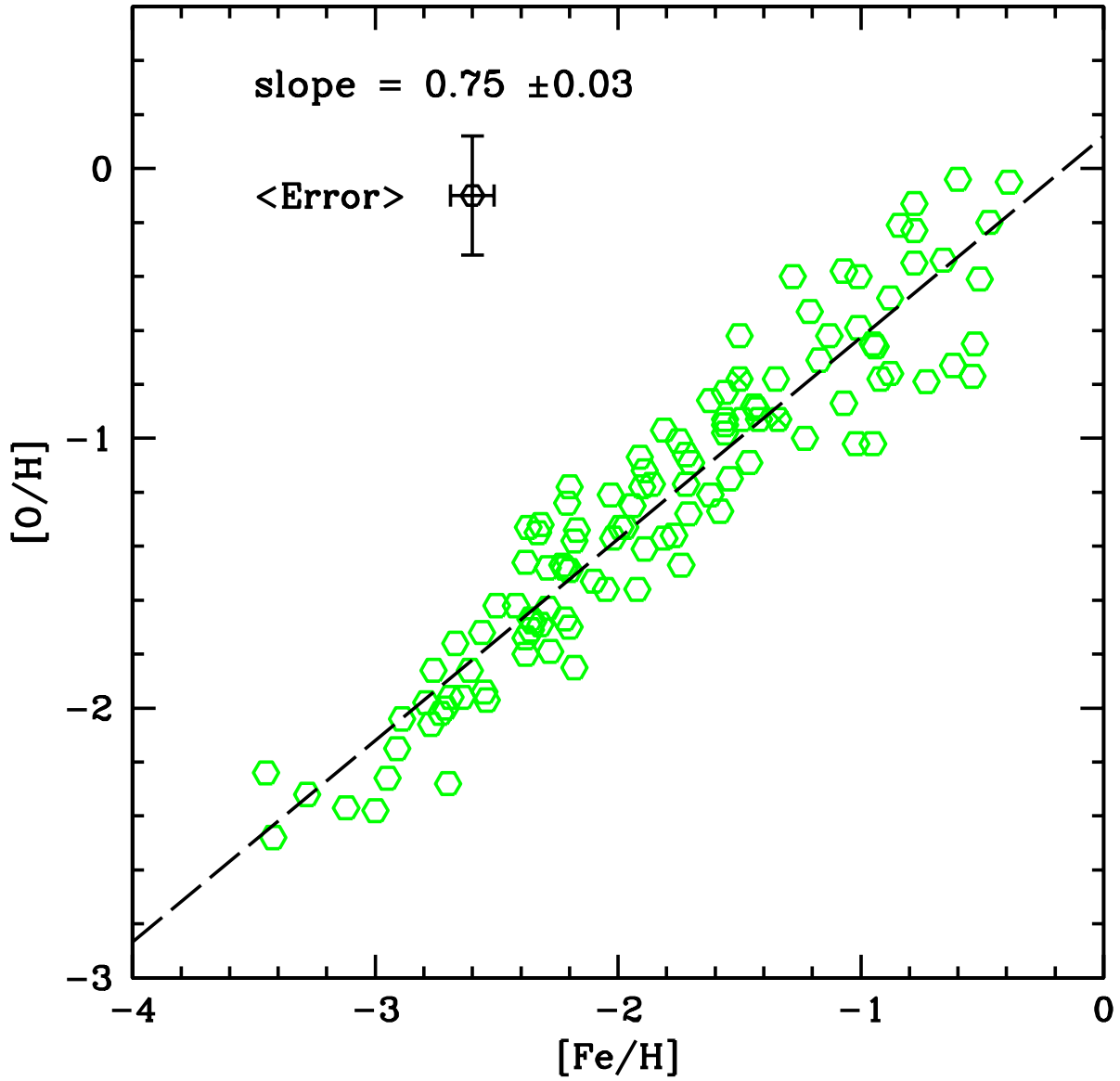


Fig. 13.— The relationship between  $[O/H]$  and  $[Fe/H]$ . This shows a good linear fit with smaller scatter than in the  $A(\text{Be})$  vs.  $[Fe/H]$  plot in Figure 11. This in turn implies that the slope change in Figure 12 is due to Be, not O, even though the  $1\sigma$  error bar is larger for  $[O/H]$  than for  $A(\text{Be})$ .



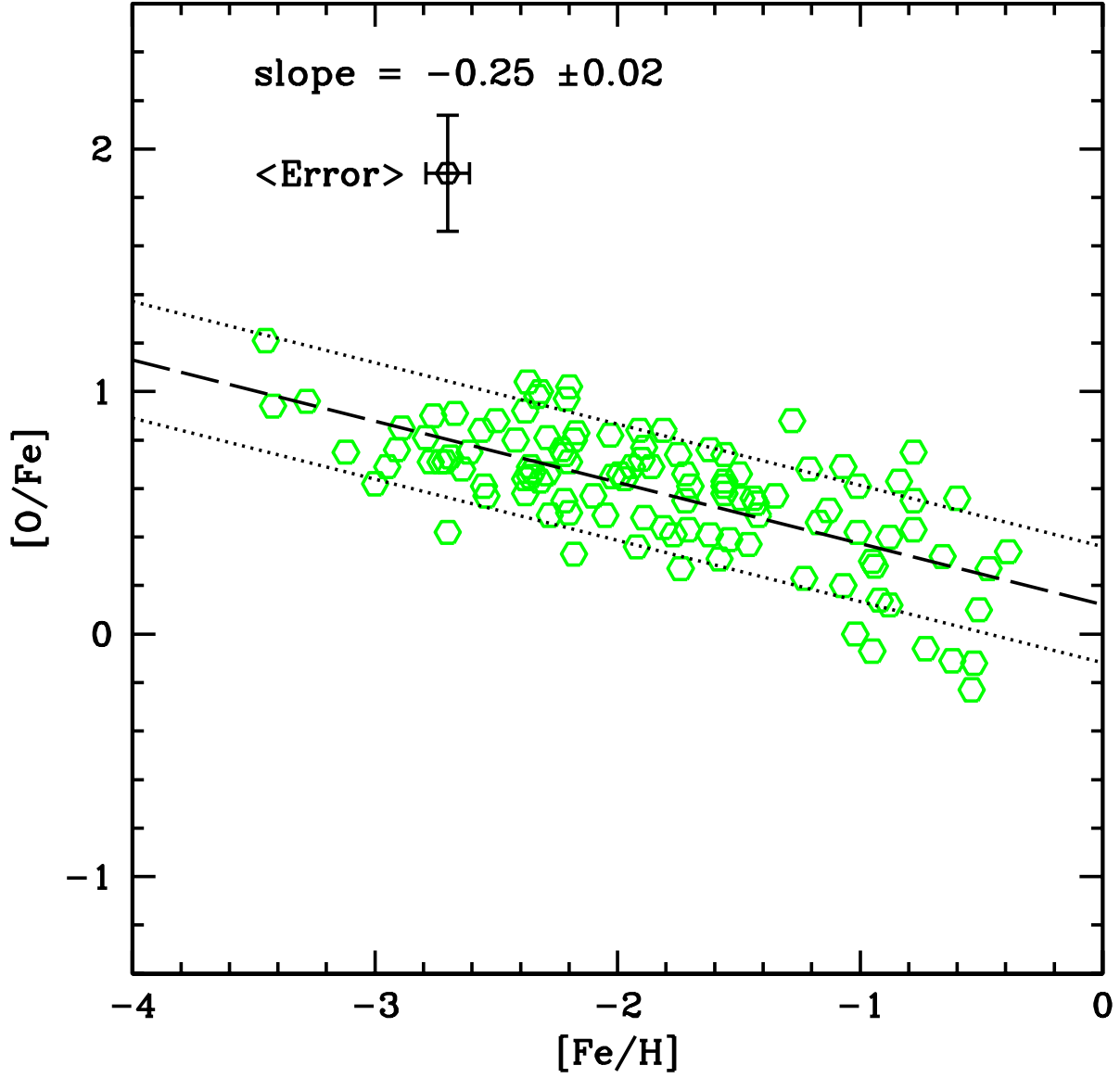


Fig. 14.— Oxygen as normalized to Fe vs. Fe. The  $1\sigma$  error bars due to  $[O/Fe]$  are drawn parallel to the best fit. There is more scatter in  $[O/Fe]$  for values of  $[Fe/H] > -1.4$ .

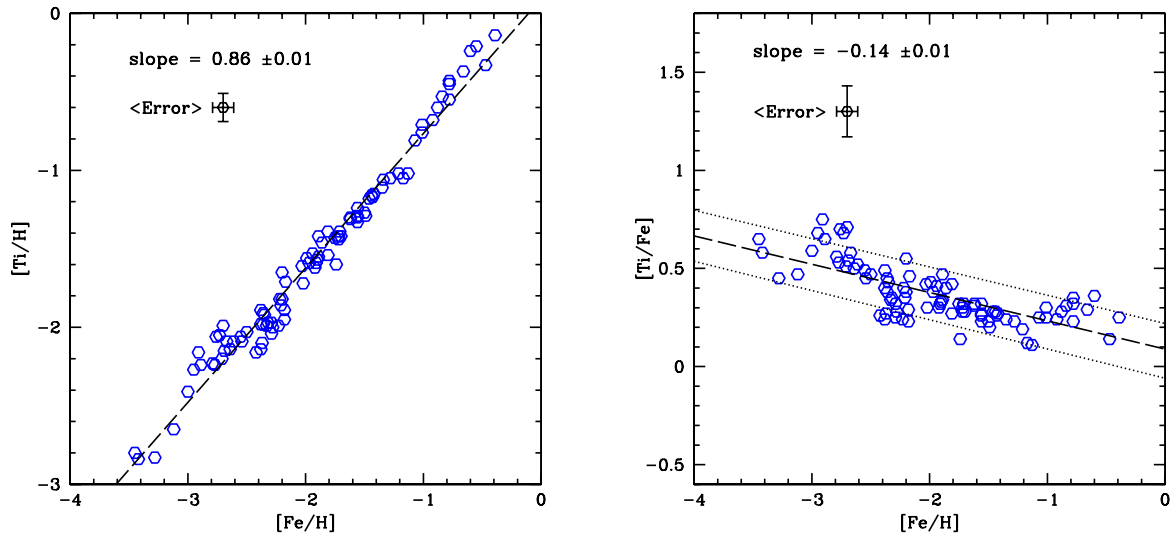


Fig. 15.— These plots are the analogs of Figures 13 and 14 for Ti instead of O. The correlation between  $[\text{Ti}/\text{H}]$  and  $[\text{Fe}/\text{H}]$  is remarkably tight.

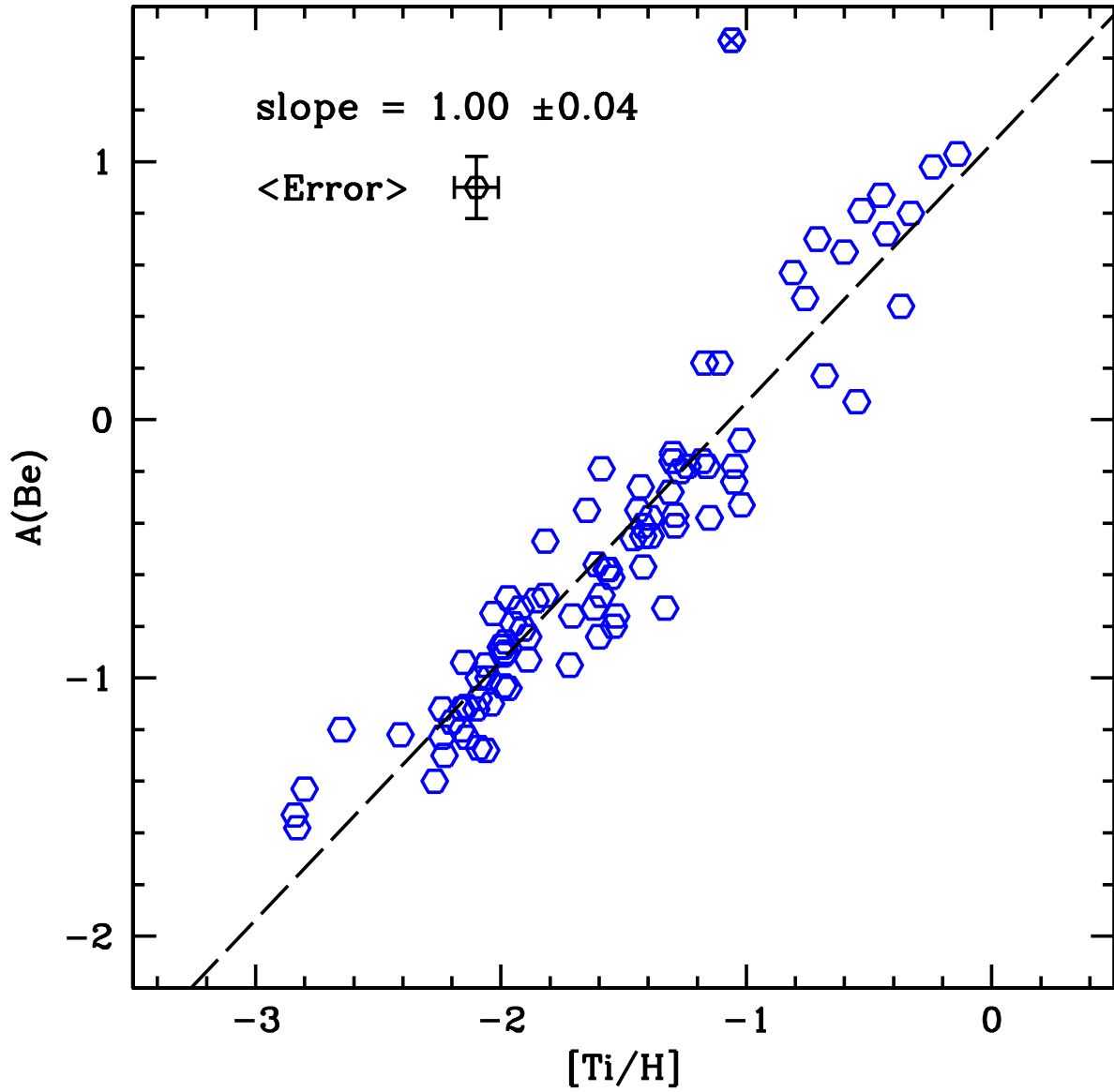


Fig. 16.— The relationship between the alpha-element, Ti, with Be. This correlation is considerably tighter than Be and O in Figure 11. The Be-rich star, HD 106038 is the hexagon with the cross in it and was not used to find the slope. (We do not have a Ti abundance for the other Be-rich star.)

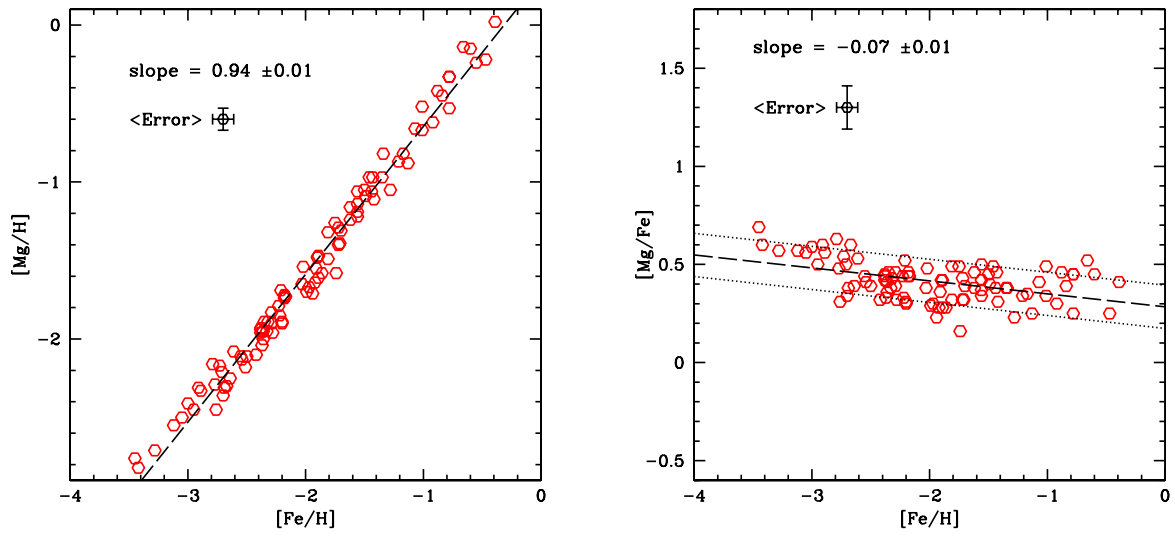


Fig. 17.— These plots are the analogs of Figures 13 and 14 for Mg instead of O. There is a very tight correlation between  $[Mg/H]$  and  $[Fe/H]$ .

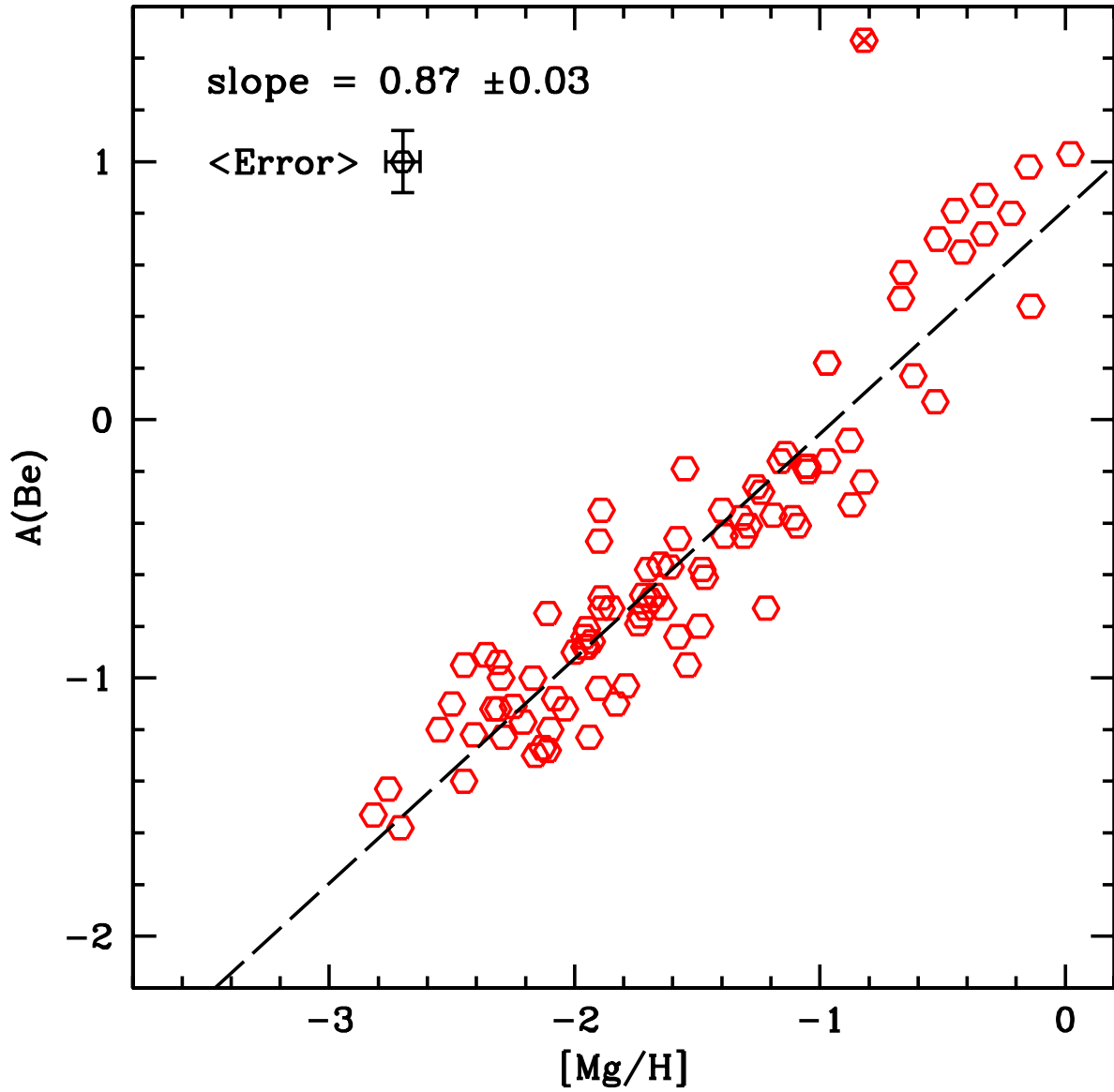


Fig. 18.— The relationship between the alpha-element, Mg, with Be. This correlation is considerably tighter than Be and O in Figure 11. The Be-rich star, HD 106038 is the hexagon with the cross in it and was not used to find the slope. (We do not have a Mg abundance for the other Be-rich star.)

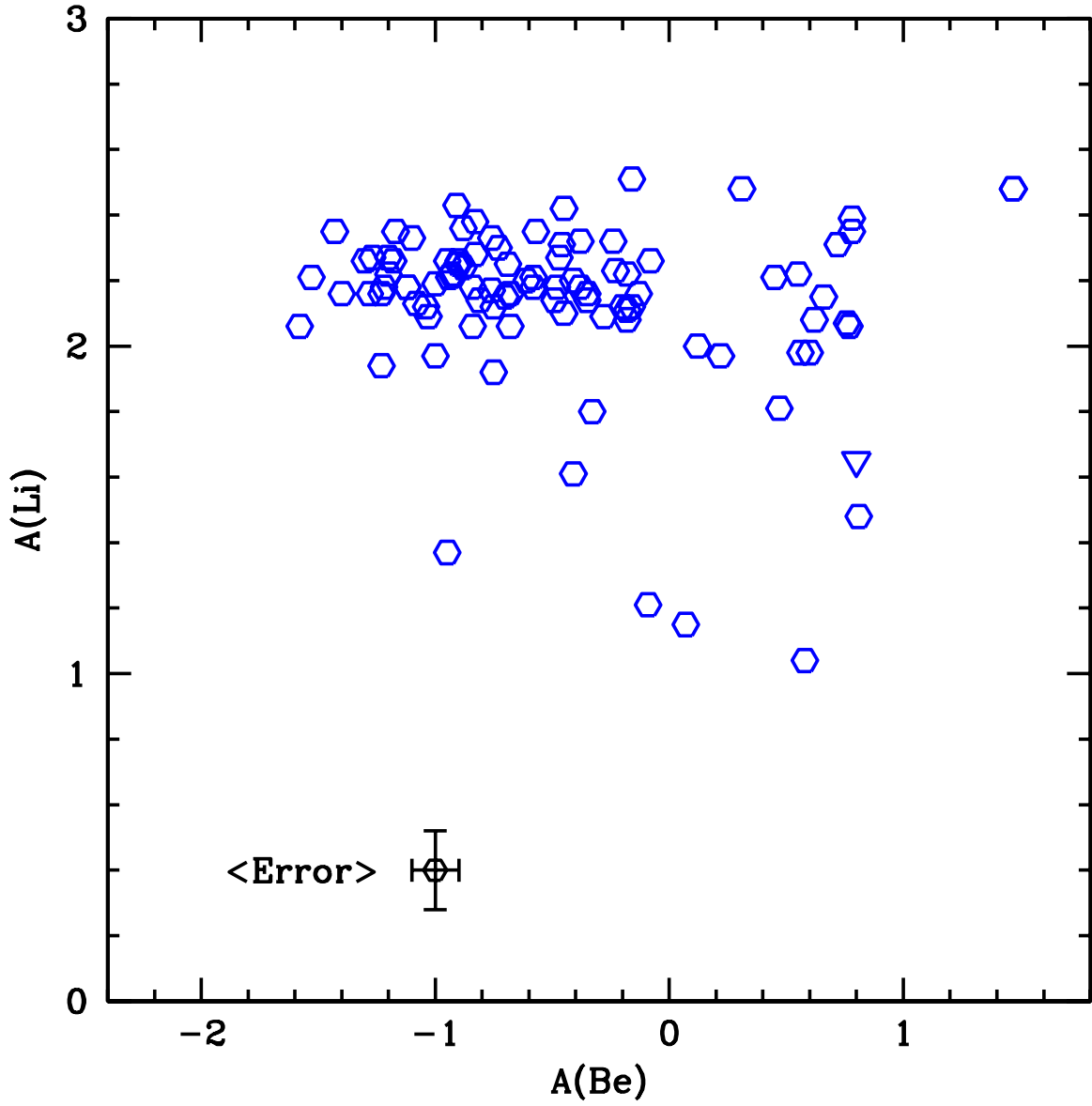


Fig. 19.— Our Be abundances compared with Li abundances in the literature. There are seven stars that are Li-depleted, but are apparently normal in Be.

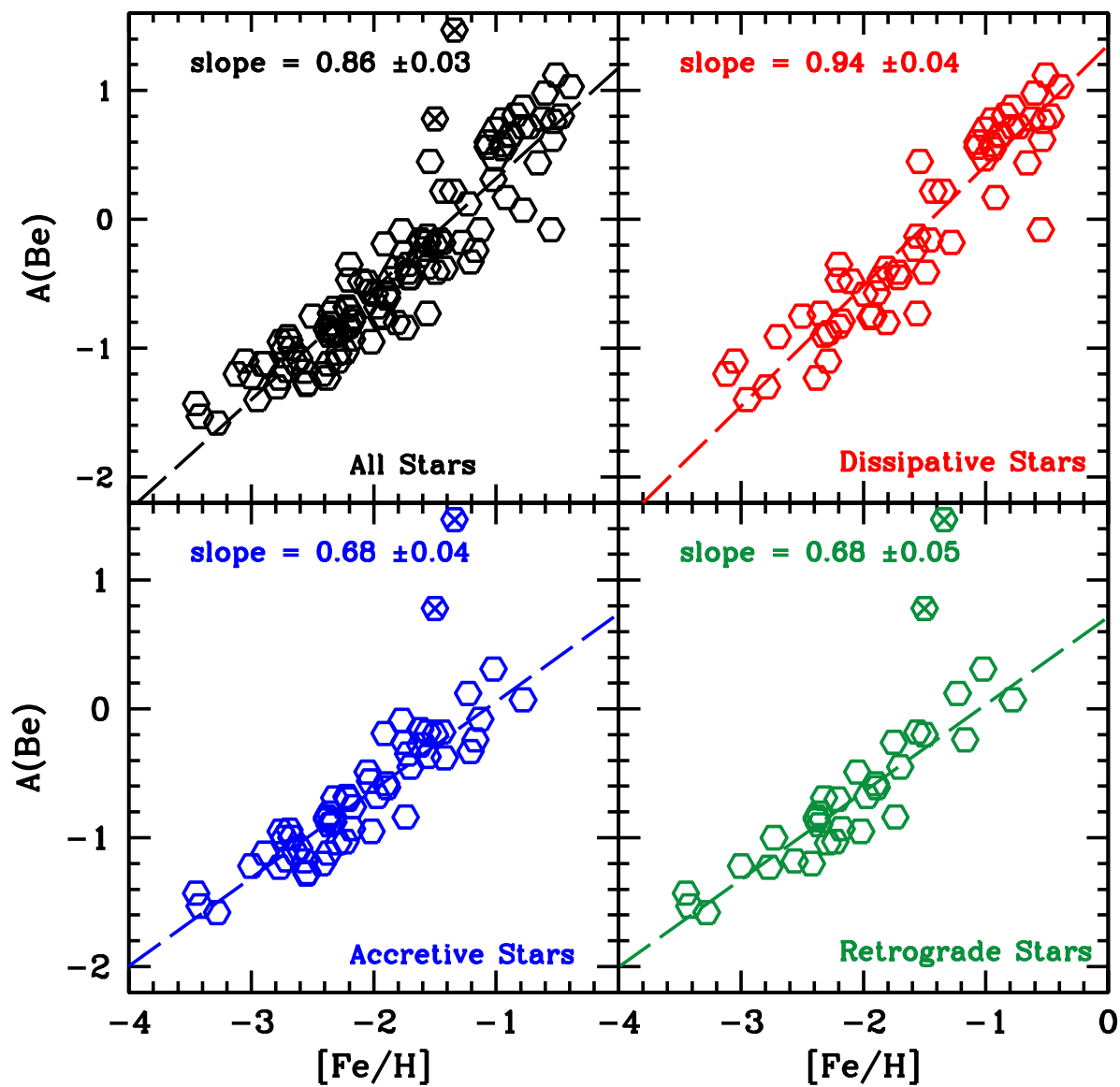


Fig. 20.— The distribution of  $A(\text{Be})$  with  $[\text{Fe}/\text{H}]$  for our total sample, for the dissipative stars, for the accretive stars, and for retrograde subset of the accretive stars. There is a steeper slope, 0.94, for the dissipative stars than for the accretive stars, 0.68. The hexagons with the crosses are the Be-rich stars which are both accretive and retrograde.

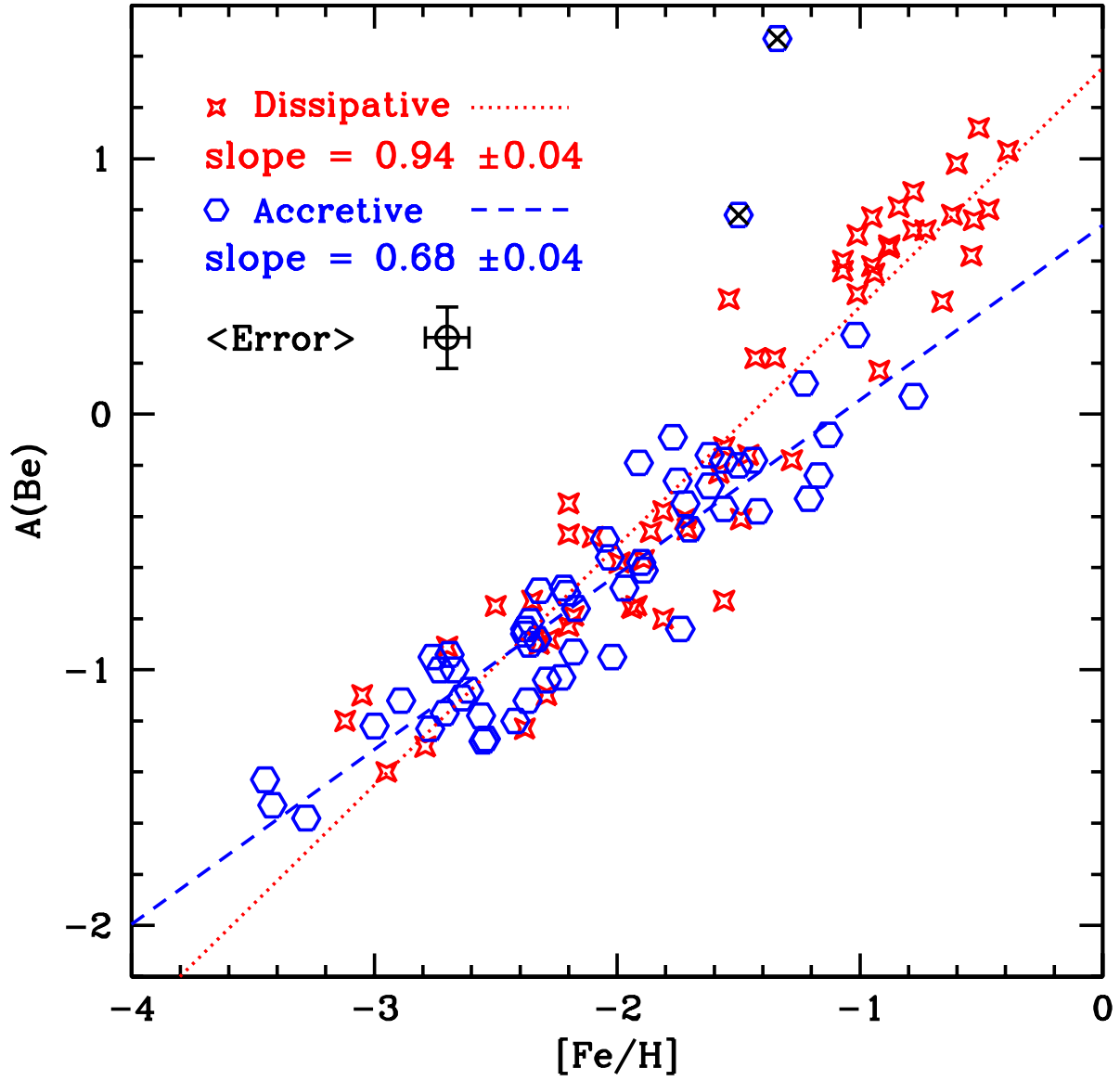


Fig. 21.— The dissipative stars (starred crosses) and their slope (dotted line) and the accretive stars (hexagons) and their slope (dashed line) are shown together.



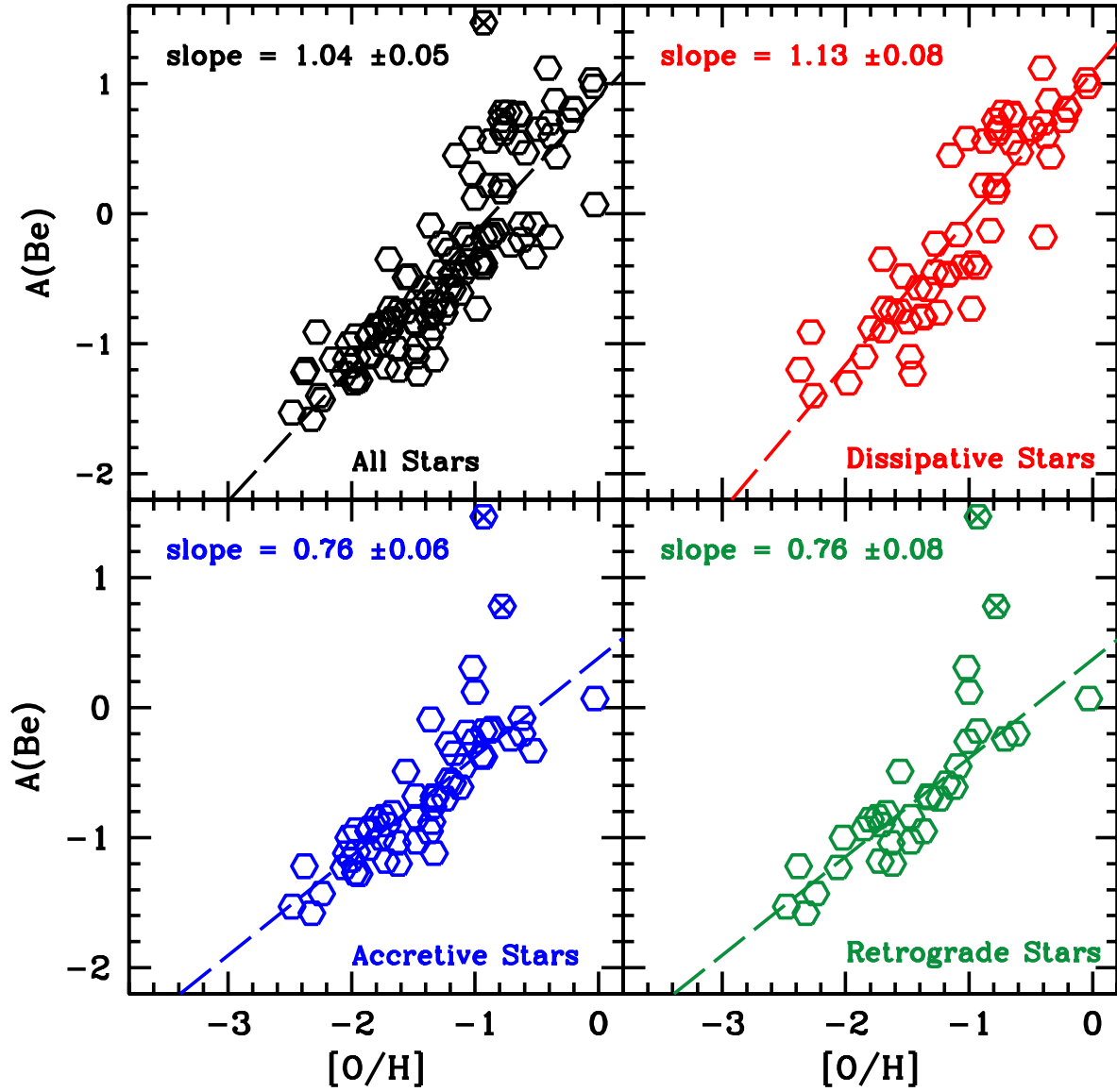


Fig. 22.— The distribution of  $A(\text{Be})$  with  $[\text{O}/\text{H}]$  for our total sample, for the dissipative stars, for the accretive stars, and for retrograde subset of the accretive stars. There is a steeper slope, 1.13, for the dissipative stars than for the accretive stars, 0.76. The hexagons with the crosses are the Be-rich stars which are both accretive and retrograde.

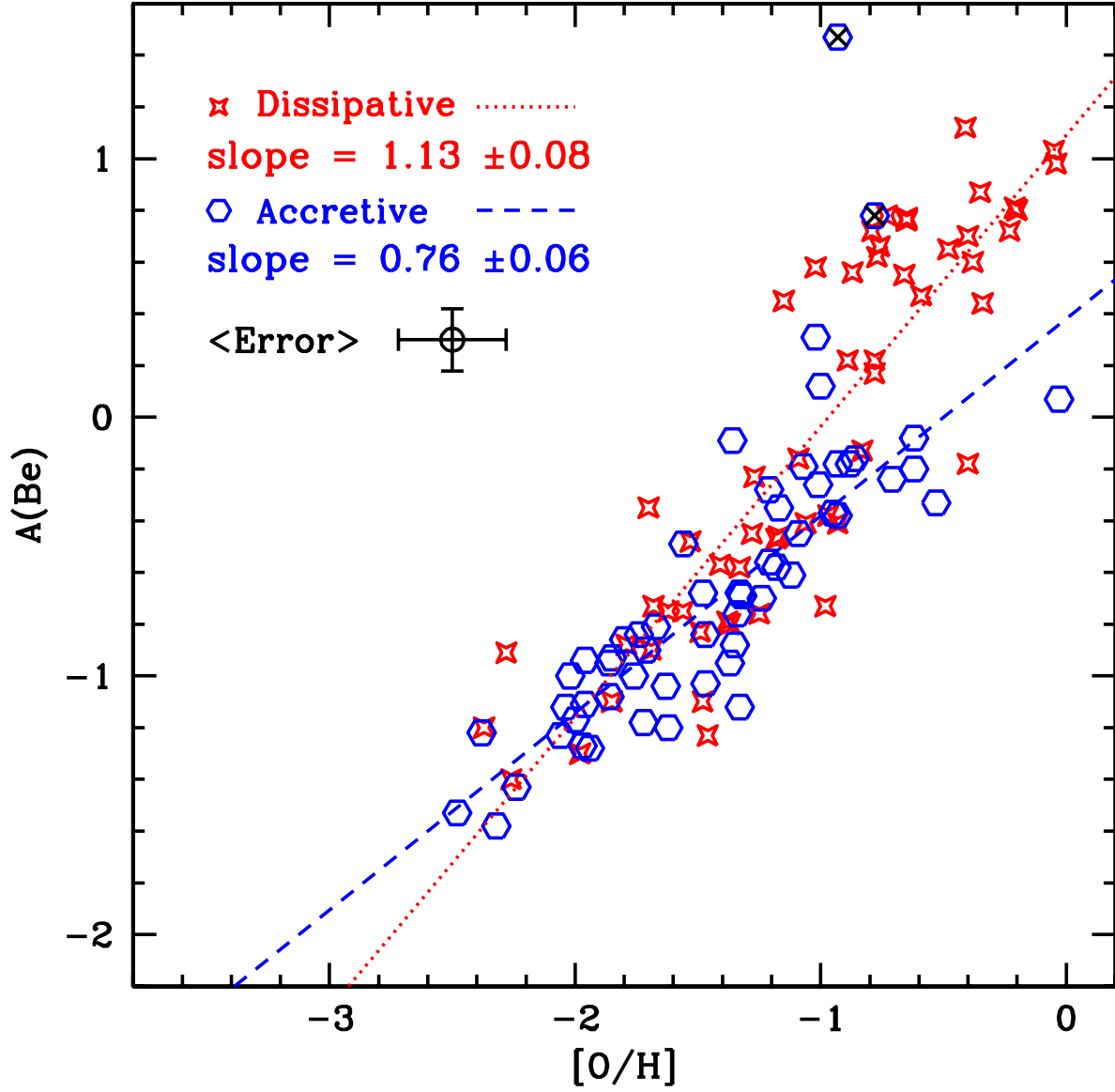


Fig. 23.— The dissipative stars (starred crosses) and their slope (dotted line) and the accretive stars (hexagons) and their slope (dashed line) are shown together.

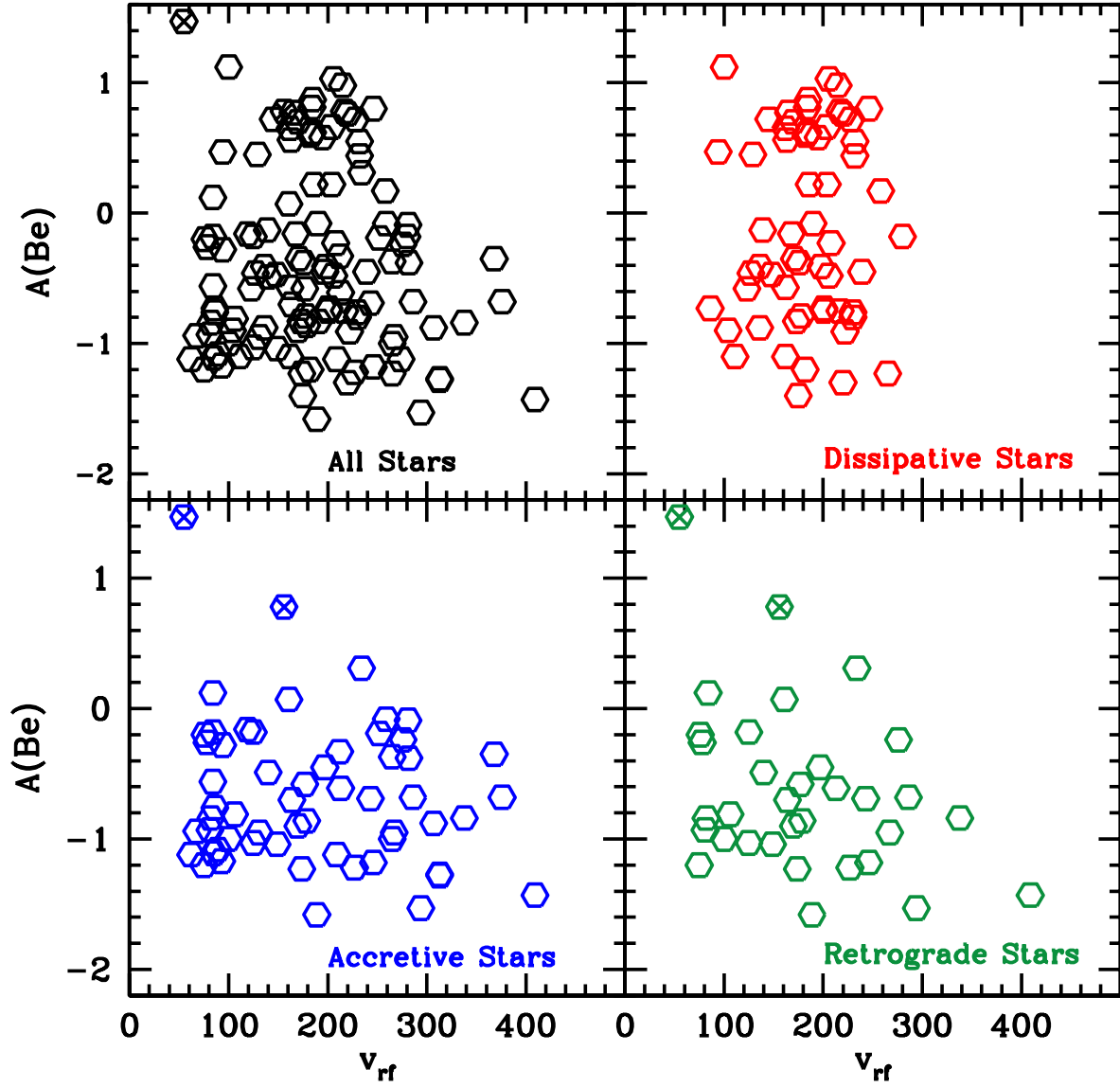


Fig. 24.— The values of  $A(\text{Be})$  shown as a function of the rest-frame velocity for the different groupings of stars.

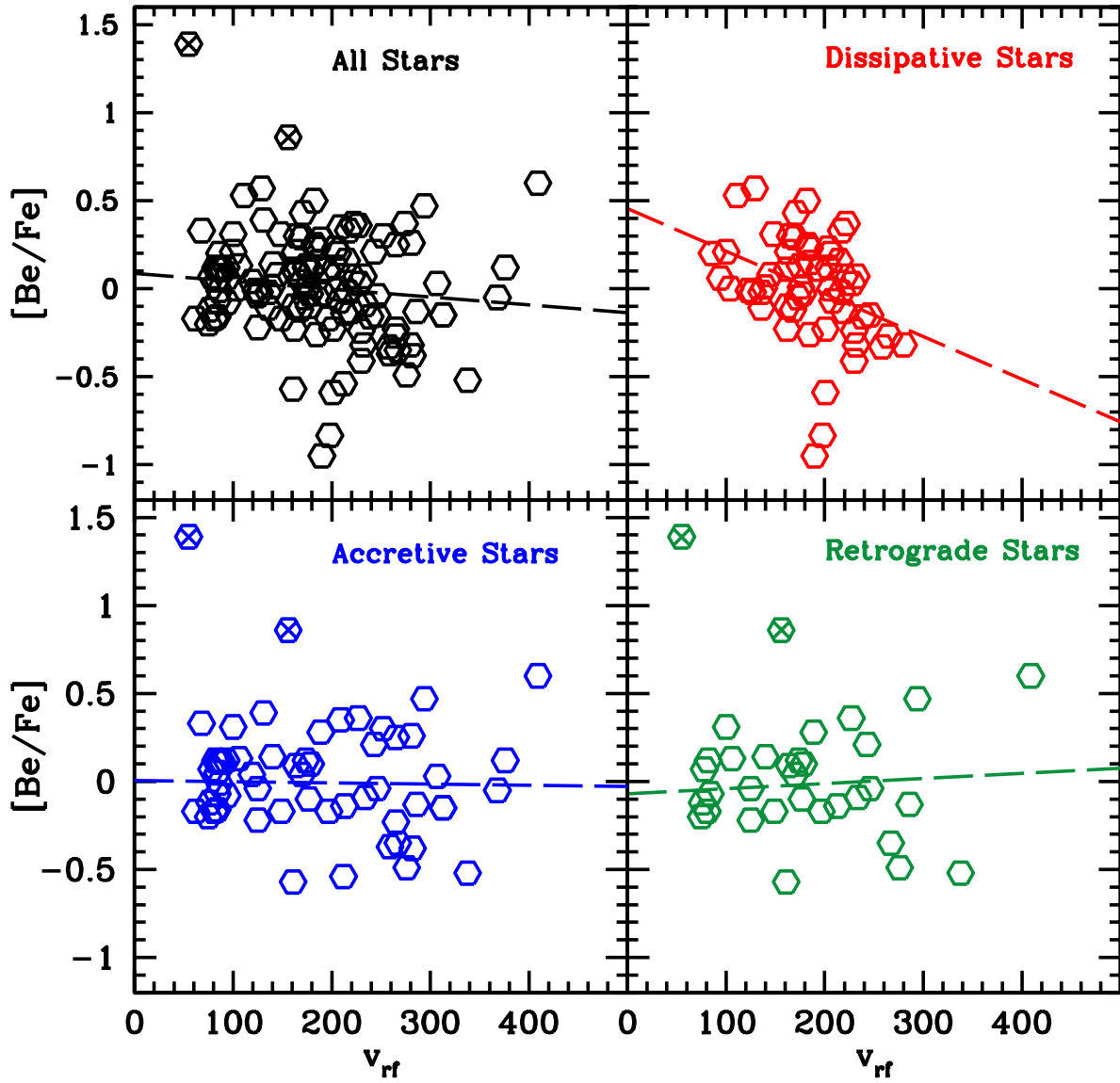


Fig. 25.— The Be abundances normalized to Fe as a function of the rest-frame velocity for the different groupings of stars. In the bottom two panels the highest-velocity point is G 64-12.

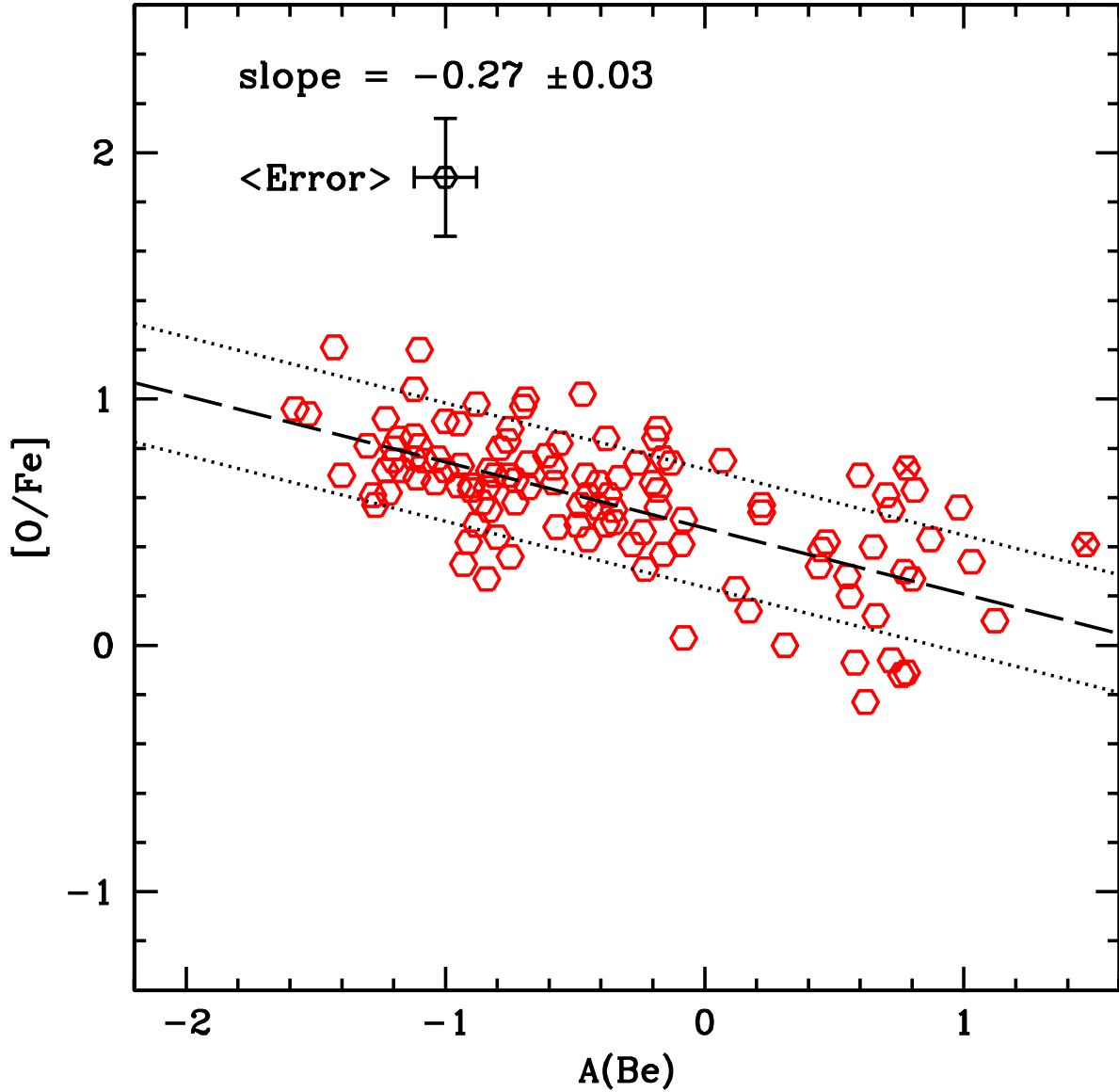


Fig. 26.—  $[O/Fe]$  as a function of the Be abundance,  $A(Be)$ . The dashed line is the linear fit and the dotted lines are plus and minus the error in  $[O/Fe]$ . There is more scatter at the higher values of  $A(Be)$  where more of the disk stars reside. Comparison of this with Figure 14, where  $[Fe/H]$  is the abscissa, shows that  $[Fe/H]$  is a better chronometer than  $A(Be)$  overall.

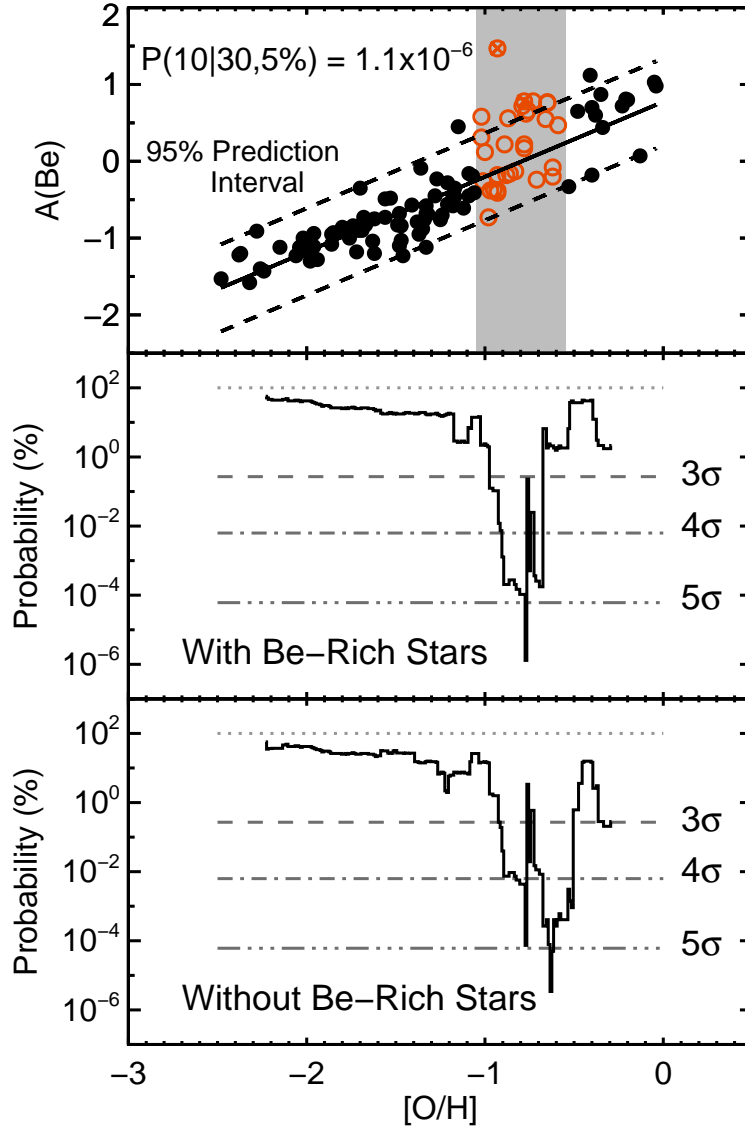


Fig. 27.— Example of our  $A(\text{Be})$  spread analysis for  $[\text{O}/\text{H}]$ . The top panel shows the test for the interval centered at  $[\text{O}/\text{H}] = -0.8$  with a width of 0.5 dex (gray shaded region). We use the data outside the interval (black filled circles) to derive the best-fit line and prediction interval we expect the data to follow within the interval (red open circles). In this example 10 out of 30 points lie outside the 95% prediction interval. Based on the binomial theorem, the probability of this occurring by chance is  $1.1 \times 10^{-6}$ . This process is repeated in running steps of 0.01 dex, producing the probability curve shown in the middle panel. For central values of  $[\text{O}/\text{H}]$  between  $\sim -0.75$  to  $-0.95$  (or a range from  $\sim 0.5$  to  $-1.2$ ), there appears to be a spread in Be at  $>4\text{-}\sigma$  for a given  $[\text{O}/\text{H}]$ . In the bottom panel we show the results ignoring the two Be-rich stars HD 106038 and HD 132475 (marked with crosses in the top panel); even in this case the spread appears to be significant.